Boore-Atkinson NGA Ground Motion Relations for the Geometric Mean Horizontal Component of Peak and Spectral Ground Motion Parameters

David M. Boore
U.S. Geological Survey, Menlo Park, California

and

Gail M. Atkinson
Department of Earth Sciences
University of Western Ontario, Canada

PEER Report 2007/01
Pacific Earthquake Engineering Research Center
College of Engineering
University of California, Berkeley

May 2007

Appendices

INTRODUCTION

A number of appendices are contained in this report. Some of them are new, and some are based on notes created by the first author during the progress of the NGA project (many of these notes are available from *http://quake.wr.usgs.gov/~boore/daves_notes.php*). We have included a number of the earlier "notes" because they represent work the first author did on the project, and we felt that this work should be documented in the final report.

Several appendices document problems that the first author found with data in the NGA flatfile; some of these problems have been fixed, but we have not had time to check the current version of the flatfile to see if all of them have been corrected.

Because it is inaccurate to refer to "we" when the first author was solely responsible for the notes, the more accurate pronoun "I" is used in some of the appendices to refer to David M. Boore.

Appendix A: Terminology

A.1 "GMPES" VS. "ATTENUATION RELATIONS"

I propose that we do away with the term "attenuation relations" to describe the equations predicting ground motion. I realize that this term is deeply ingrained in our profession, but like jargon in other fields, does not promote a clear understanding of the subject. The problem in earthquake engineering is that the equations do more than predict attenuation (the change of amplitude with distance); they also predict absolute levels of ground motion and therefore also the change in amplitude as a function of earthquake magnitude at a given distance (as controlled largely by source scaling). In addition, ground motions along a given profile might actually increase with distance (think "Moho bounce"), and in the future more sophisticated path- and/or regionally dependent predictions of ground motion might include an increase of motion at some distance ranges. Finally, there is the potential for confusion because some people really do mean *Q* and geometrical spreading when using the term "attenuation relations." What do I suggest as a replacement? I doubt that any term is without potential misunderstanding or would receive universal approval, but here are several possibilities: "ground-motion prediction equations," although some people do not like the word "prediction"; "ground-motion estimation equations"; or "ground-motion models" (a term preferred by Ken Campbell, recognizing that some models are in the form of look-up tables rather than equations). All of the phrases can be preceded by one of these qualifiers, as appropriate: empirical, hybrid, or theoretical. In this report we use "GMPEs." This is to be pronounced "gumpys."

For your entertainment, here is Tom Hanks's view of the matter, (Hanks, T.C., and C.A. Cornell, "Probabilistic Seismic Hazard Analysis: A Beginner's Guide," to be published in *Earthquake Spectra)*: "… we need what's known in the trade as a ground-motion attenuation relation. (What is really meant here is the excitation/attenuation relationship, admittedly a

polysyllabic mouthful for our language-challenged colleagues who nevertheless know perfectly well that earthquake strong ground motion is a function of magnitude (excitation) and distance (attenuation)).”

A.2 MODIFIERS OF “FREQUENCY” AND “PERIOD”

Just as frequencies are usually described as being “low” or “high,” and periods are described as being “short” or “long,” we should use “longest useable period” rather than “highest useable period.” But to be perverse, we use “maximum useable period” and “T_{MAX}” instead.

A.3 “LOW-CUT FILTER” OR “HIGH-PASS FILTER”?

We prefer “low-cut filter” to “high-pass filter,” although both refer to the same thing; “high-pass filter” probably derived from analog circuits that only “passed” certain frequencies, whereas the active process of a digital filter is to remove or cutout frequencies—thus “low-cut” rather than “high-pass.” Unfortunately, many engineers have not caught up with the newer terminology.

Appendix B: Comparing NGA Flatfiles v. 7.2 and 7.27

In the NGA flatfile, values of PSA are provided for periods up to 10 s no matter what low-cut filtering was needed to remove long-period noise. The lowest useable frequency, based on the low-cut filter frequency and the order and type of the filter, is provided for each record in the flatfile, and this variable is used to guide the choice of the portion of the PSA for each record to be used in the regression. (We find it more convenient to work with the longest useable period, which we denote T_{MAX}, rather than the lowest useable frequency; T_{MAX} is the reciprocal of the lowest useable frequency.) In developing the NGA database, the first version of the flatfile to provide GMRotI (version 7.2) based on the choice of the rotation angle used to compute GMRotI on all periods to 10 s, regardless of the filter cutoff used in processing each record. Formally, it is not valid to include portions of the response spectrum above T_{MAX} in choosing the rotation angle used to compute GMRotI because the spectrum at periods greater than T_{MAX} might not correspond to the actual ground-motion spectrum that would exist in the absence of the noise that required the low-cut filter in the first place. This error was corrected in what we call version 7.27 of the NGA flatfile (this is not a new flatfile distributed to the developers by Brian Chiou, but one that the first author made by inserting the information in *727brian.xls* into the v. 7.2 flatfile; the file *727brian.xls* was distributed to the developers, but it was up to each developer to replace the incorrect values in the flatfile with the correct values). Two things are included in this Appendix: (1) a comparison of GMRotI from the version 7.2 and version 7.27 flatfiles and (2) some plots relevant to whether GMRotD should be used instead of GMRotI (only a brief discussion of this is given, with no conclusions).

The ratios are shown in Figures B.1–B.8, for PGV, PGA, and PSA for oscillator periods $T_{OSC} = 0.1$, 0.2, 1.0, 3.0, 5.0, and 10.0 s (the y-axis title can be used to identify the period). The ratios are values from version 7.27 divided by values from version 7.2. A few outliers have been flagged with the NGA flatfile record number, event, and recording station. The comparison between the version 7.27 and 7.2 ground-motion values is worse for longer period measures of ground-motion intensity. Note the color coding indicating whether T_{OSC} is less than or greater than T_{MAX}. Our expectation was that most of the scatter of the ratio away from unity for the longer oscillator periods would correspond to recordings for which $T_{MAX} < T_{OSC}$, but that does not seem to be the case. This is easiest to see in Figures B.4–B.8, which show the ratios of ground motions plotted against T_{OSC} / T_{MAX}. The red symbols indicate ratios for which $T_{MAX} < T_{OSC}$, but the ratios for these recordings are no farther removed from unity than are the ratios for recordings for which T_{MAX} is much greater than T_{OSC}. Although there appears to be considerable scatter, particularly at longer periods, the graphs are misleading---they do not show that many observations have ratios close to unity. Statistical tests of the kurtosis show that the distributions are not normal. In the worst case ($T_{OSC} = 10.0$ s), 50% of the ratios are between 0.992 and 1.005, and 90% of the values are between 0.880 and 1.072. Our conclusion is that it should make little or no difference in the GMPEs if version 7.2 of the flatfile is used rather than version 7.27.

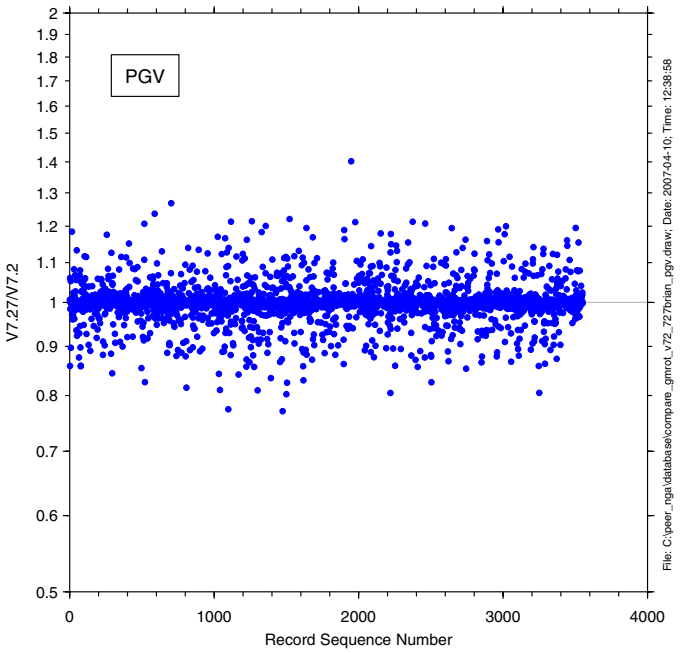

Fig. B.1 Ratio of PGV values from NGA flatfile, versions 7.27 and 7.2.

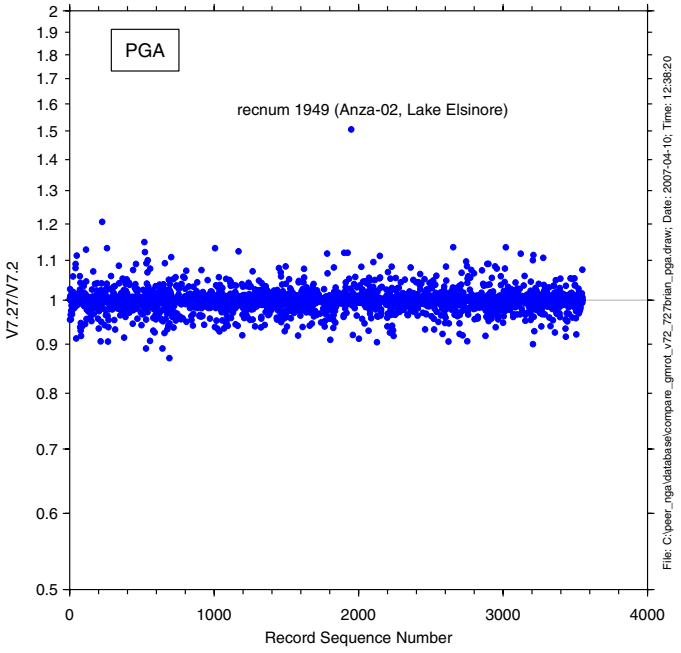

Fig. B.2 Ratio of PGA values from NGA flatfile, versions 7.27 and 7.2.

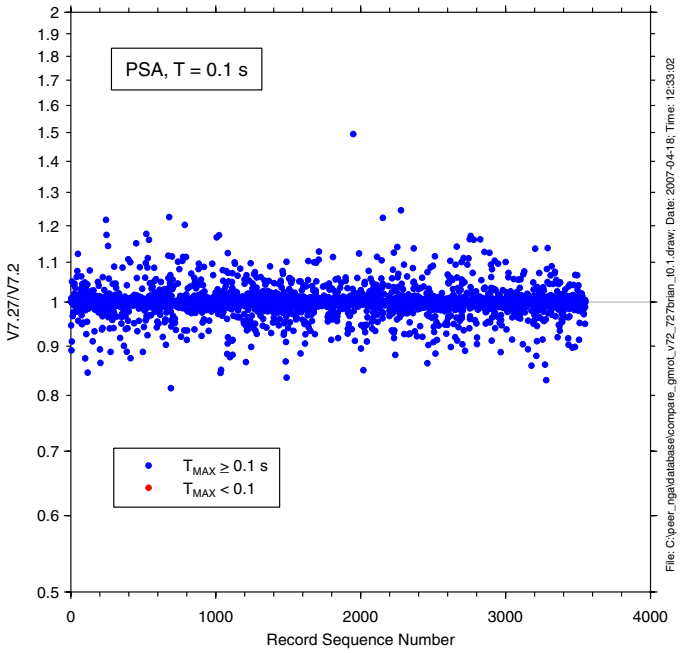

Fig. B.3 Ratio of 5%-damped 0.1 s PSA values from NGA flatfile, versions 7.27 and 7.2. As indicated in legend, symbol colors indicate values for which highest useable period (T_{MAX}) is greater than or less than oscillator period. In this case, period is so short that T_{MAX} s for all records are greater than oscillator period.

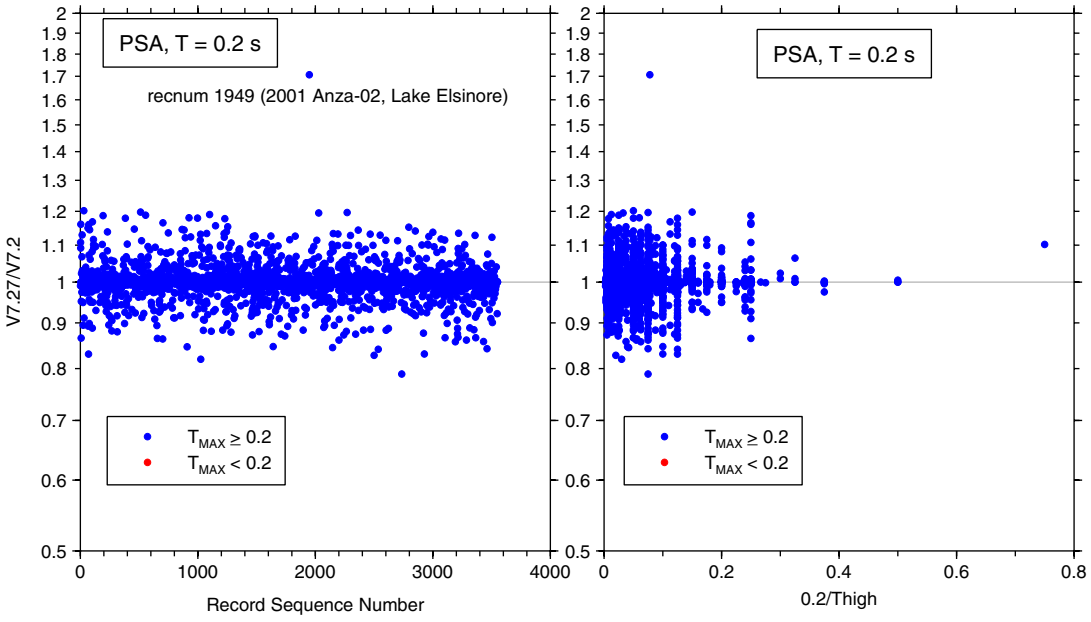

Fig. B.4 Ratio of 5%-damped 0.2 s PSA values from NGA flatfile, versions 7.27 and 7.2. As indicated in legend, symbol colors indicate values for which highest useable period (T_{MAX}) is greater than or less than oscillator period. In this case, period is so short that T_{MAX} s for all records are greater than oscillator period.

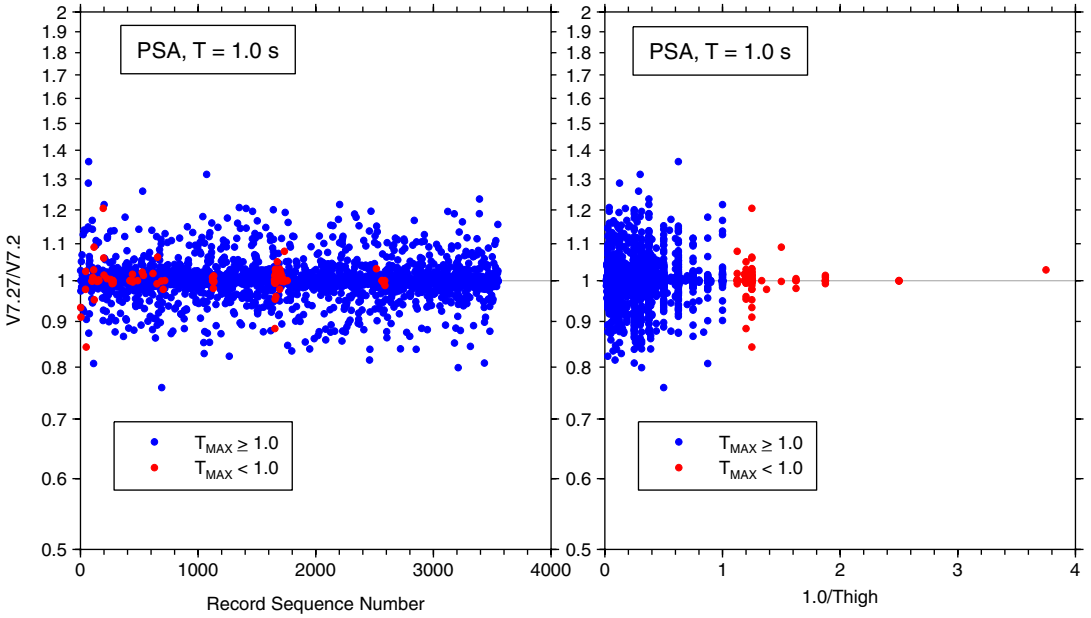

Fig. B.5 Ratio of 5%-damped 1.0 s PSA values from NGA flatfile, versions 7.27 and 7.2. As indicated in legend, symbol colors indicate values for which highest useable period (T_{MAX}) is greater than or less than oscillator period.

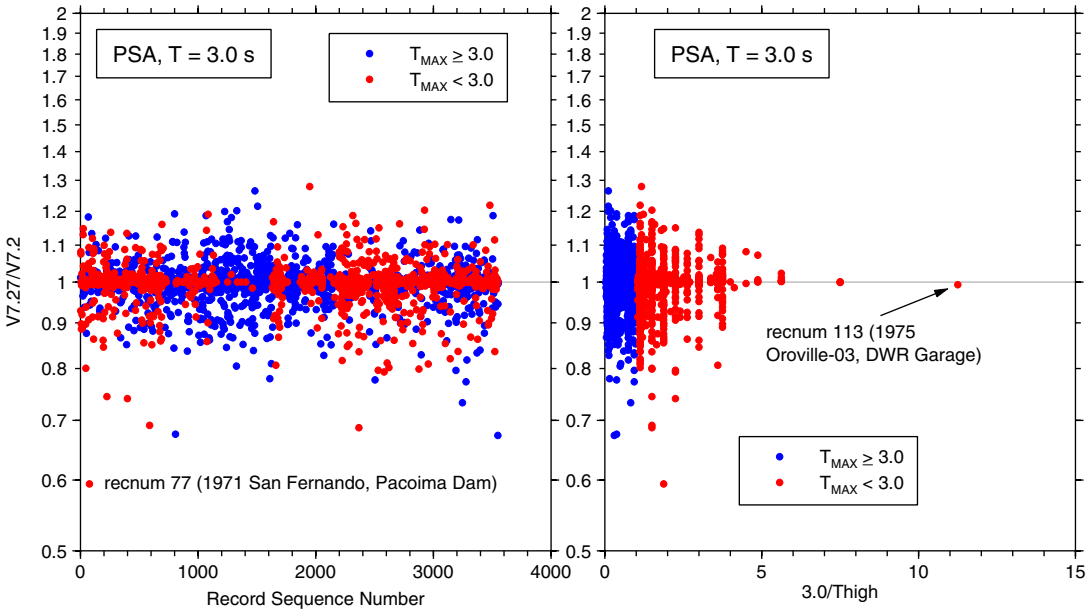

Fig. B.6 Ratio of 5%-damped 3.0 s PSA values from NGA flatfile, versions 7.27 and 7.2. As indicated in legend, symbol colors indicate values for which highest useable period (T_{MAX}) is greater than or less than oscillator period.

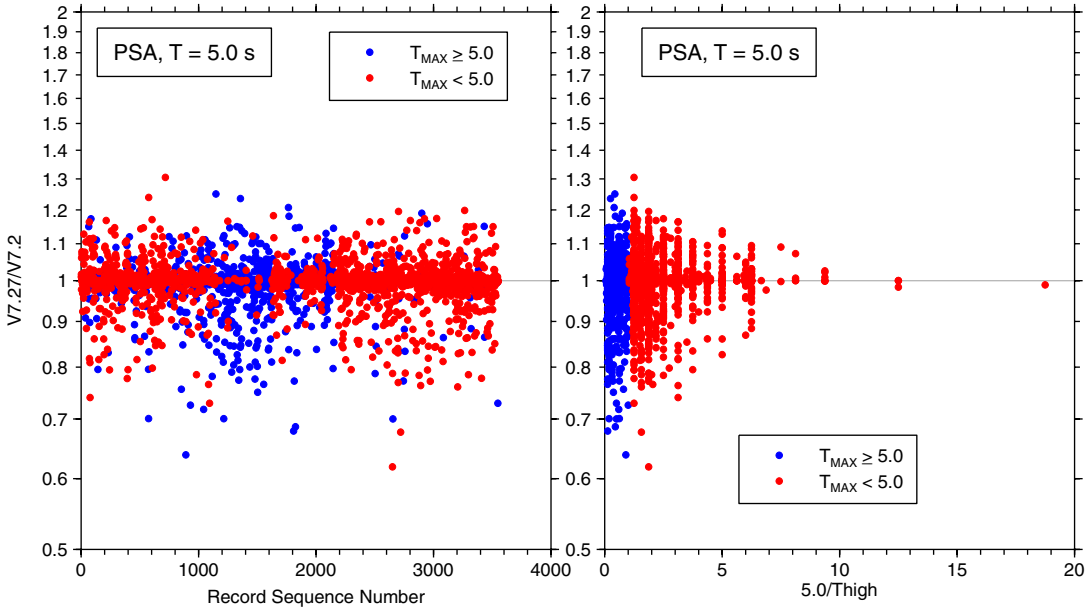

Fig. B.7 Ratio of 5%-damped 5.0 s PSA values from NGA flatfile, versions 7.27 and 7.2. As indicated in legend, symbol colors indicate values for which highest useable period (T_{MAX}) is greater than or less than oscillator period.

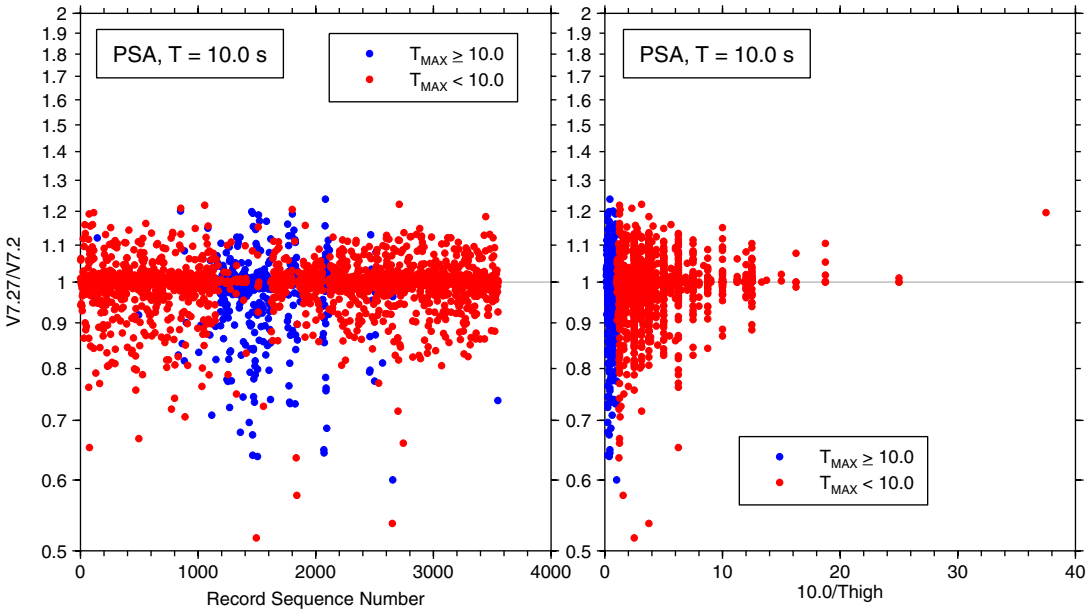

Fig. B.8 Ratio of 5%-damped 10.0 s PSA values from NGA flatfile, versions 7.27 and 7.2. As indicated in legend, symbol colors indicate values for which highest useable period (T_{MAX}) is greater than or less than oscillator period.

As noted in Boore et al. (2006), GMRotI can be sensitive to the range of periods used in computing the penalty function, which is not the case for GMRotD. (Note: Boore et al., 2006, used the terminology "GMRotI50" and "GMRotD50" to stand for what we are calling "GMRotI" and "GMRotD"). This raises a question of whether it would be better to use GMRotD instead of GMRotI. We include here a few figures adapted from Boore et al. (2006), the first (Fig. B.9) showing the ratio of GMRotI to GM as recorded (and the standard deviation of the logarithm of the ratio, expressed as a factor), and the second (Fig. B.10) showing the ratio of GMRotI to GMRotD (and the standard deviation of the logarithm of the ratio, expressed as a factor). Clearly there are significant trends for longer periods. It is not possible to say whether the numerator or the denominator contributes most to the standard deviation, but in either case, the factor is small compared to the inter- and intra-event uncertainties. These plots show that the ratio of GMRotI to GMRotD varies little from unity (the maximum being a 1% reduction at 10 s period); we conclude that it makes no difference if GMRotI instead of GMRotD is used in developing the GMPEs.

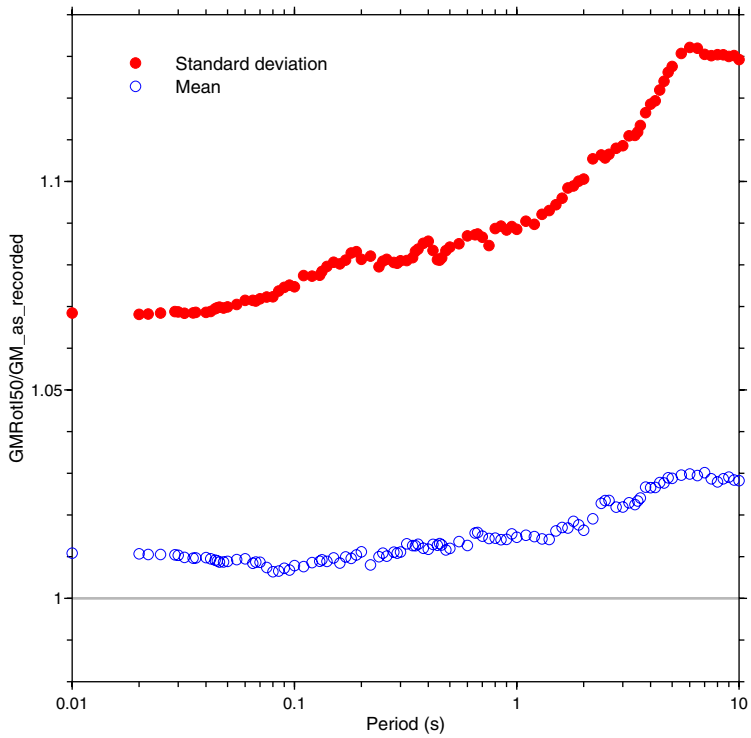

Fig. B.9 Average of ratio of GMRotI to as-recorded geometric mean and standard deviation of ratio, as function of oscillator period.

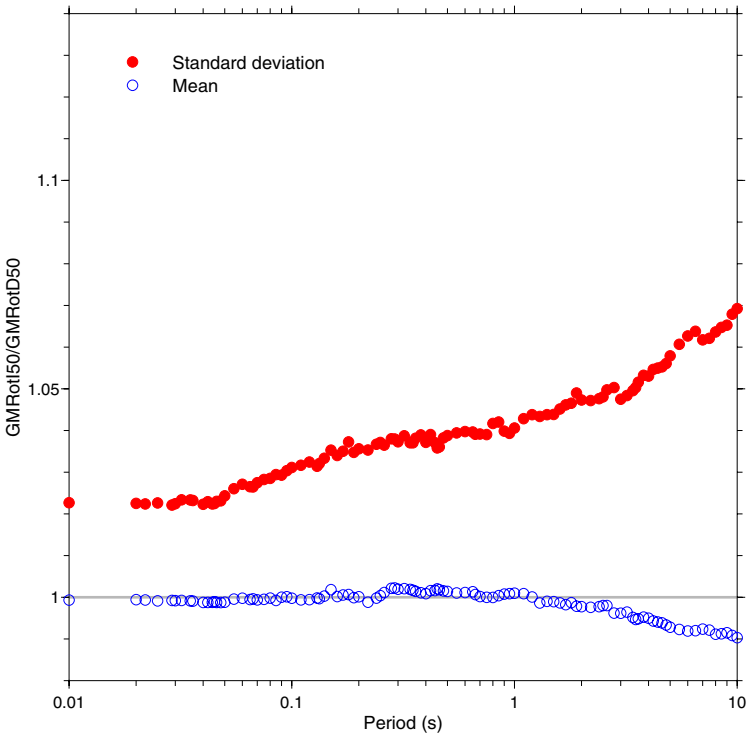

Fig. B.10 Average of ratio of GMRotI to GMRotD and standard deviation of ratio, as function of oscillator period.

Appendix C: Why We Don't Provide GMPEs for PGD

We do not provide GMPEs for PGD because PGD can be very sensitive to the low-cut filter corner. We show some examples in this appendix. We also discuss a possible bias in PGD in the NGA flatfile from accelerograms for which the NGA project only had access to records previously filtered by data providers and not to the original, unprocessed records. We also point out that some of the NGA processing may have been too conservative in the choice of low-cut filters, thus reducing the number of records available for determination of GMPEs at long periods.

C.1 SENSITIVITY TO LOW-CUT FILTER FREQUENCIES: RECORDS FROM 1999 CHI-CHI EARTHQUAKE

As shown earlier (Fig. 2.5), the number of data for which the longest useable period is greater than the oscillator period decrease rapidly for $T_{OSC} > 2$ s. For that reason, every effort should be made to choose the low-cut filter frequencies (f_{LC}) as low as possible, consistent with the noise. As is well known, this is a subjective process. Figure C.1 shows that there are many digital recordings for which T_{MAX} is less than 10 s. This seems a bit surprising, but we do not have time to look into the processing in detail for each record in the NGA flatfile. We were struck, however, with the large number of near-fault recordings from the 1999 Chi-Chi earthquake for which f_{LC} is less than 0.1 Hz (for most records, $T_{MAX} = 0.8 / f_{LC}$). Figure C.2 shows where these stations are located with respect to the fault. As Figure C.3 shows, many of these stations are close to GPS measurements of residual displacement. We have looked in detail at the horizontal

component recordings at stations TCU071 and TCU074. We computed displacement time series for a series of acausally filtered acceleration time series. These are shown for TCU074 in Figure C.4. We show the results for this station first because it is one of the rare examples where double integration of unfiltered data produces a displacement time series unaffected by long-period drifts. As the figure shows, the residual displacements are very close to those from the GPS measurements (particularly for the EW component). The filters used in the processing that gave the PGD values in the NGA flatfile are indicated in the figure. This is a very instructive figure. We first make the assumption that the noise increases with decreasing frequency; this assumption is based on extensive experience with double integration of accelerograms. Because of the lack of long-period drifts and the good correspondence of the residual displacements from the doubly-integrated accelerograms and the GPS measurements, we can then conclude that all of the filtered traces represent filtered signal and are not affected by noise. This allows us insight into the character of acausally-filtered ground motions with nonzero residual displacements; without this example, we think that many people would conclude that the character of the waveforms shown in Figure C.4 for the lower filter frequencies (e.g., 0.02 and 0.04 Hz) are controlled by noise. Instead, the "peculiar" features of the waveforms are the filter transients produced when a time series with a finite offset is filtered using an acausal filter. This being so, we think that the NGA filter corner frequencies are too high (we understand from personal communication with W. Silva that many of the recordings of the Chi-Chi earthquake have been reprocessed, but the new values are not in the NGA flatfile). Figure C.5 shows that PGD is sensitive to the filter corner frequency.

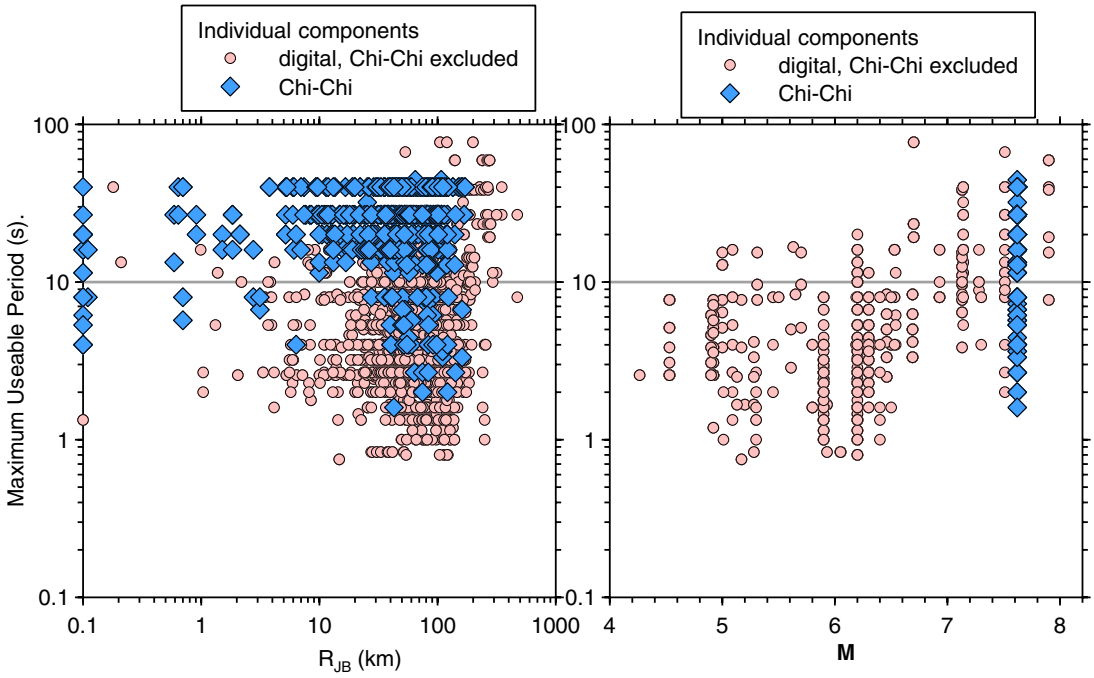

Fig. C.1 Maximum useable period (T_{MAX}) of data in NGA flatfile.

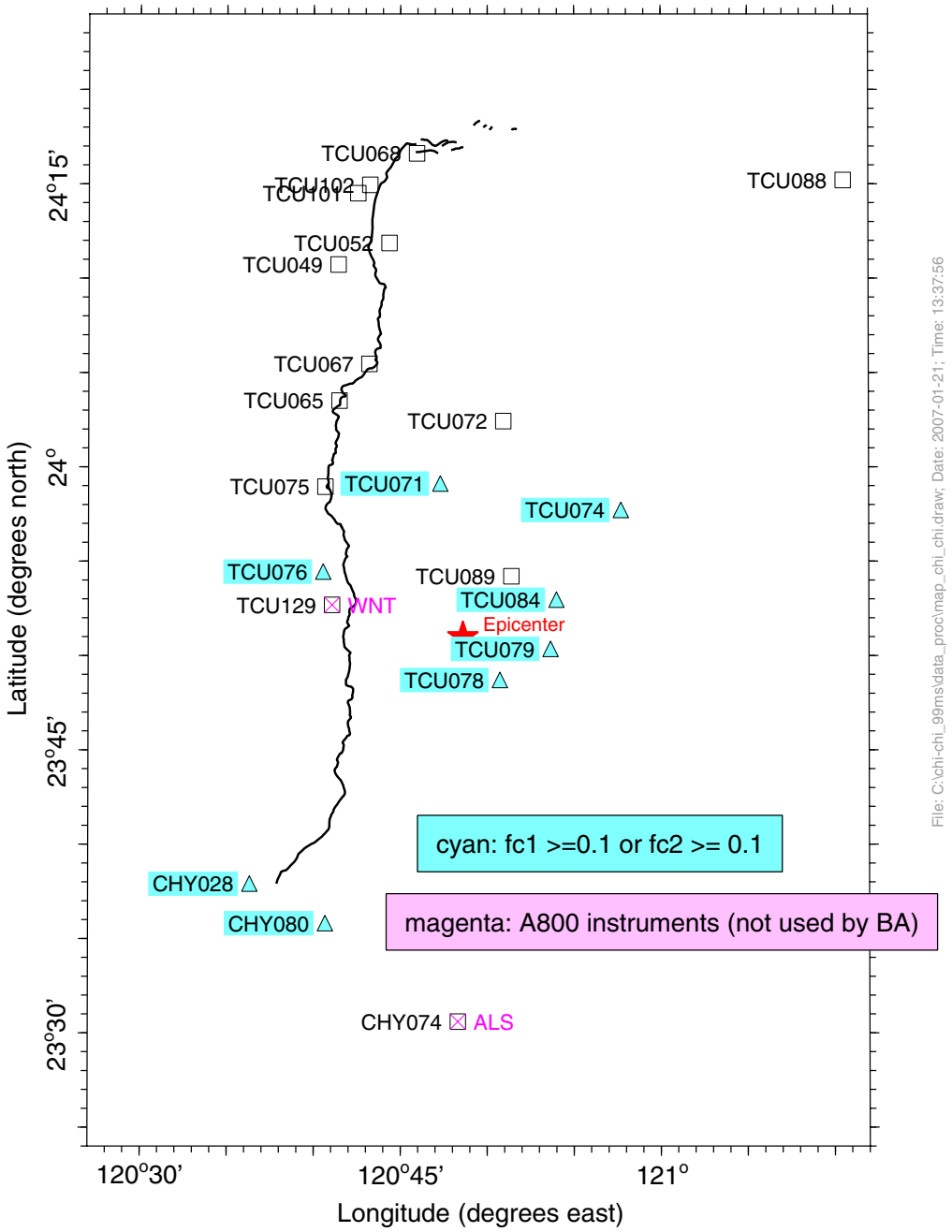

Fig. C.2 Map of near-fault stations that recorded 1999 Chi-Chi earthquakes, highlighting stations for which one of filter corners in NGA flatfile is less than 0.1 Hz.

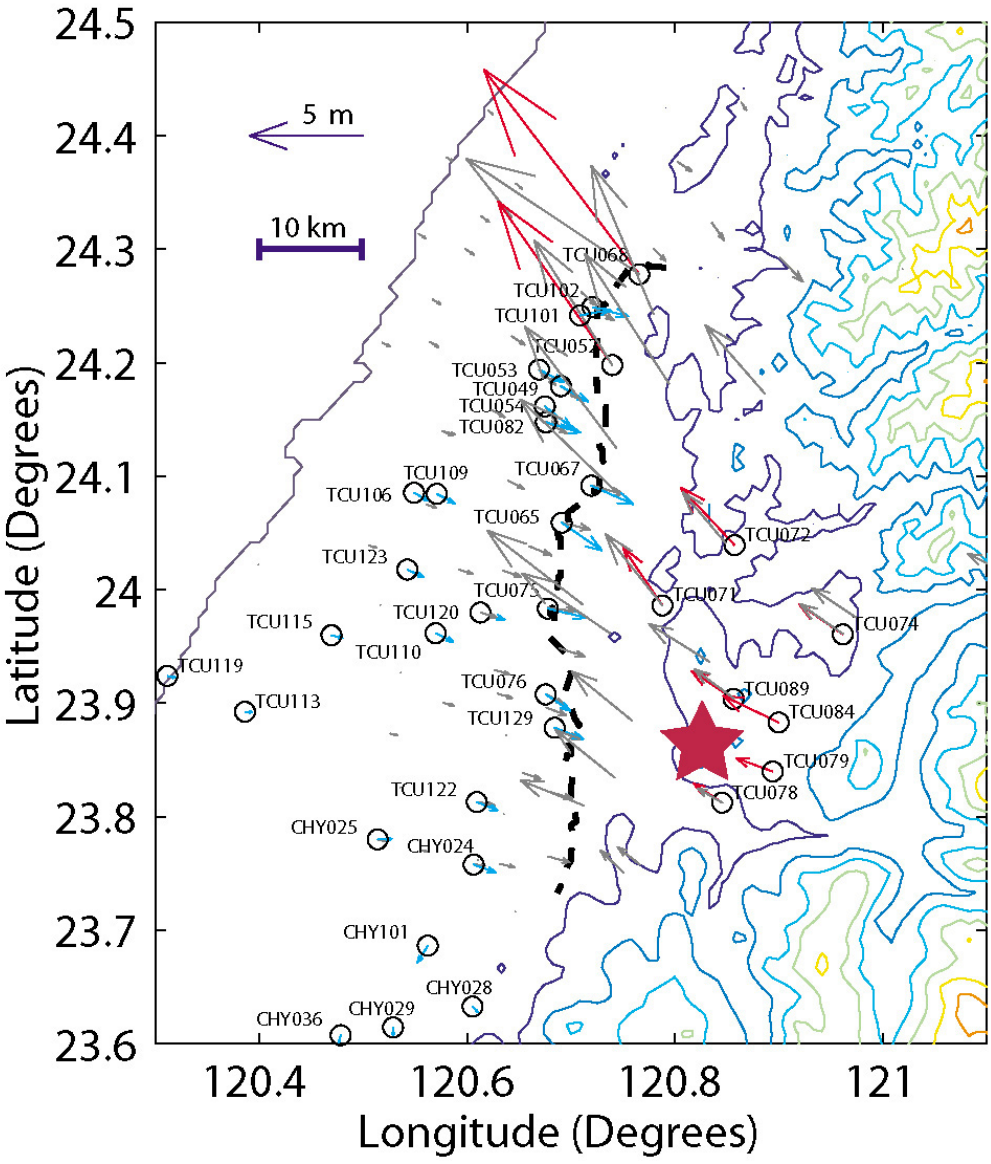

Fig. C.3 Comparison of residual displacements obtained from accelerometer recordings and from GPS measurements (from Oglesby and Day 2001).

.

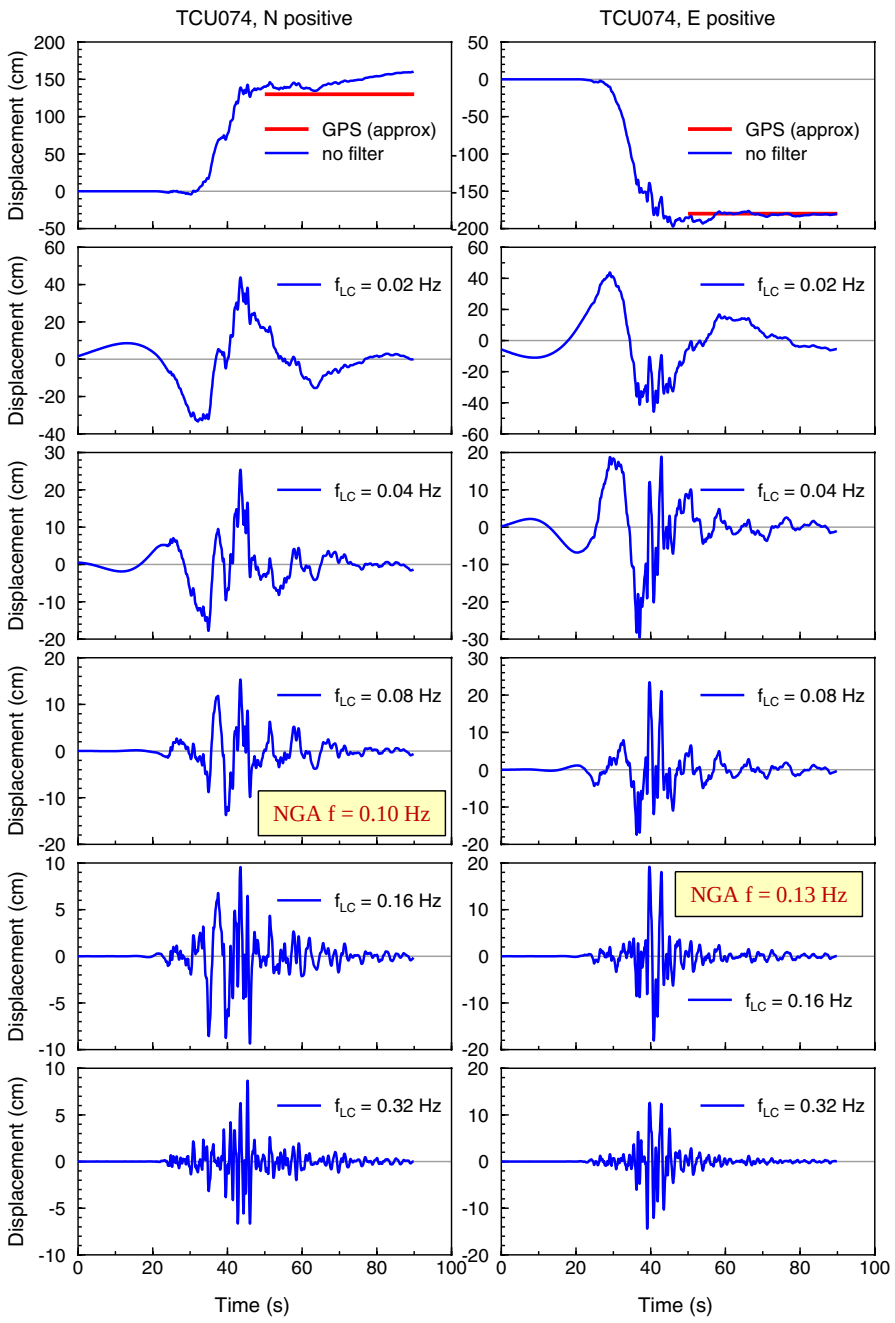

Fig. C.4 Displacements at TCU074, obtained by double integration of filtered accelerometer recordings of 1999 Chi-Chi earthquake. Each column corresponds to different horizontal component. GPS displacements scaled from Fig. 2 of Oglesby and Day (2001). Low-cut filter frequencies used in processing data in NGA flatfile indicated by text boxes placed on time series filtered with corner frequency close to NGA frequency.

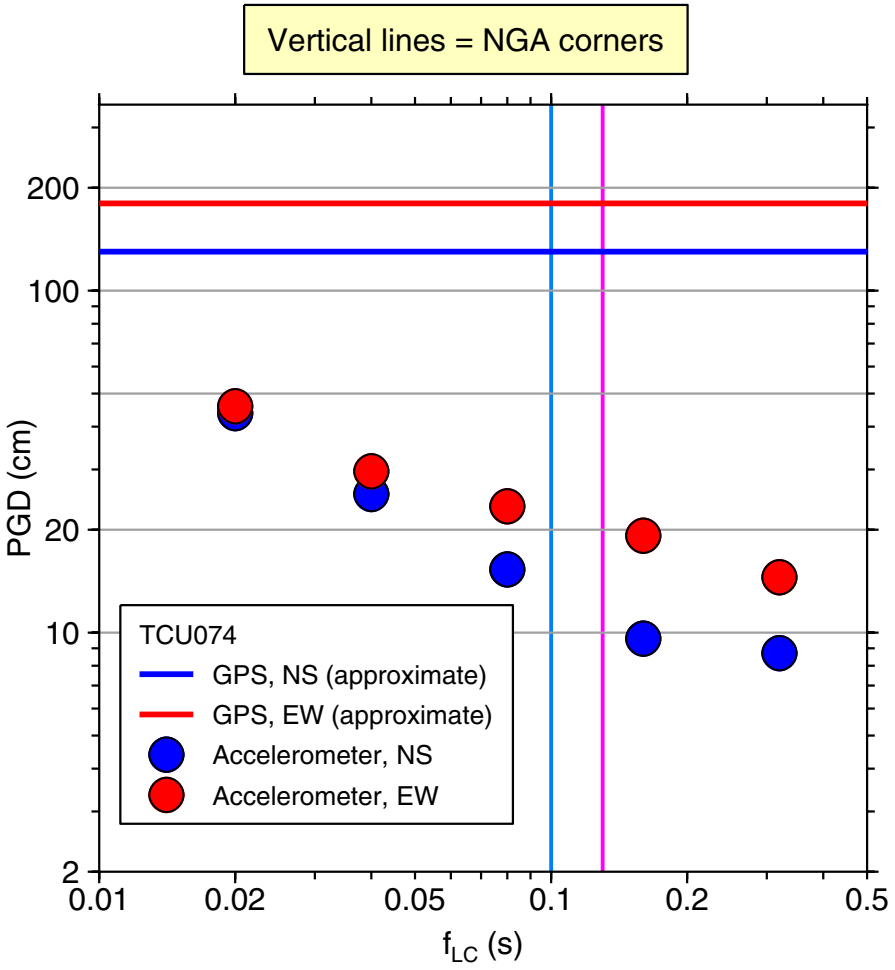

Fig. C.5 PGD from various time series shown in previous figure. Also shown are GPS residual displacements and low-cut filter corner frequencies used in processing data in NGA flatfile.

We did the same exercise with the horizontal component records from TCU071, as shown in Figures C.6 and C.7. For this record, it is clear that the typical long-period drifts exist, due to double integration of long-period noise in the acceleration time series. For that reason we cannot be sure that the traces filtered with low corner frequencies represent signal only. But the waveforms for $f_{LC} = 0.02$ Hz are similar to those for TCU074, so it is likely that most of the displacements in the filtered traces represent signal. One other point is that it is not clear why there is such a large difference in the NGA corner frequencies for the two components of motion. The lowest useable frequency in the NGA flatfile is determined by the maximum of the low-cut filter corners for the two horizontal components, which for TCU071 is 0.2 Hz (according to the

NGA flatfile, the lowest useable frequency for this record is 0.25 Hz). This means that with the NGA processing, the recording at this station contributes no information for the GMPEs developed for periods greater than 4 s.

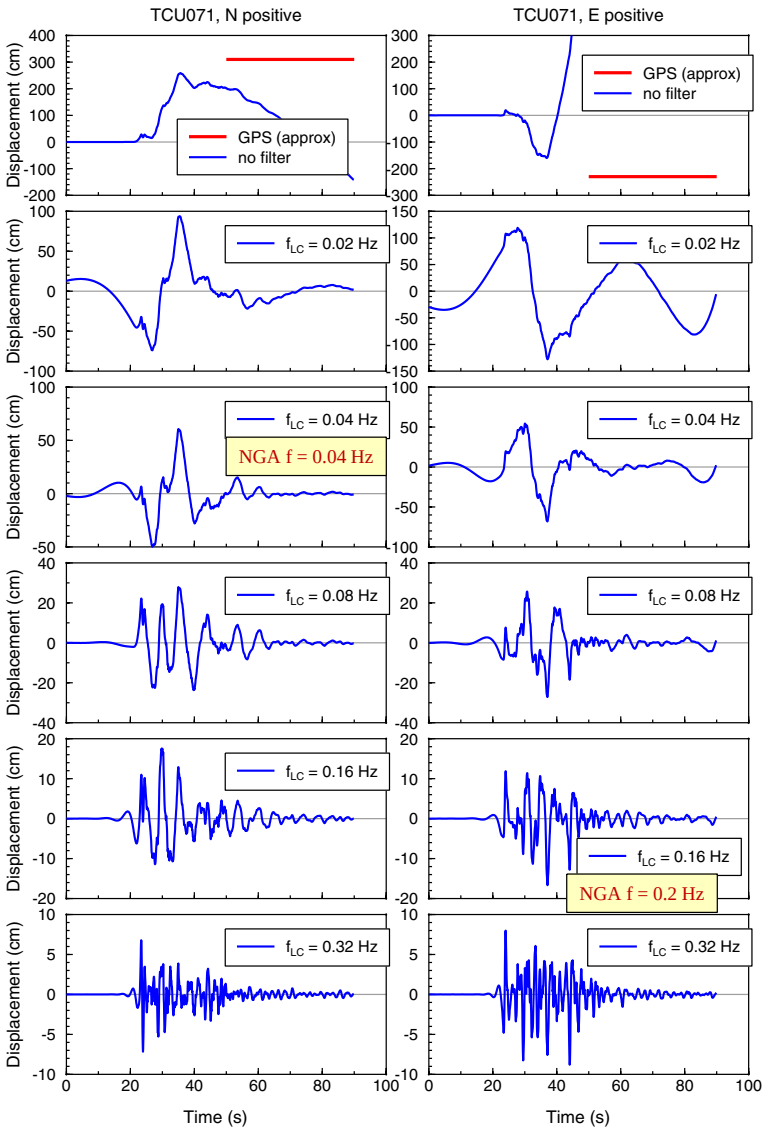

Fig. C.6 Displacements at TCU071, obtained by double integration of filtered accelerometer recordings of 1999 Chi-Chi earthquake. Each column corresponds to different horizontal component. GPS displacements scaled from Fig. 2 of Oglesby and Day (2001). Low-cut filter frequencies used in processing data in NGA flatfile indicated by text boxes placed on time series filtered with corner frequency close to NGA frequency.

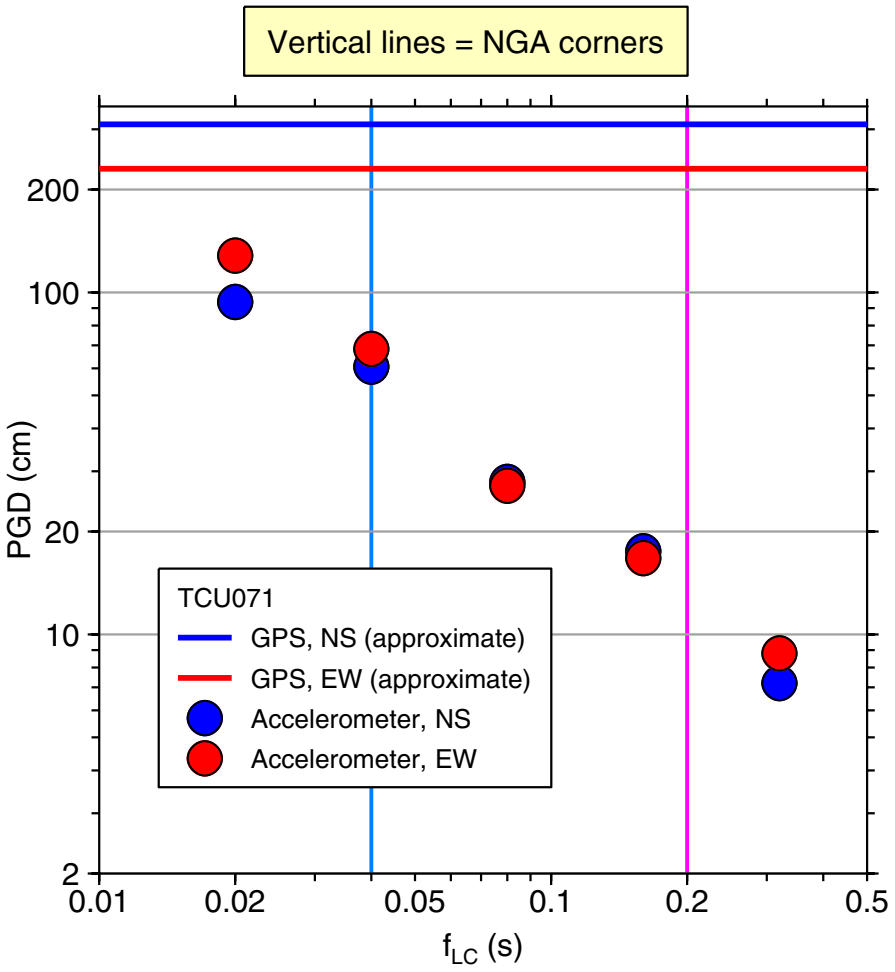

Fig. C.7 PGD from various time series shown in previous figure. Also shown are GPS residual displacements and low-cut filter corner frequencies used in processing data in NGA flatfile.

C.2 POSSIBLE SYSTEMATIC OVERESTIMATION OF PGD FOR "PASS-THROUGH" DATA

For several reasons, not all of the NGA data were processed starting from original, unfiltered records. Some of the acceleration time series provided by data agencies had already been filtered and/or baseline corrected to remove long-period noise. These records are referred to as "pass-through" records by W. Silva. The seismic-intensity measures other than PGA were computed from these pass-through data. Unfortunately, the pass-through data rarely, if ever, are distributed

with the zero pads that were added if acausal filtering was used to remove long-period noise. As discussed by Boore (2005), subsequent processing of pad-stripped data can lead to incompatible PSA, PGV, and PGD. This is shown in Figure C.8. The first blue and red traces are the displacement time series provided by the U.S. Geological Survey for two horizontal components recorded at the Monte Nido Fire Station during the 1994 Northridge earthquake. Note that the displacements are not zero at zero time. This is because the original processing included pre-event pads, which were stripped off the processed records made available to the public. Double integration of the pad-stripped acceleration leads to drifts in the displacements, as shown in the second traces. This was recognized in developing the NGA flatfile, but rather than use the displacement traces available from the data agencies, ad-hoc corrections were made to remove the drifts (the corrected NGA-determined displacement time series are the third time series in each set). These time series look like those from the data agency, but note the difference in PGD: 2.6 cm vs. 3.3 cm and 1.9 cm vs. 2.1 cm for the USGS-provided and PEER NGA, for the two components, respectively. We have made similar comparisons of a small set of data from the 1992 Cape Mendocino, 1992 Landers, and 1994 Northridge earthquakes. The results are summarized in Figure C.9, which shows the ratio of PGD from the NGA time series and from the reporting agency (the latter PGD were obtained from the padded and filtered acceleration time series). The results suggest a bias in the NGA values relative to the correct values. We show these results only to indicate other possible problems with PGD in the NGA flatfile. We have not done a systematic study of all pass-through data, nor have we investigated the differences in PSA and PGV. Both PSA and PGV were determined from the pad-stripped data, and therefore they may also be different than the values from the data providing agencies; we suspect, however, that the problem will be most severe for PGD.

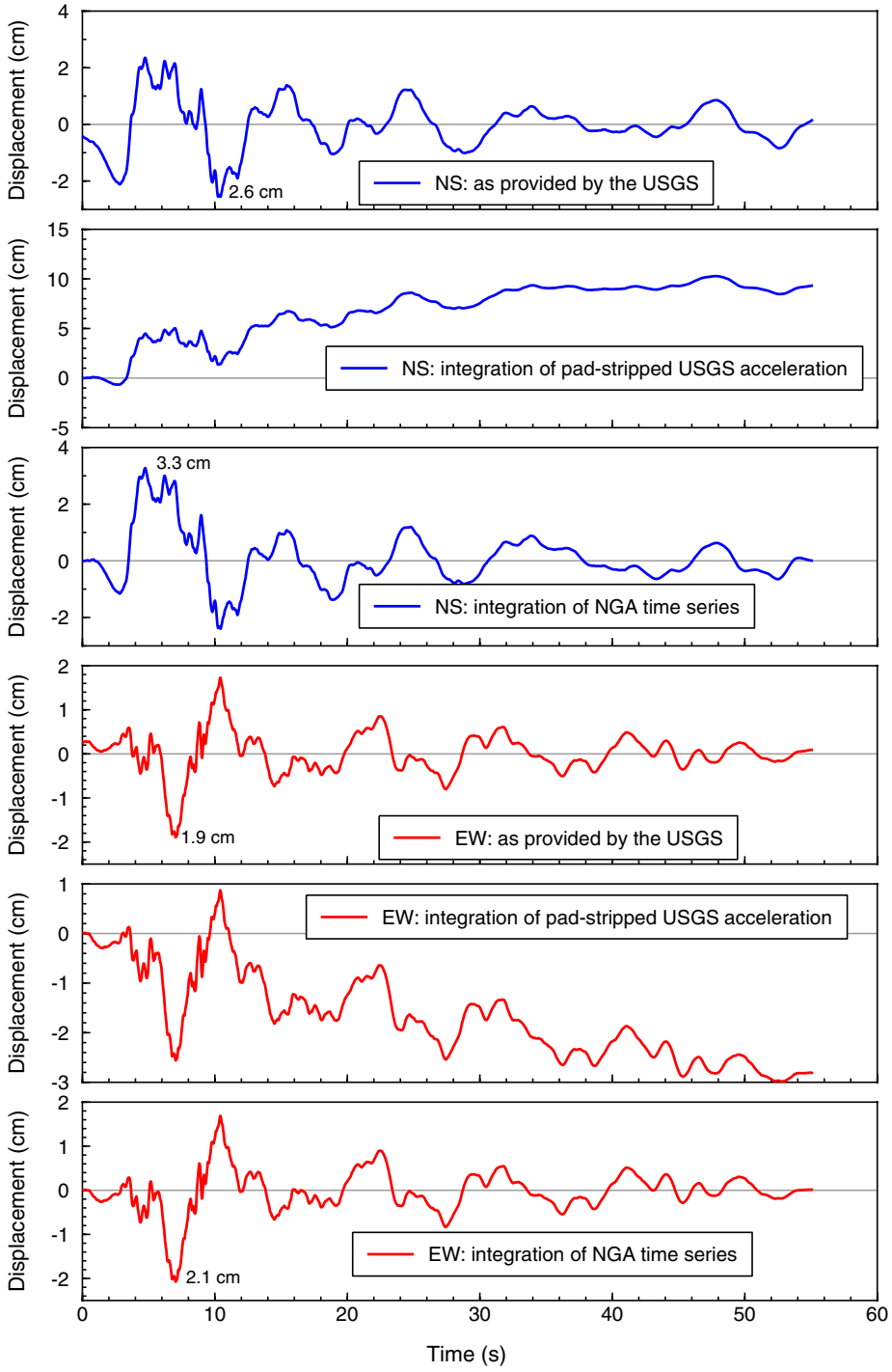

Fig. C.8 Displacements for two components of Monte Nido recording of 1994 Northridge earthquake, processed in various ways. Values of PGD labeled for second and third time series in each set.

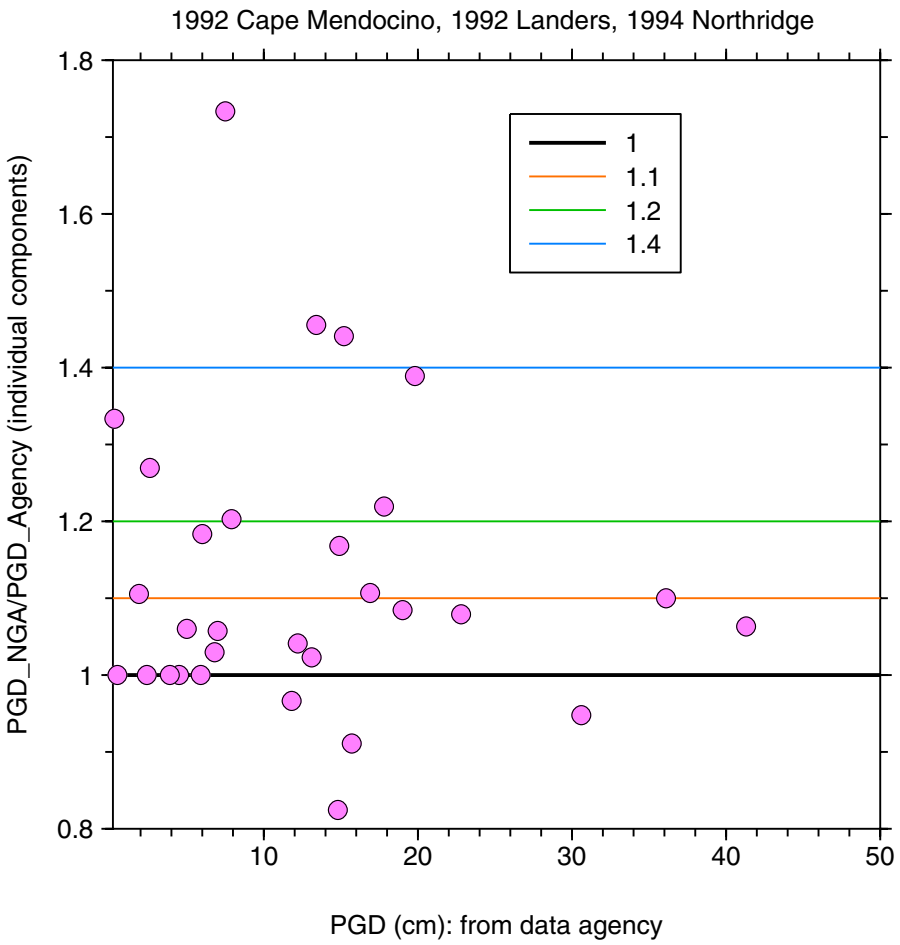

Fig. C.9 Ratio of PGD from NGA flatfile to that from agency providing data, showing bias in NGA flatfile values of PGD.

Appendix D: Classifying Fault Type Using P- and T-Axes

Rather than including a continuously varying quantity such as rake angle as the fault-type predictor variable, most, if not all, previous GMPEs group earthquakes into a few fault types (this is analogous to the use of "soil" and "rock" rather than V_{S30} as the predictor variables for site amplification). These fault types are most commonly given the names "strike-slip," "reverse," and "normal," sometimes with "oblique" appended to these names. The classification of a particular earthquake into one of these groups is usually defined in terms of rake angle, although the mapping of rake angle into a fault type can vary amongst authors (Bommer et al. 2003). For earthquakes in which one of the two possible fault planes is shallowly dipping, however, the classification into a fault type based on rake angle will be different for the two planes. A way of removing this ambiguity is to classify earthquake fault type using the plunges of the P-, T-, and B-axes. Several mappings of the plunge angles into fault types have been proposed (e.g., Frohlich and Apperson 1992 and Zoback 1992). In deciding which scheme to use, we classified the earthquakes in an early version of the NGA flatfile using Zoback (1992). Her scheme is given in the following table:

Table D.1 Definitions of fault type based on plunges of P-, T, and B-axes (after Table 3 in Zoback 1992). (*pl* in table is plunge angle, from horizontal.)

P-axis plunge	B-axis plunge	T-axis plunge	Fault Type
$pl \geq 52°$		$pl \leq 35°$	Normal
$40° \leq pl < 52°$		$pl \leq 20°$	Normal Oblique
$pl < 40°$	$pl \geq 45°$	$pl \leq 20°$	Strike-slip
$pl \leq 20°$	$pl \geq 45°$	$pl < 40°$	Strike-slip
$pl \leq 20°$		$40° \leq pl < 52°$	Reverse Oblique
$pl \leq 35°$		$pl \geq 52°$	Reverse

The classifications of the NGA data using Zoback's definitions are shown in Figure D.1. Note that only three events were not classified using the scheme, and two of these would have been classified with slight changes in the plunges. In addition, for the NGA dataset the criteria involving the plunge of the B axis is redundant (the plunge of the P- and T-axes suffices). By looking at the above figure we recommend the following simplification to Zoback's classification scheme:

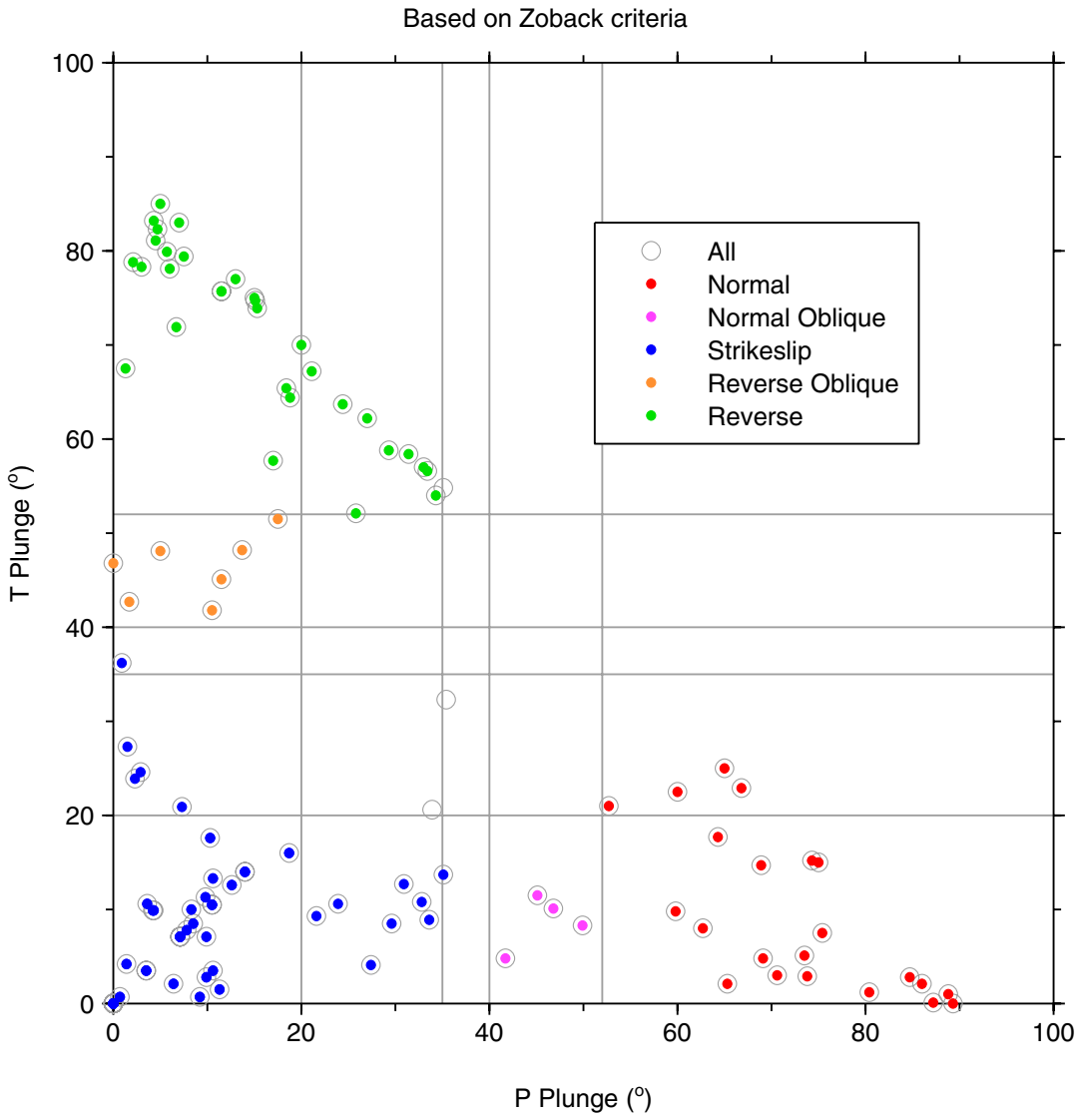

Fig. D.1 Classification using Zoback (1992).

We showed earlier (Fig. 2.6) that this simplified classification scheme agrees with that used by Boore et al. (1997); only a few singly recorded earthquakes were not classified when using Table D.2.

Table D.2 The BA07 fault-type definitions (pl is plunge angle, from horizontal).

P-axis plunge	T-axis plunge	Fault Type
$pl > 40°$	$pl \leq 40°$	Normal
$pl \leq 40°$	$pl > 40°$	Reverse
$pl \leq 40°$	$pl \leq 40°$	Strike-slip
$pl > 40°$	$pl > 40°$	undefined

To see how the classification based on the P- and T-axes compares to various classifications based on rake angles, we attach a series of figures using both the NGA flatfile definition of fault type in terms of rake angle and a definition based on 45-degree wedges of rake angle. As seen in Figures D.2–D.11, there is considerable overlap in the ways of classifying the fault types. We have not attempted to look into those events that have different classifications using the various schemes.

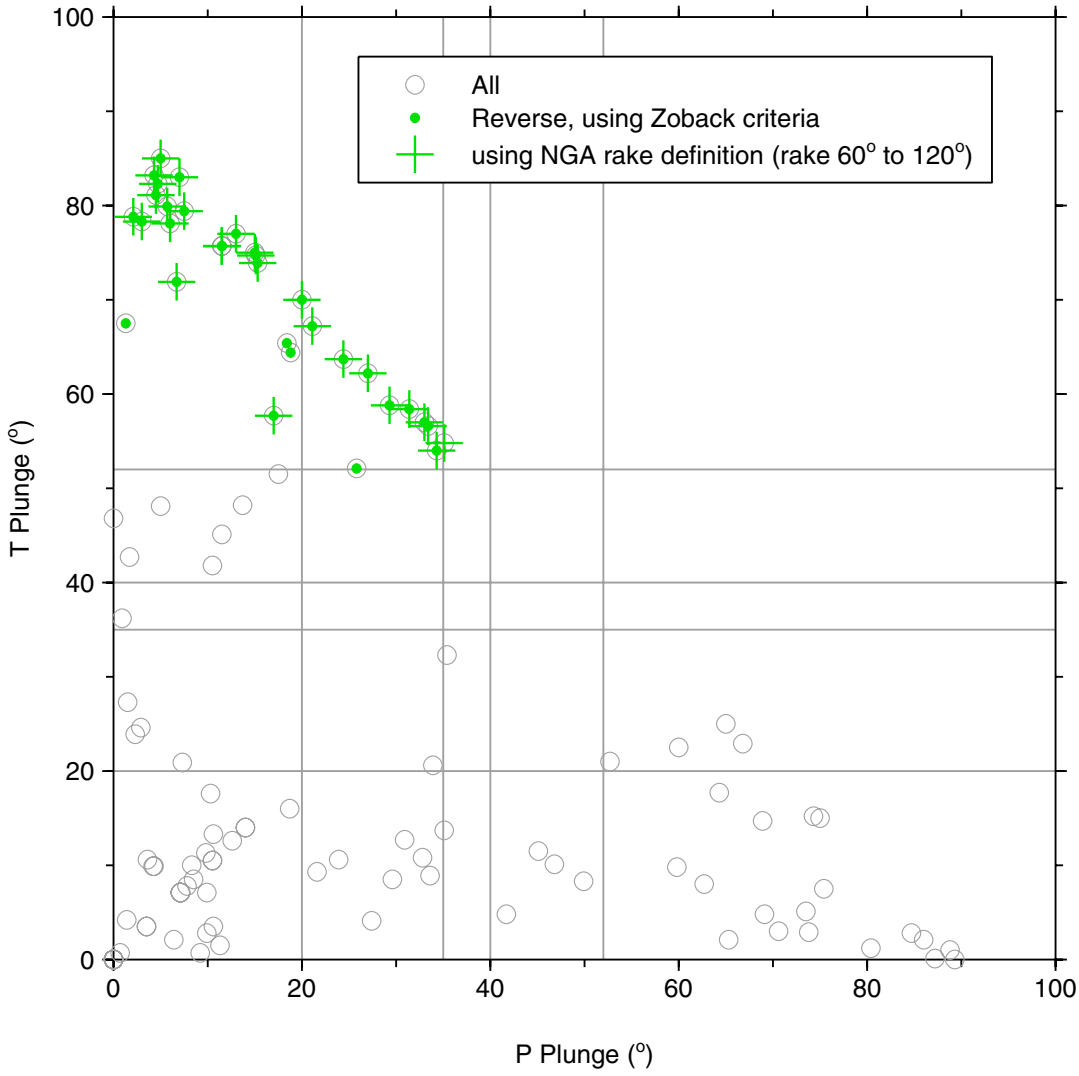

Fig. D.2 Classifications based on Zoback (1992) and rake angles (using NGA definition, shown in legend): reverse-slip earthquakes.

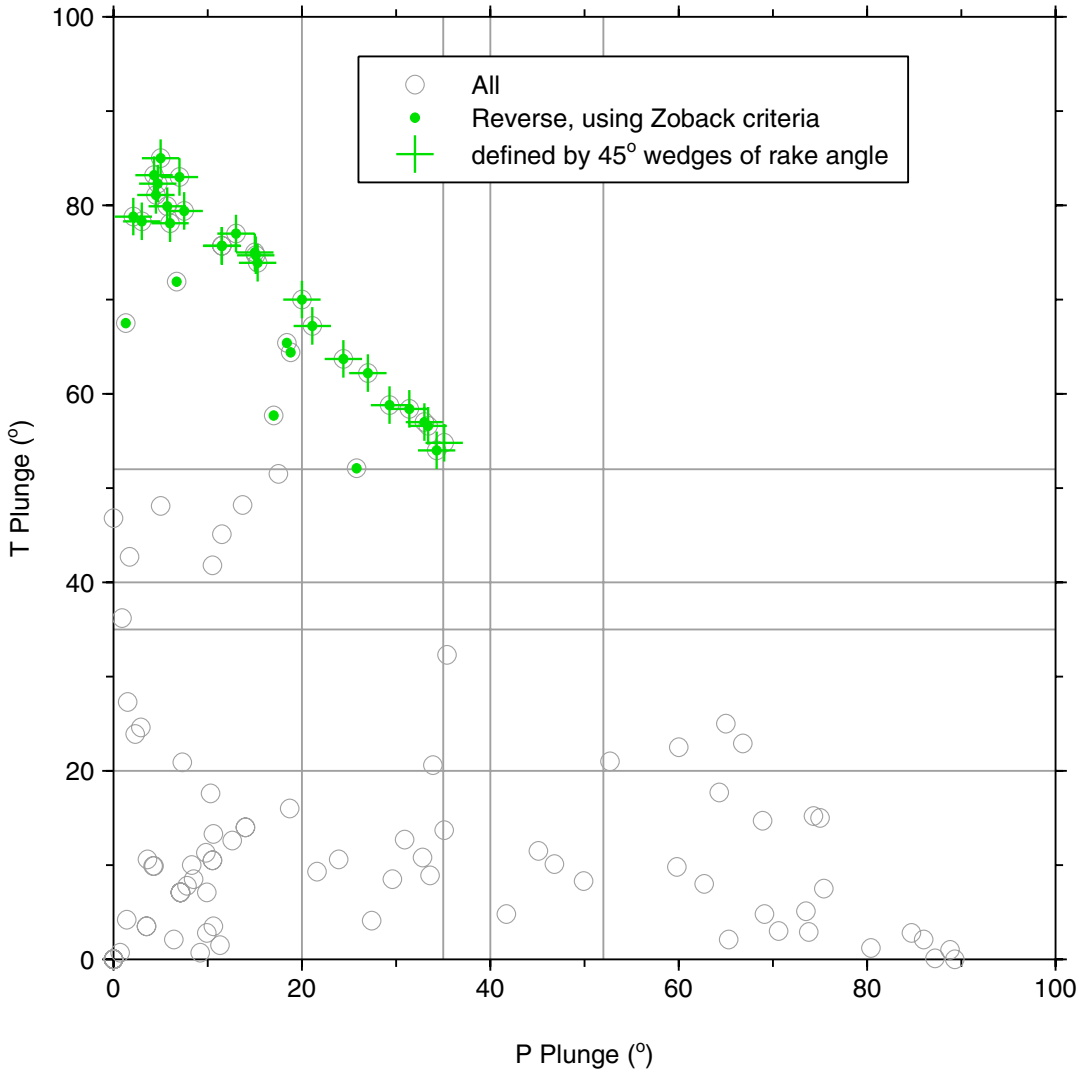

Fig. D.3 Classifications based on Zoback (1992) and using 45-degree wedges of rake angle: reverse-slip earthquakes.

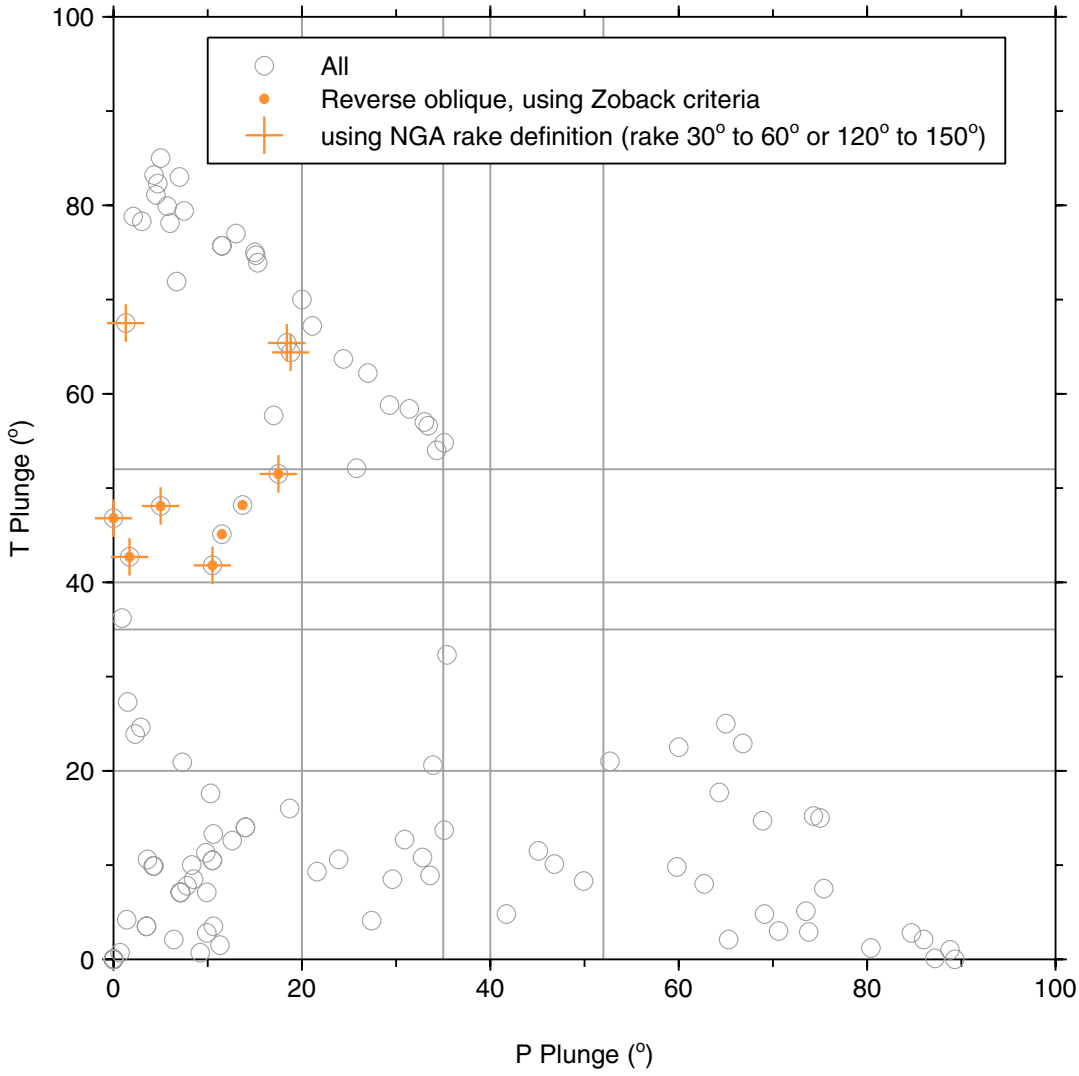

Fig. D.4 Classifications based on Zoback (1992) and rake angles (using NGA definition, shown in the legend): reverse-oblique-slip earthquakes.

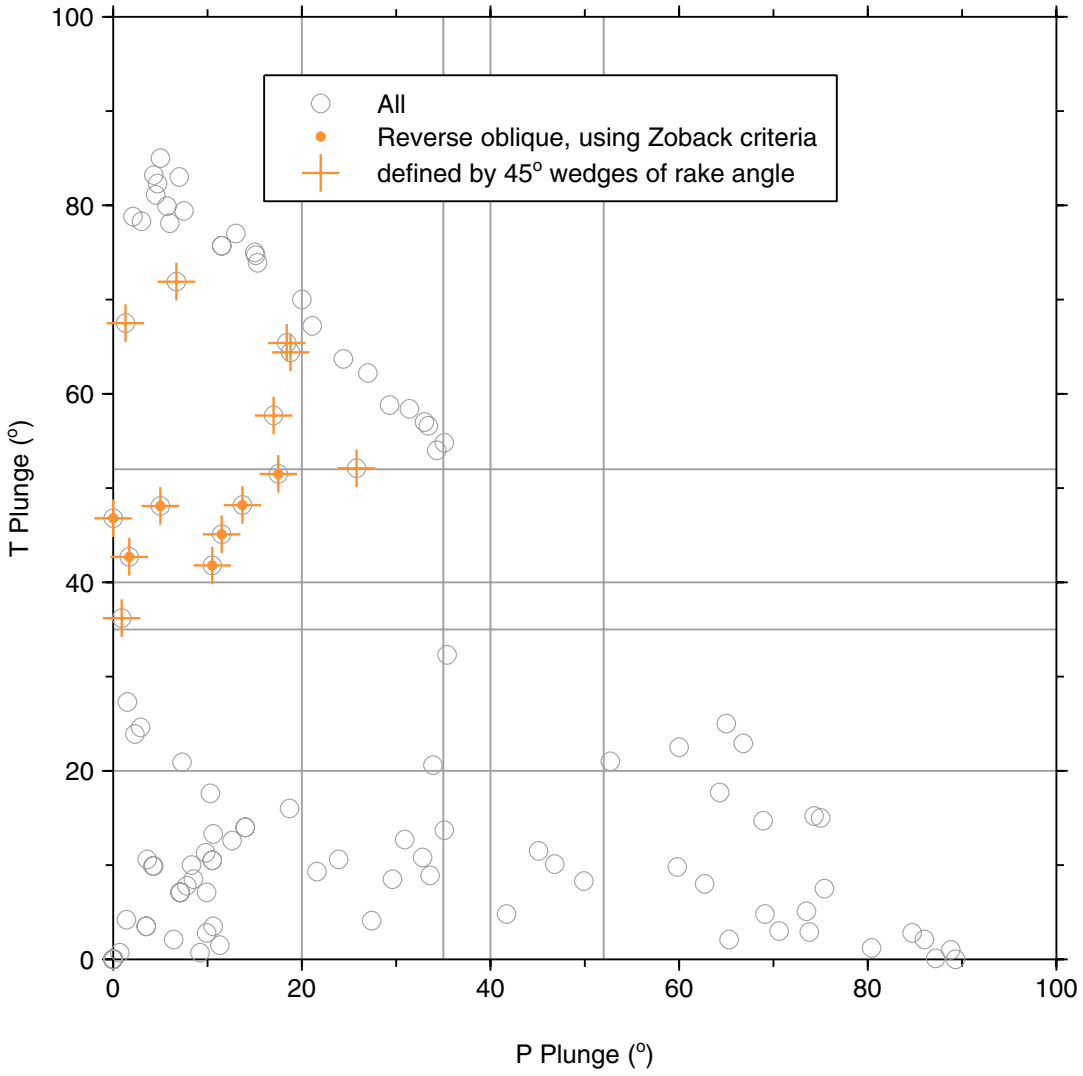

Fig. D.5 Classifications based on Zoback (1992) and using 45-degree wedges of rake angle: reverse-oblique-slip earthquakes.

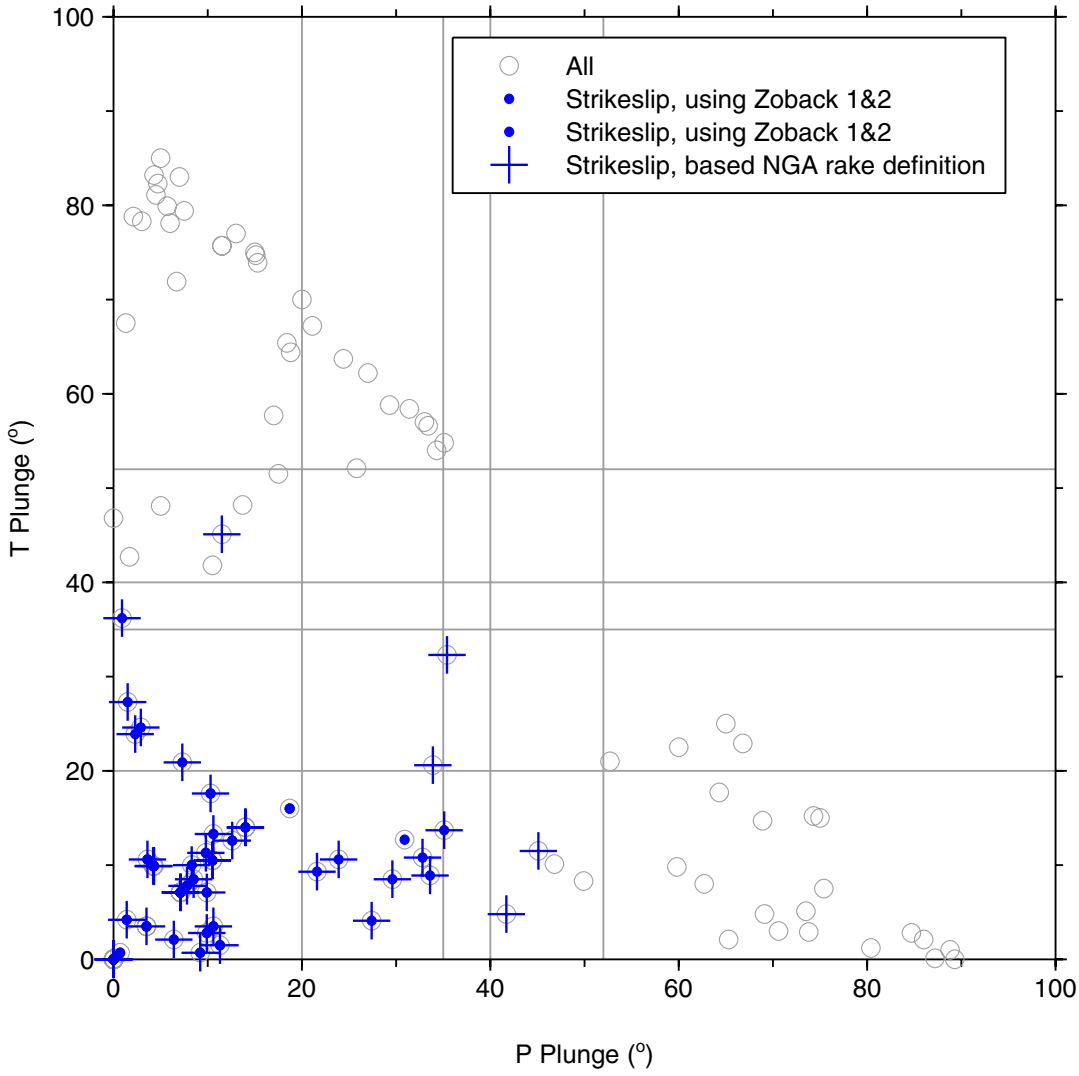

Fig. D.6 Classifications based on Zoback (1992) and rake angles (using NGA definition, shown in legend): strike-slip earthquakes.

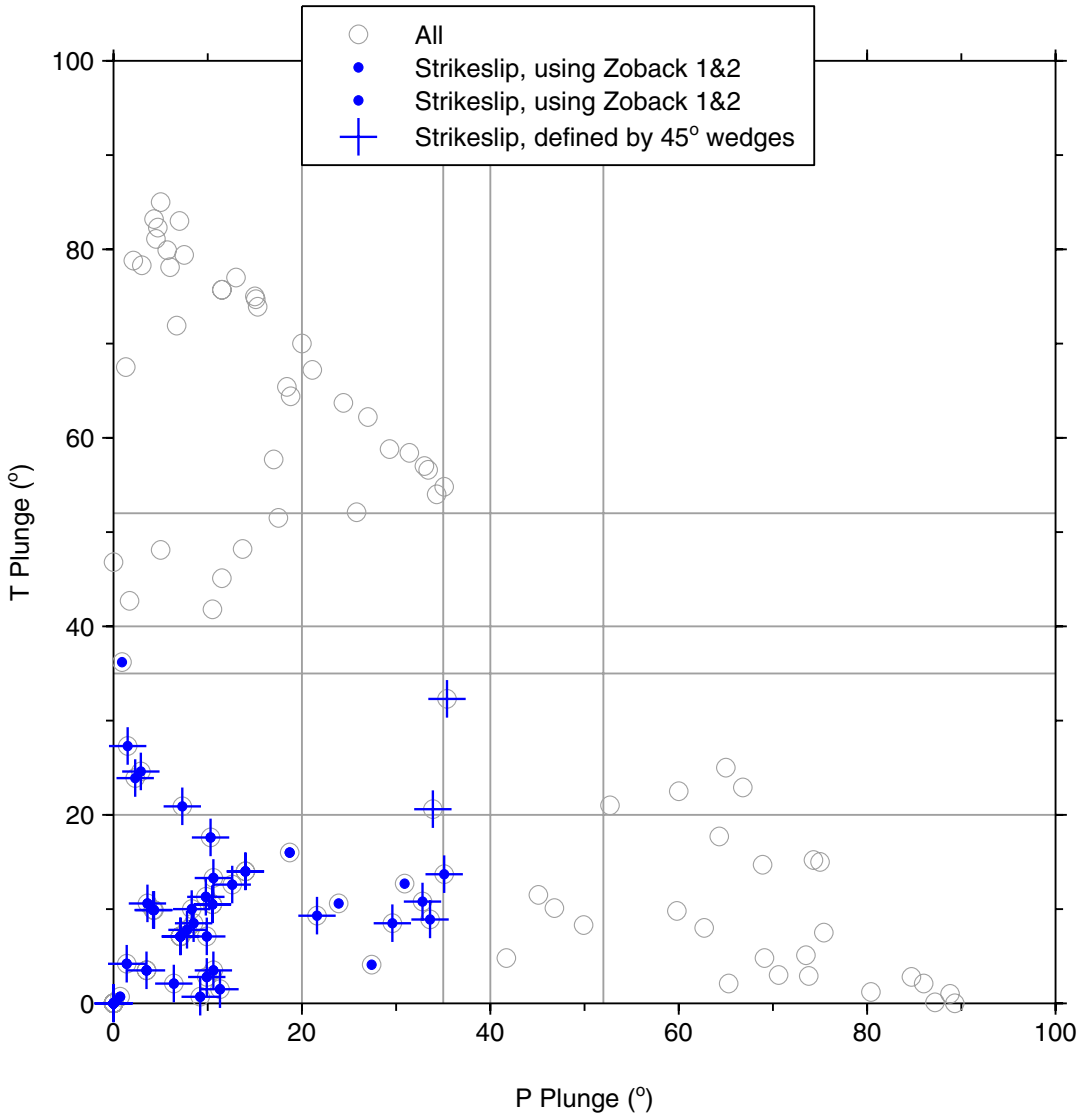

Fig. D.7 Classifications based on Zoback (1992) and using 45-degree wedges of rake angle: strike-slip earthquakes.

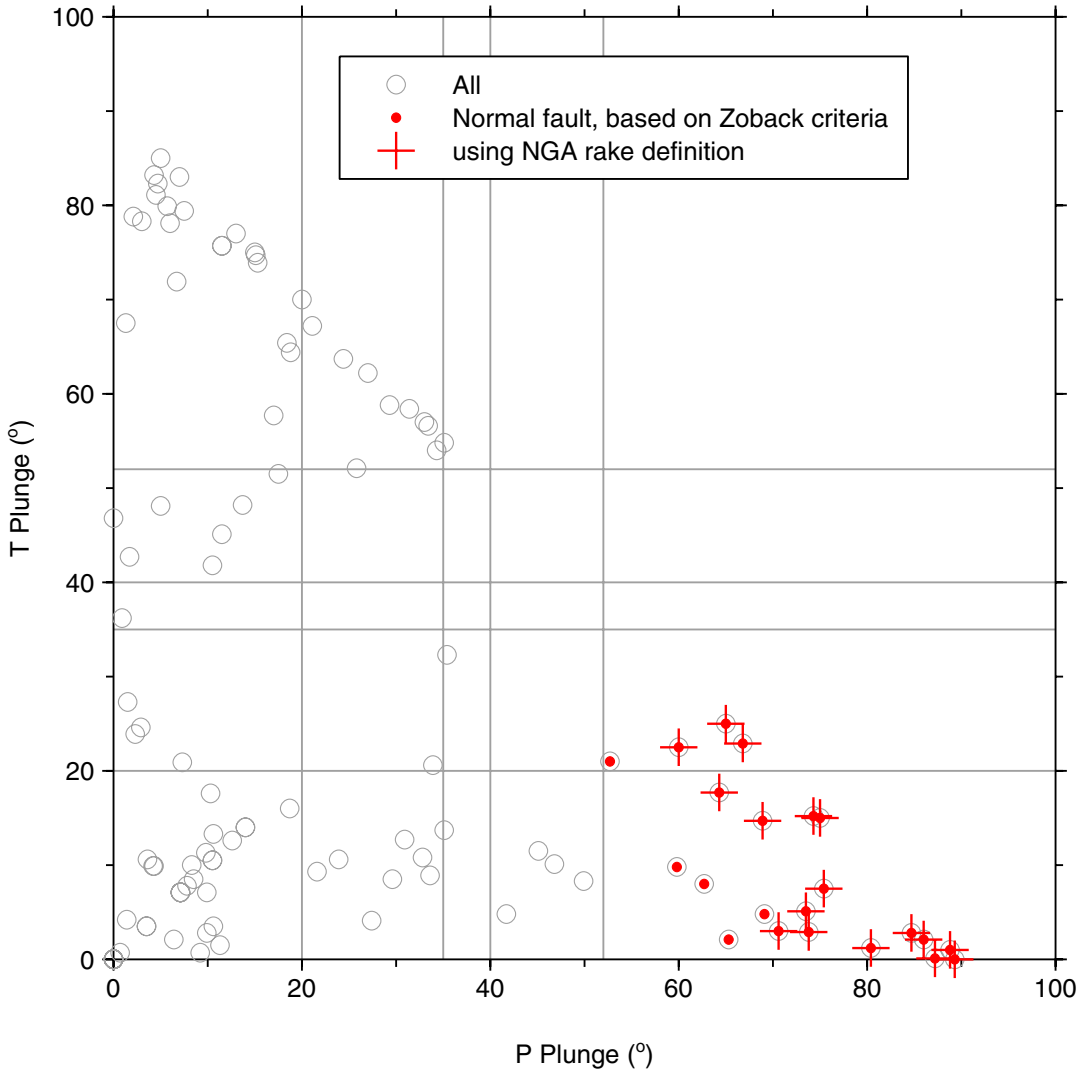

Fig. D.8 Classifications based on Zoback (1992) and rake angles (using NGA definition, shown in legend): normal-oblique-slip earthquakes.

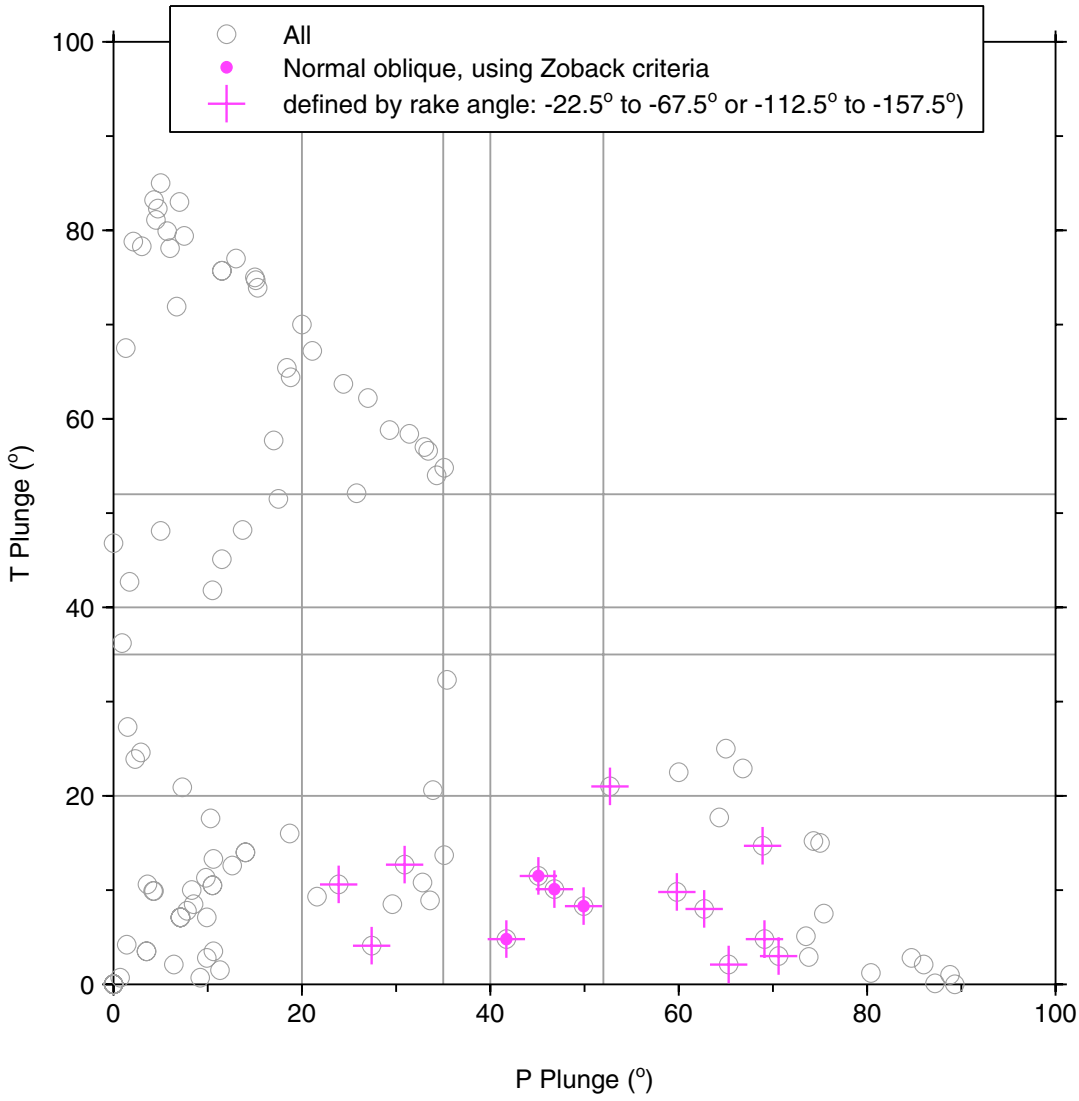

Fig. D.9 Classifications based on Zoback (1992) and using 45-degree wedges of rake angle: normal-oblique-slip earthquakes.

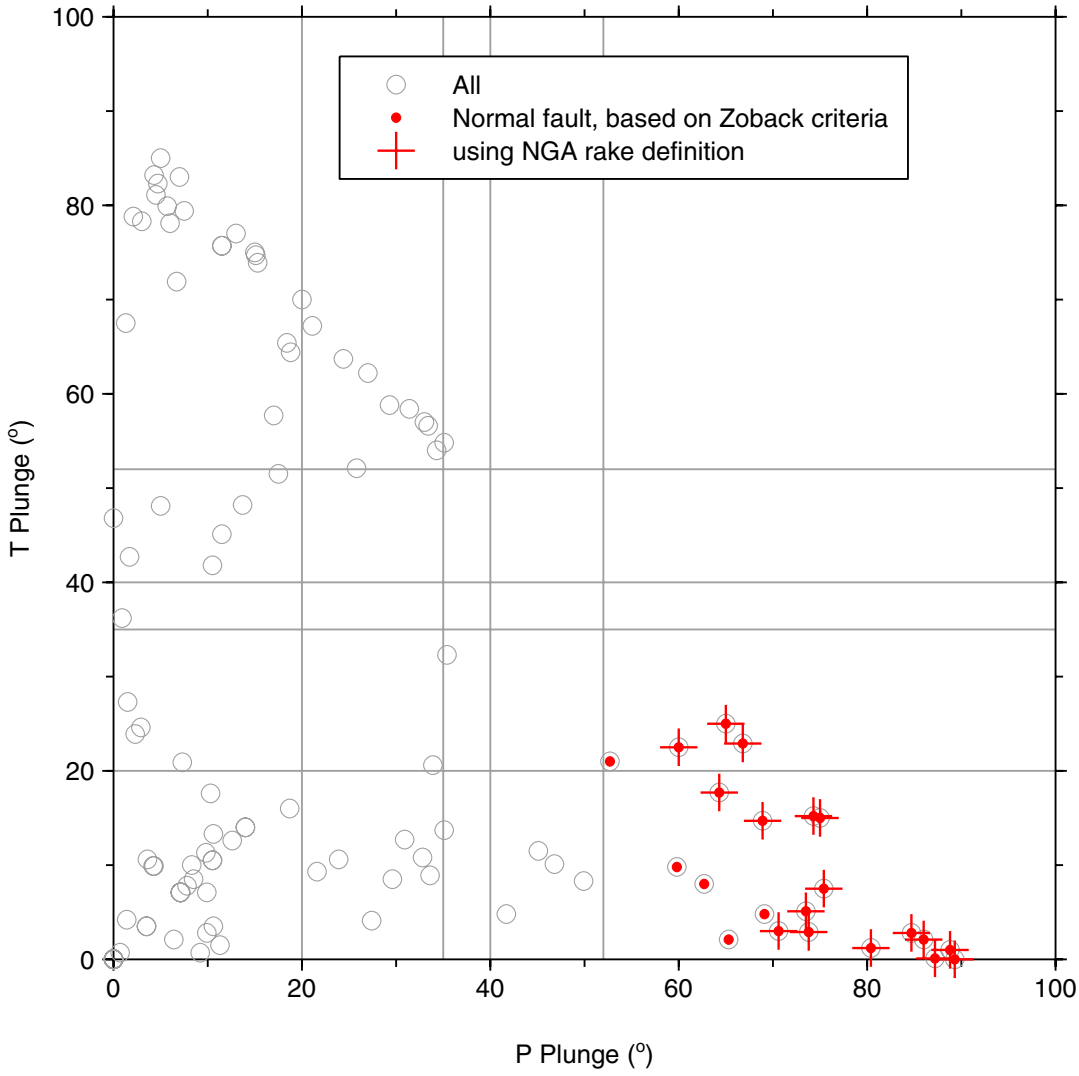

Fig. D.10 Classifications based on Zoback (1992) and rake angles (using NGA definition, shown in legend): normal-slip earthquakes.

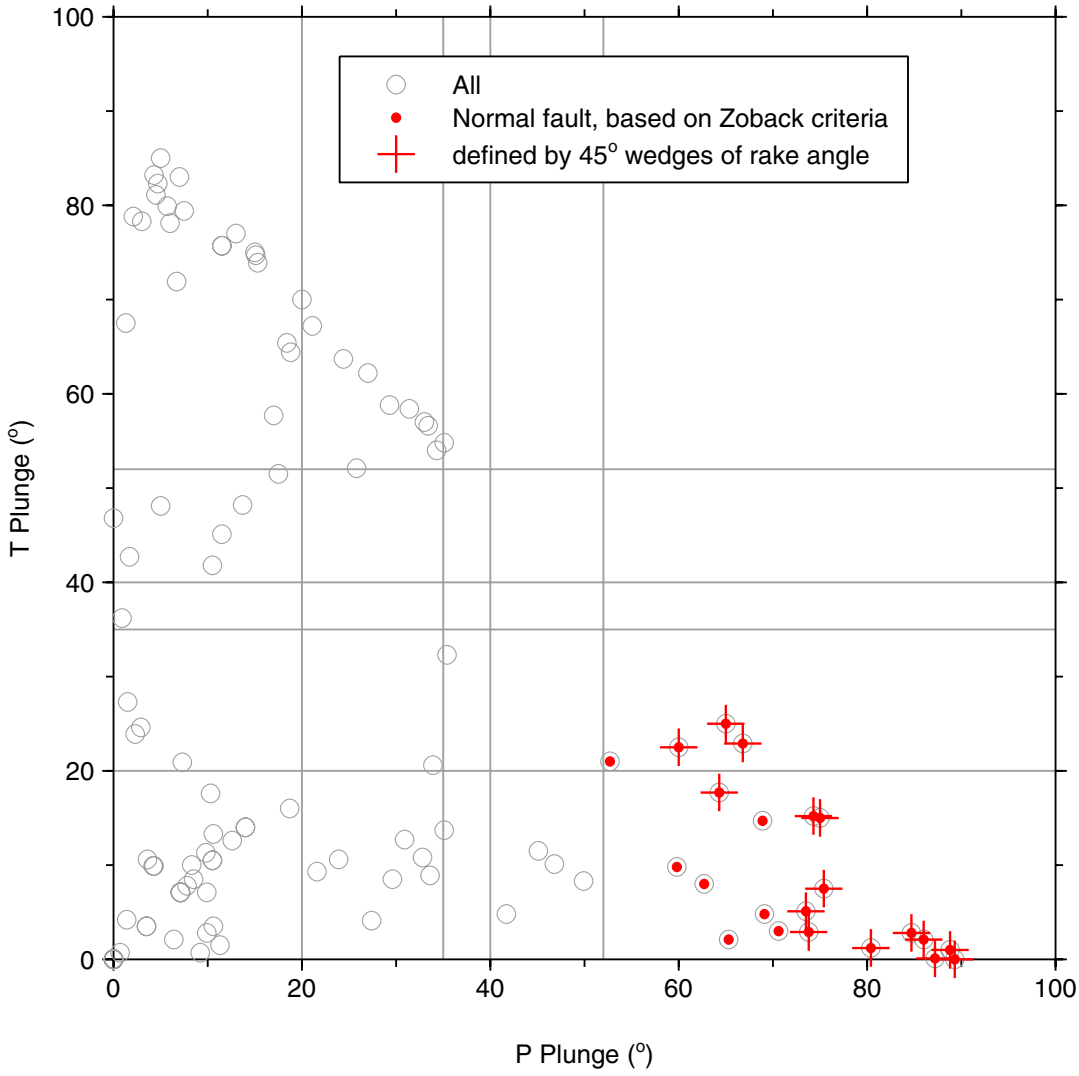

Fig. D.11 Classifications based on Zoback (1992) and using 45-degree wedges of rake angle: normal-slip earthquakes.

Appendix E: Choice of V30 for NEHRP Class

The need sometimes arises to evaluate GMPEs for a particular NEHRP site class. Because the PEER NGA GMPEs use the continuous variable V_{S30} as the predictor variable for site amplification, the question naturally arises as to what value of V_{S30} to use for a specific NEHRP class. To explore that question, I used the distribution of V_{S30} values from the borehole compilation given in Boore (2003) and from the NGA flatfile, and computed the geometric means of the average of the V_{S30} values in each NEHRP class.

I used the geometric mean of V_{S30} in each NEHRP class, as these will give the same value of $\ln Y$ as the average of the $\ln Y$'s obtained using the actual V_{S30} values in the dataset. Here is the analysis:

Because

$$\ln Y \approx b \ln V_{30}$$

the average of $\ln Y$ for a number of V_{S30}'s in a site class is:

$$\overline{\ln Y} \approx b \frac{1}{N} \sum_{i=1}^{N} \ln(V_{30})_i$$

and the same value of $\ln Y$ is obtained using the value of V_{S30} given by:

$$\ln \overline{V_{30}} = \frac{1}{N} \sum_{i=1}^{N} \ln(V_{30})_i$$

But does that mean that the values of V_{S30} in the NGA database should be used to determine the average value of V_{S30} that will be substituted into the GMPEs for a given NEHRP site class? Yes, under the assumption that the distribution of V_{S30} in the NGA database is similar to the one that would be obtained if a random site were selected. I discuss this in more detail at the end of this appendix.

To determine the geometric means of V_{S30} from the NGA flatfile, I used the Excel function *vlookup* to select only one entry per station. Figure E.1 shows the histograms. For the Boore (2003) dataset, I used values of V_{S30} for which the borehole velocities had to be extrapolated less than 2.5 m to reach 30 m. The top graph shows histograms for the Boore (2003) velocities; the middle graph shows histograms for NGA velocities for which the values of V_{S30} are based on measurements (source = 0 and 5); and the bottom graph is for NGA values from measurements and estimations (source = 0, 1, 2, and 5). In choosing the most representative value of V_{S30} for each NEHRP class, I gave most weight to the middle graph in Figure E.1. Those histograms used more data than in Boore (2003), but they are not subject to the possible bias in using an estimated value of V_{S30}, in which the value might be based on the assignment of a NEHRP class to a site, with someone else's correlation between NEHRP class and V_{S30} (correlations that may or may not have used the geometric mean of V_{S30}). I am trying to find the appropriate value independently.

The gray vertical lines in Figure E.1 are the geometric means in each NEHRP class for the data used for each graph; the black vertical lines in Figure E.1 are the V_{S30} values I recommend be used for each NEHRP class; they are controlled largely by the analysis of the source = 0 and 5 NGA data. Table E.1 contains the values of V_{S30} determined for the different histograms. Based on these values, the second-to-last column in the table contains the observation-based representative values that could substituted into the NGA GMPEs for specific NEHRP classes. The last column contains another possible set of values for evaluating the GMPEs for a specific NEHRP class; these values are the geometric means of the velocities defining each NEHRP class, rounded to the nearest 5 m/s (e.g., for NEHRP class D the value from the class definition is $\sqrt{180 \times 360} = 255$ m/s).

As mentioned before, the values in the second-to-last column of Table E.1 are valid representations of the different NEHRP classes if the distribution of velocities in the geographic region of interest is the same as that for the data used in the analysis above. Most of the measured values in the NGA database, however, come from the Los Angeles and San Francisco areas of California, so there is the potential for a bias if the V_{S30} values for those regions are not representative of a generic site. An alternative set of representative V_{S30} values for each NEHRP site class is given by the geometric mean of the velocities defining the site-class boundaries. These are given in the last column of Table E.1. The values in the last two columns of Table E.1 are similar, but to assess the impact of the two sets of representative values, I evaluated the ratios of ground motions for the two values for each NEHRP class, for a wide range of periods and distances. The differences in ground motions using the two possible sets of V_{S30} values are less than 8%, 5%, and 3% for NEHRP classes B, C, and D, respectively. The differences are largest at long periods for classes B and C and for short periods for class D. The differences in ground motions for each site class obtained using the alternative sets of representative V_{S30} values are so small that either set of could be used. The choice of one set or the other as the standard should be a group decision; I have provided information that might be used by such a group in making a choice.

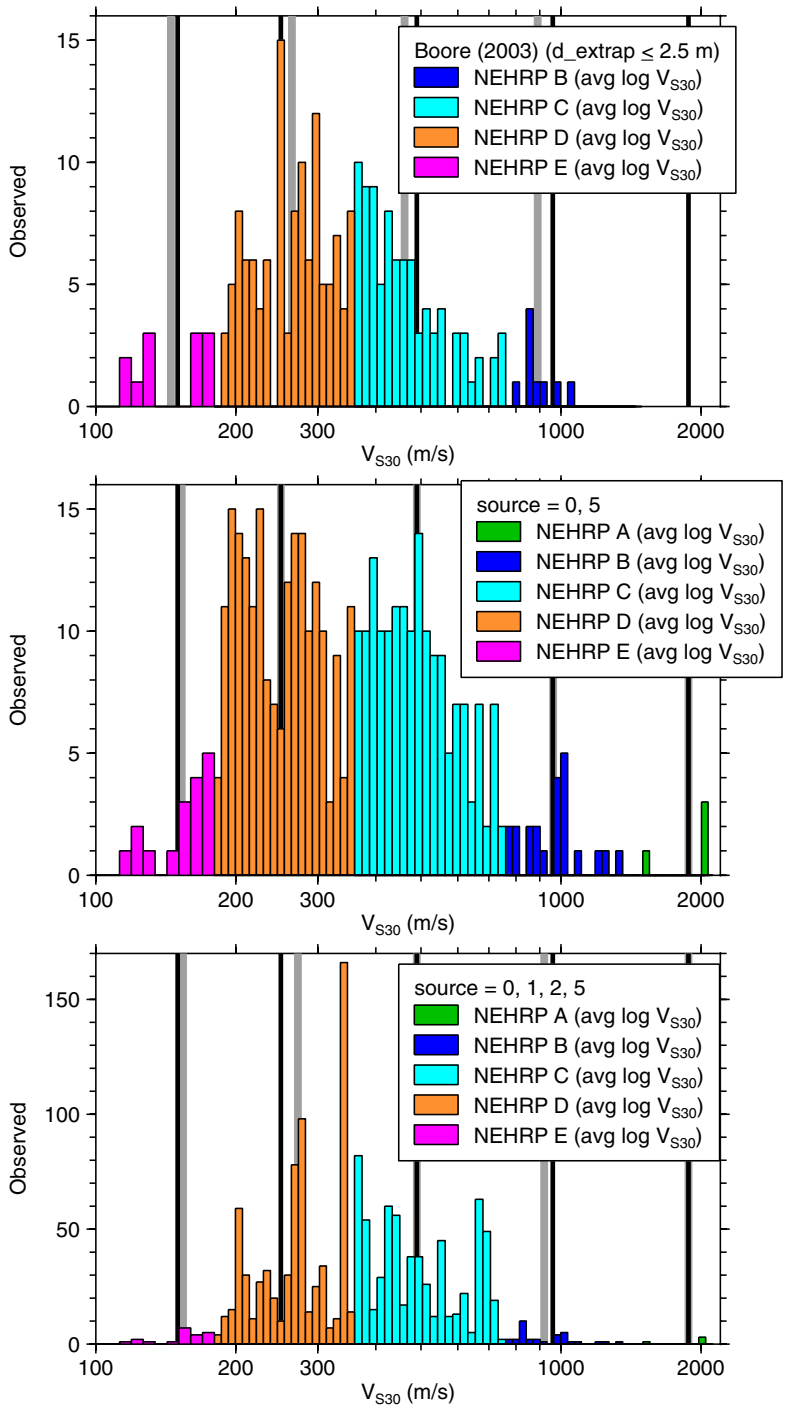

Fig. E.1 Histograms of V_{S30} used to determine value of V_{S30} to use in evaluating NGA GMPEs for particular NEHRP class (see text for details).

Table E.1 Correspondence between NEHRP class and geometric mean V_{S30} (see text).

NEHRP	nga,src0,5	nga,src0,1,2,5	Boore (2003)	Based on measured velocities	From class definitions
A	1880.5	1880.5		1880	
B	962.3	919.6	891.2	960	1070
C	489.8	489.9	461.4	490	525
D	249.8	271.5	263.7	250	255
E	153.3	153.7	145.0	150	

Appendix F: Questioning NGA Filter Values for Pacoima Dam Recording of 1971 San Fernando Earthquake

There is a large difference in the GMRotI values at long periods in the v 7.2 Excel file and those of the more recent *727brian.xls* file for the Pacoima Dam recording of the 1971 San Fernando earthquake. The reason for this is that one of the filter corners was 0.5 Hz for the 254-degree component, which trumps the filter corner of 0.1 Hz used for the 164-degree component. This results in a lowest useable frequency of 0.625 Hz. In my processing of the Pacoima data I was satisfied with a filter corner near 0.1 Hz, so I wanted to look into the reason for the large difference in filter corners for the two components. I show in Figure F.1 the displacements from the NGA processing and from my processing. For my processing I used filter corners of 0.1, 0.2, and 0.5 Hz. The first thing to note is that my results for $f_{LC} = 0.1\,\text{Hz}$ are close to those in the NGA flatfile for the 164-degree component, which confirms that my processing and the NGA processing return similar results for the same filter corner, at least in this case. But the next thing to note is that the dependence on filter corner is much more extreme for the 164-degree component than it is for the 254-degree component. What this tells me is that there is not much low-frequency content in the unfiltered 254-degree component record. So why was a value of 0.5 Hz used for the filter for that component?. I think it is easier to justify, from the appearance of the waveforms, a filter value of 0.1 Hz for the 254-degree component than for the 164-degree component! But I think that 0.1 Hz can be used as the filter corner for both components—doing this will add to the dataset at longer periods and close distances.

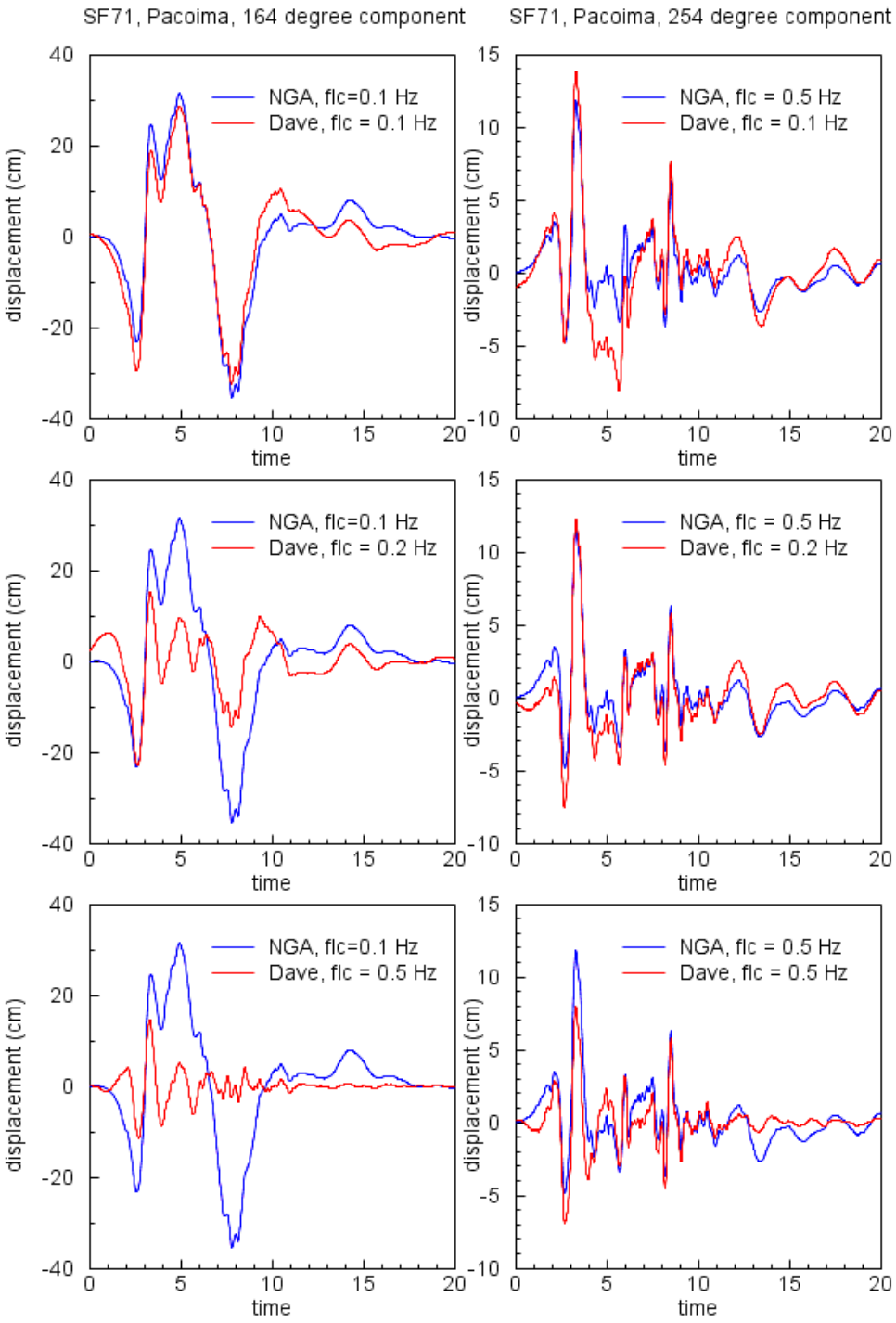

Fig. F.1 Displacements for two horizontal components at Pacoima Dam site, recorded during 1971 San Fernando earthquake, processed using different values of low-cut filter corner frequencies.

Appendix G: Notes Concerning Recordings of 1978 Tabas Earthquake

On May 7, 2004, I sent an email to all developers and a few other interested parties pointing out that the low-cut (high-pass) filter corners in the PEER NGA spreadsheet for some of the analog recordings for the 1978 Tabas, Iran, earthquake are suspiciously low (see Fig. G.1). I hypothesized that the records had had long-period noise removed via polynomial corrections, and thus the filter corners should not be used as a guide to the useable bandwidth of the response spectrum. The only reply I received was from Vladimir Graizer. As the version of the PEER NGA spreadsheet at the time that I sent the email (*Flatfile V2 (June-09-04).xls*) still contained the low-filter corners for the Tabas records, I thought I should process the data myself to get a better understanding of what is going on.

Figure G.1 contains a modified version of the plot I sent in May, 2004. In this appendix I look in detail at horizontal-component records from two stations: Tabas and Bajestan (the latter having the lowest corner of all of the Tabas recordings, although it is 120 km from the fault). I obtained the unprocessed data from the European Strong-Motion Database website. The Bajestan recording has obvious problems:. an offset at 8.3 s on the x component and spikes on the y component (Fig. G.2). Correcting for the spikes was easy—I just replaced them with the average of the two adjacent values. Dealing with the offset was more difficult. I show in Figures G.3 and G.4 the results of filtering at the PEER NGA value of 0.02 Hz, as well as at 0.1 and 0.2 Hz. Figure G.2 contains the results of filtering with no corrections for the offset on the x component. But it is clear that without removing the offset, the waveforms and peak motions are not believable for the 0.02 Hz filter. The waveforms and peaks motions are more reasonable for the higher-frequency filters, but the offset in acceleration leads to erroneous motions in the velocity and displacements with amplitudes that are close to the peak motions. I tried removing the offsets by fitting simultaneously two quadratics to the motions on each side of the offset,

constraining the linear and quadratic terms to be the same for both functions. The difference in constant terms was used as a correction. The results were not that much better. After some trial and error, I finally subtracted from the acceleration second- and fourth-order polynomials fit to the motions before and after the offset. Filtering these baseline-corrected records gave the results shown in Figure G.4. The results look better than before, but the records filtered using the 0.02 Hz filter corner are still dominated by unrealistically long-period motions. The filtered y-component record is shown in Figure G.5, after despiking. Again the motions obtained using a 0.02 Hz filter corner are not realistic. The results in Figures G.3–G.5 convince me that the filter corner given in the PEER NGA spreadsheet is not correct, at least for Bajestan (and probably not for most other records from the Tabas earthquake, the exception being the large-motion recording at Tabas).

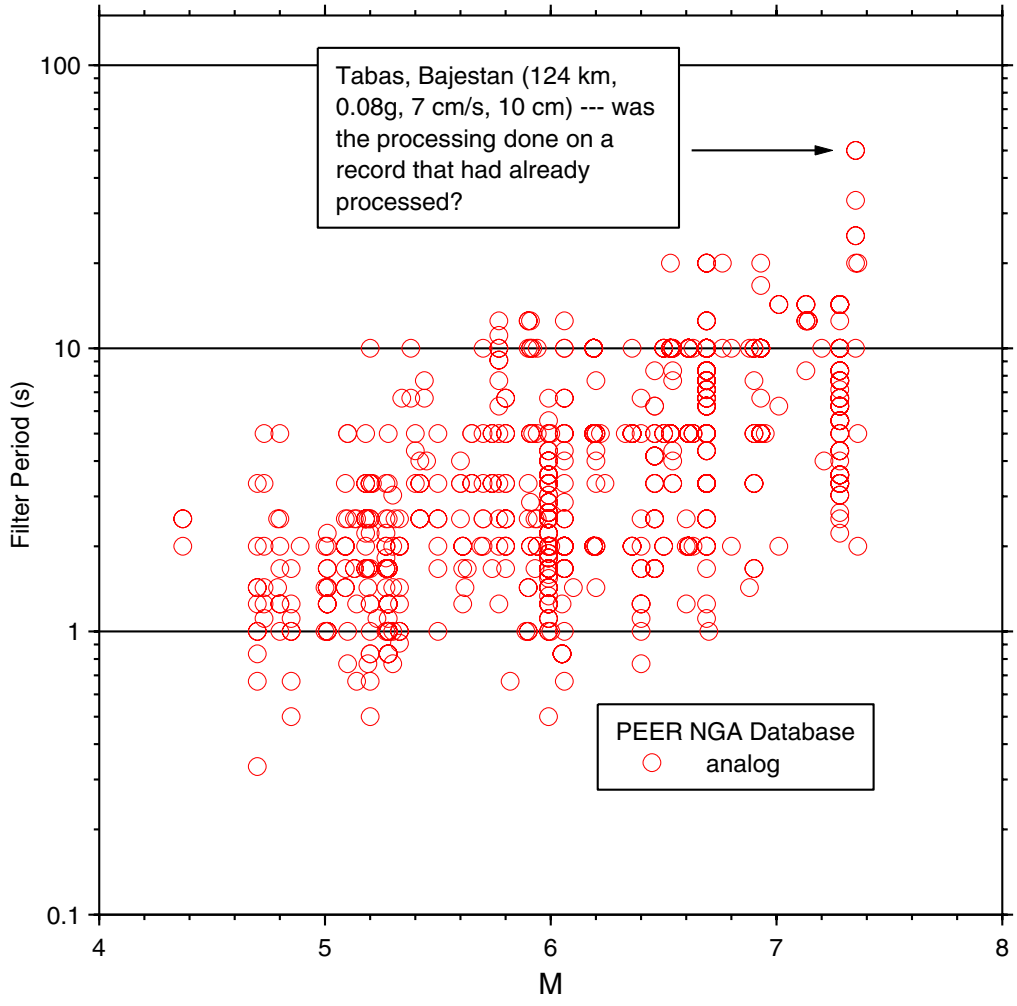

Fig. G.1 Filter period vs. M for analog records in 2004 version of NGA flatfile. Many values for Tabas earthquake seem too large.

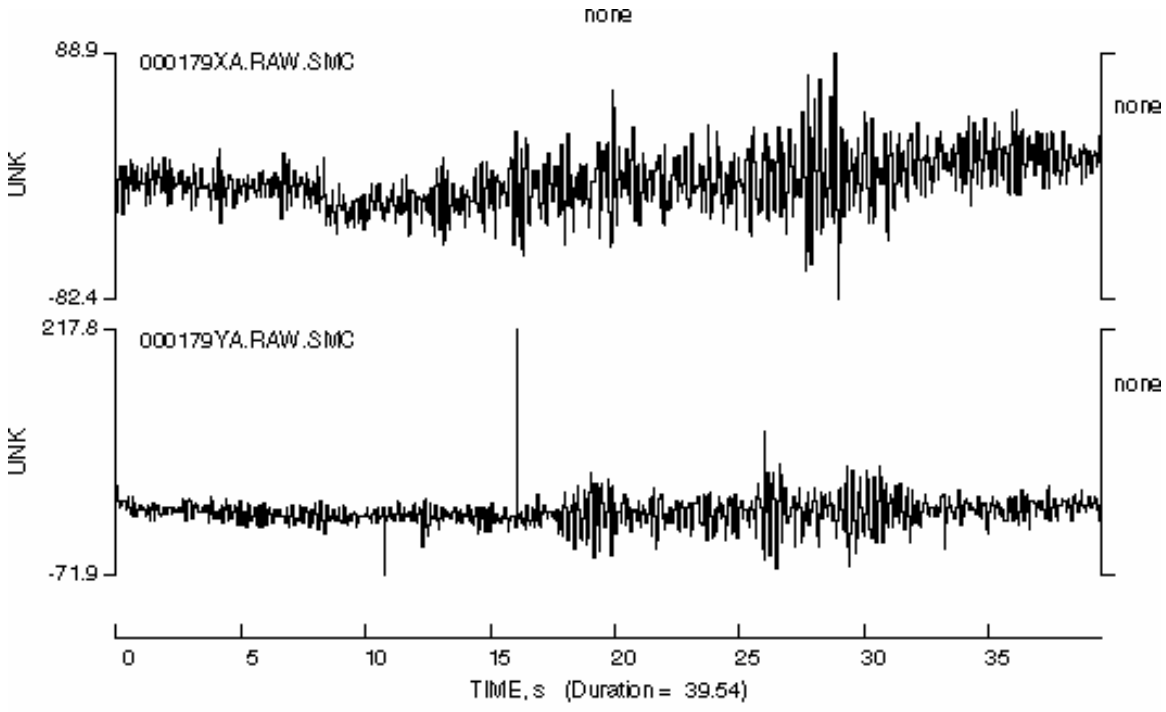

Fig. G.2 Uncorrected traces from Bajestan recording of 1978 Tabas earthquake, obtained from European Strong-Motion database website. Note step offset on x component at about 8.3 s, and large spikes on y component.

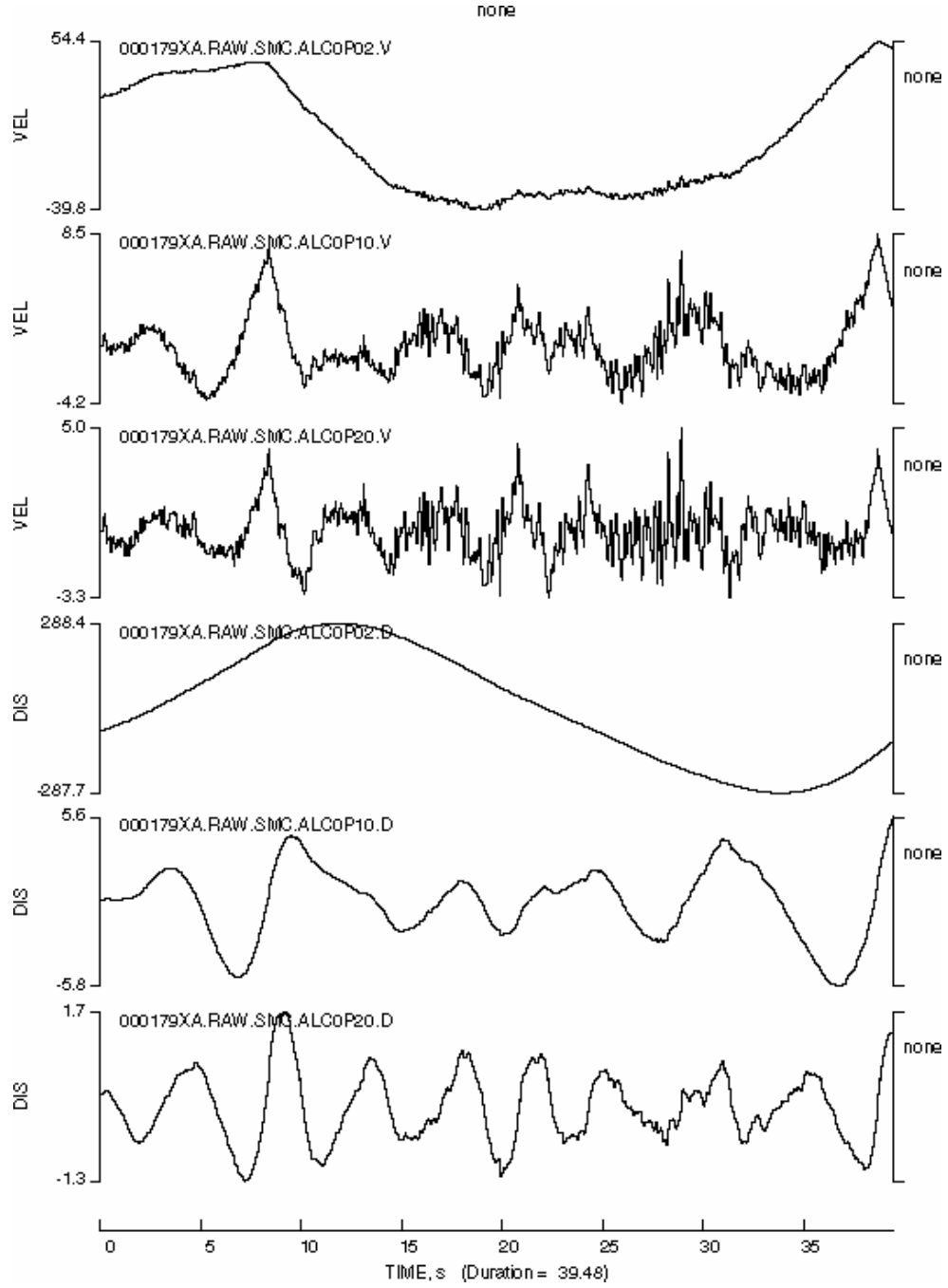

Fig. G.3 x-component velocity and displacement traces for Bajestan recording of 1978 Tabas earthquake, obtained by filtering unprocessed acceleration with acausal Butterworth filters with corner frequencies of 0.02, 0.10, and 0.20 Hz. At low-frequencies filter decays as $1/f^8$. No correction made for step offset on x component at about 8.3 s. Only original portion of processed time series shown (pre- and post-filter transients not shown).

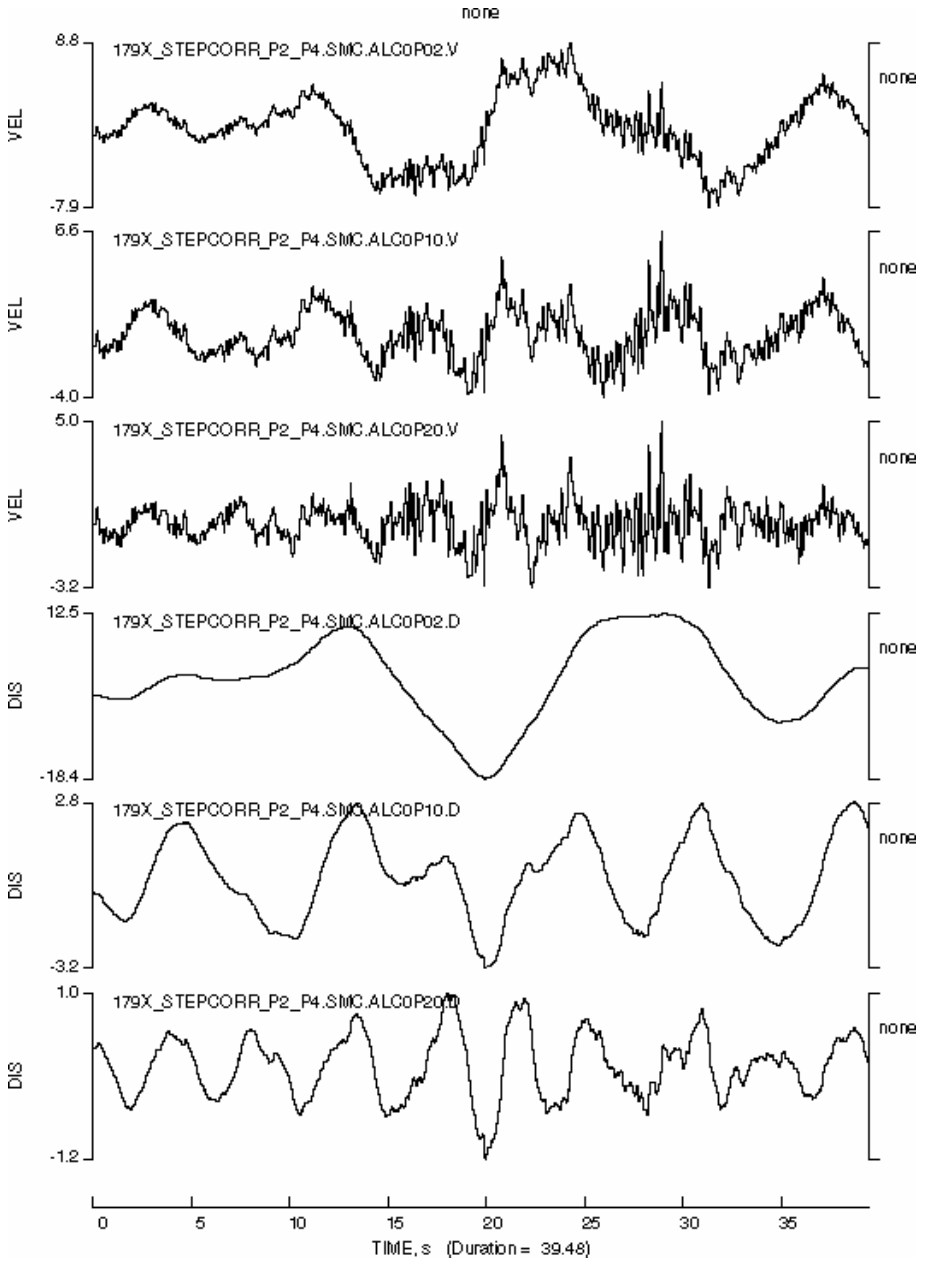

Fig. G.4 x-component velocity and displacement traces for Bajestan recording of 1978 Tabas earthquake, obtained by filtering unprocessed, step-corrected acceleration with acausal Butterworth filters with corner frequencies of 0.02, 0.10, and 0.20 Hz. At low-frequencies filter decays as $1/f^8$. Correction for step offset on x component at about 8.3 s made by subtracting from unprocessed record second- and fourth-order polynomials fit to unprocessed accelerations on each side of offset. Only original portion of processed time series shown (pre- and post-filter transients not shown).

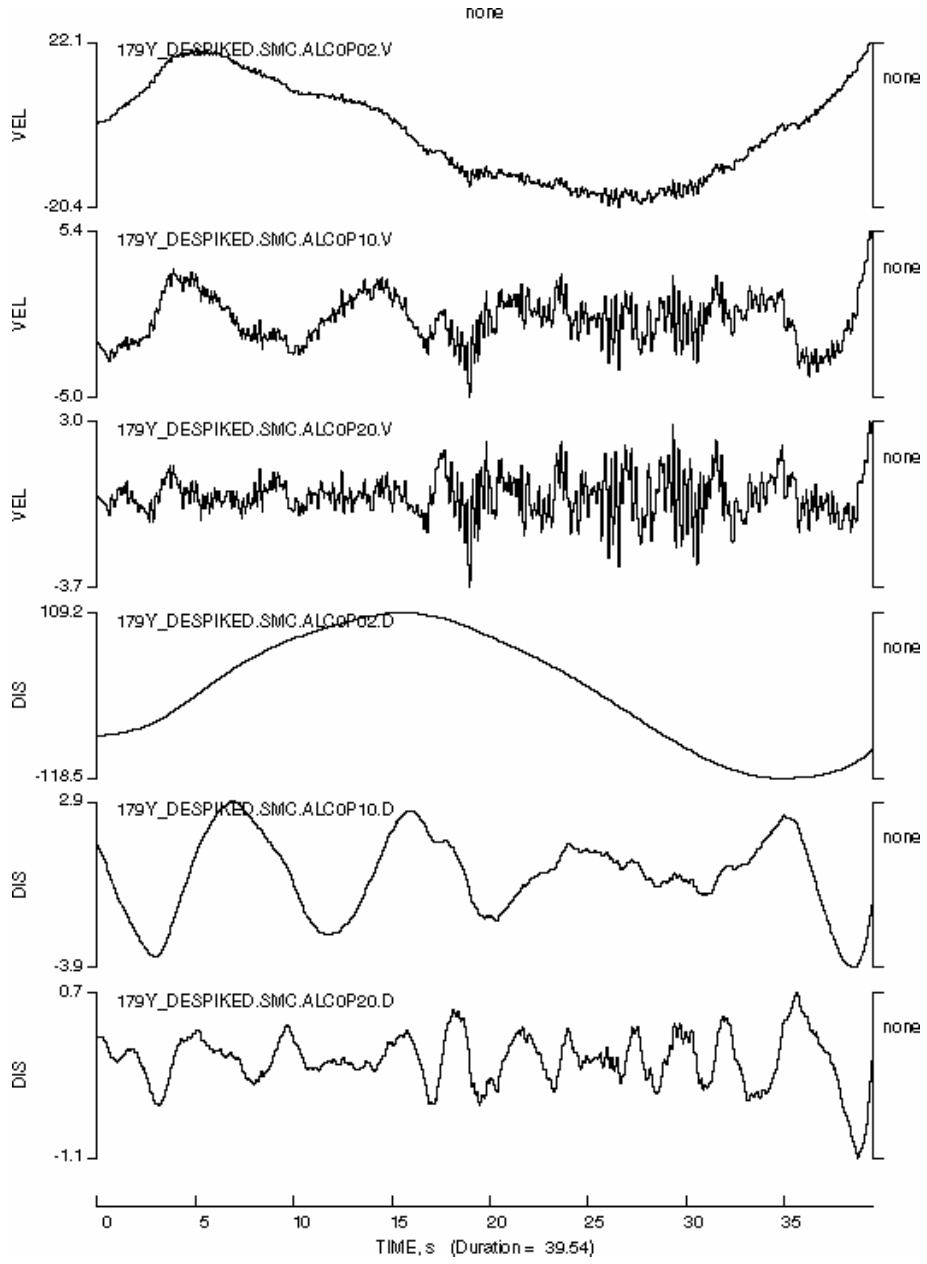

Fig. G.5 y-component velocity and displacement traces for Bajestan recording of 1978 Tabas earthquake, obtained by filtering unprocessed, step-corrected acceleration with acausal Butterworth filters with corner frequencies of 0.02, 0.10, and 0.20 Hz, after replacing spikes at 10.74, 12.26, 16.04, 25.98, and 33.2 s with averages of values on each side of spike. At low-frequencies filter decays as $1/f^8$. Only original portion of processed time series shown (pre- and post-filter transients not shown).

The processed records for the recording at Tabas are shown in Figures G.6–G.7 for the two horizontal components. The PEER NGA value of 0.05 Hz for the low-cut filter corner seems reasonable.

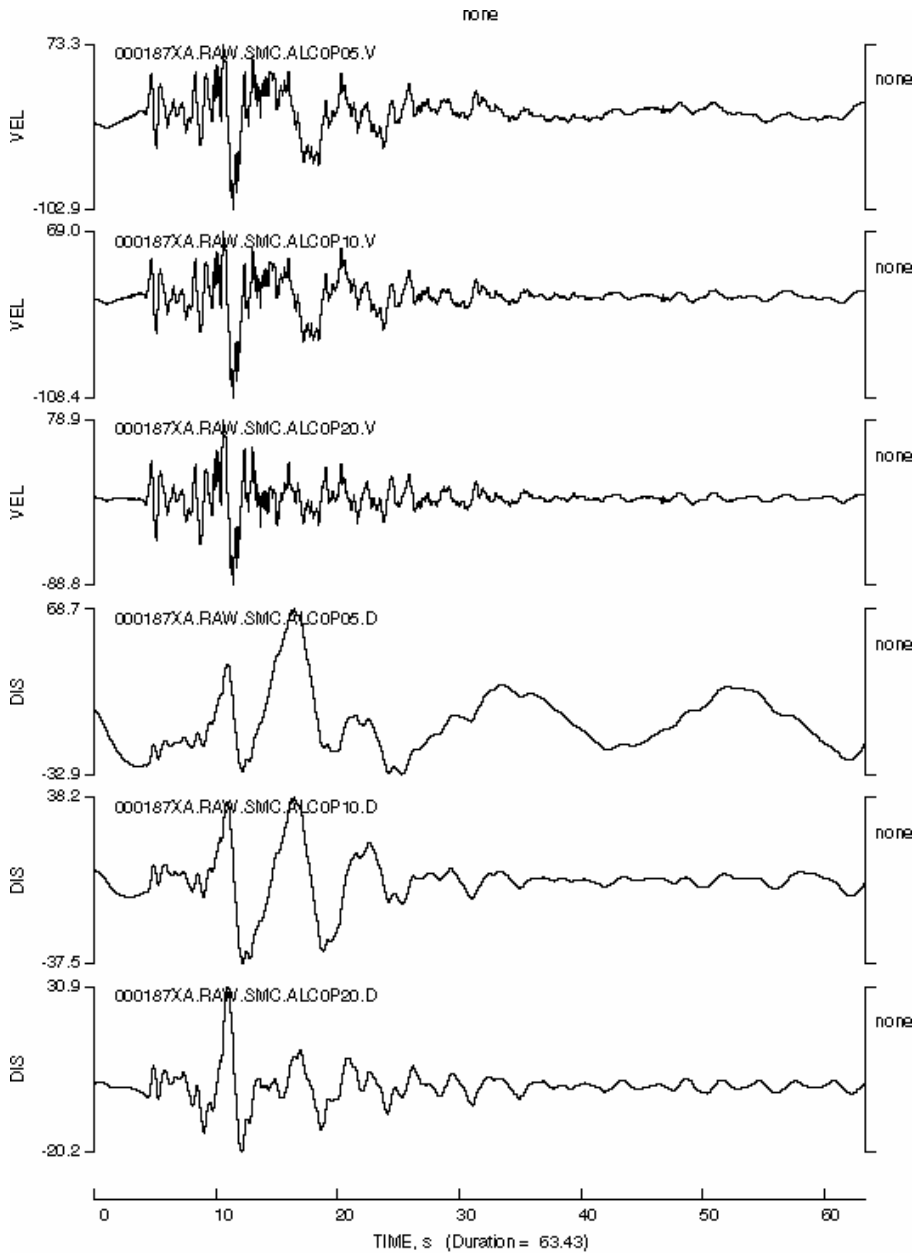

Fig. G.6 x-component velocity and displacement traces for Tabas recording of 1978 Tabas earthquake, obtained by filtering unprocessed acceleration with acausal Butterworth filters with corner frequencies of 0.05, 0.10, and 0.20 Hz.

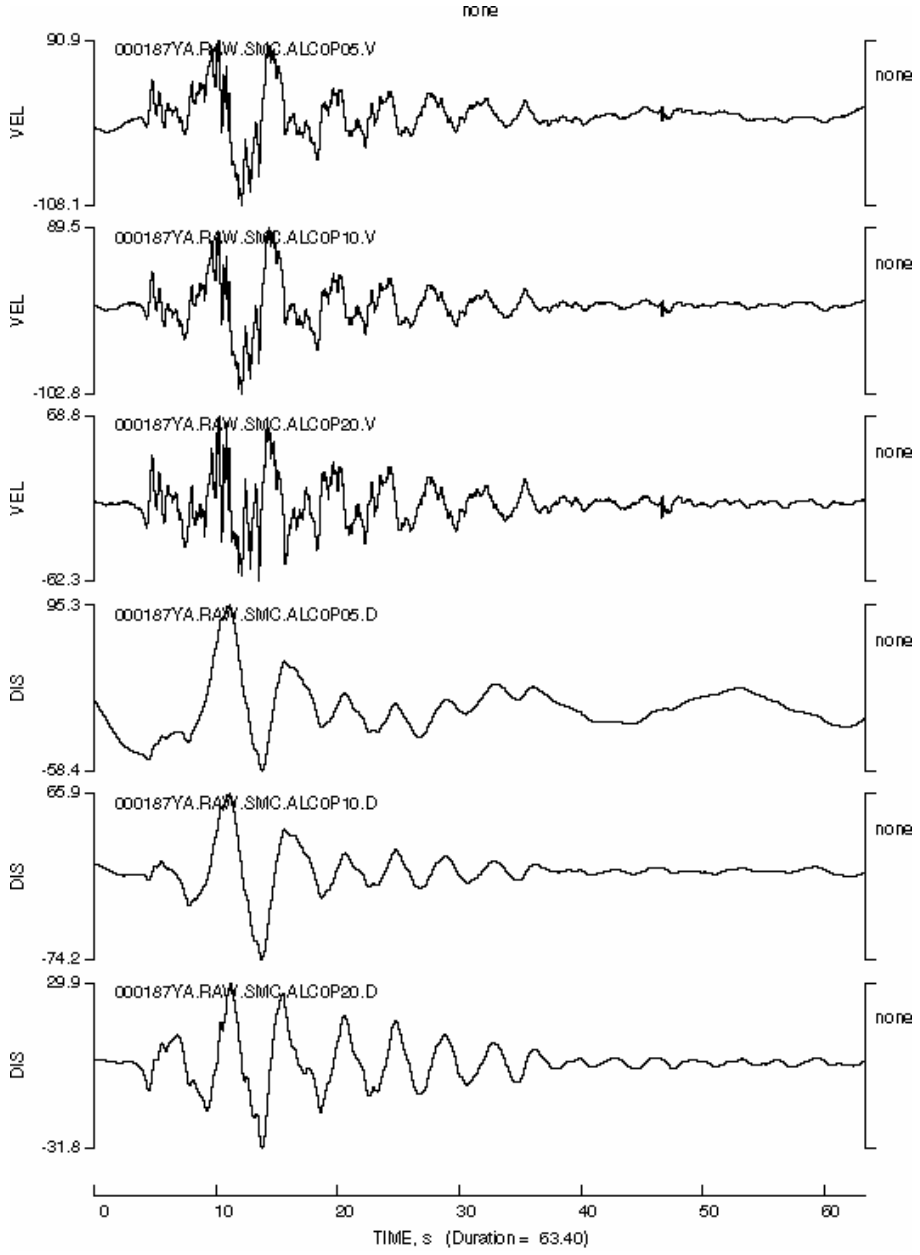

Fig. G.7 y-component velocity and displacement traces for Tabas recording of 1978 Tabas earthquake, obtained by filtering unprocessed. acceleration with acausal Butterworth filters with corner frequencies of 0.05, 0.10, and 0.20 Hz.

Table G.1 compares the geometric mean of the motions at Bajestan and Tabas obtained by my processing and contained in the PEER NGA spreadsheet (previous version). The PEER PGV value for Bajestan is similar to that obtained for a filter around 0.1 Hz, whereas the PGD value implies a lower-frequency corner (but not as low as 0.02 Hz). The Tabas values indicate that the filter corner of 0.05 Hz (the PEER NGA value) may be OK. There is relative stability in the PGV, although as often happens, the value of PGD is sensitive to the low-cut filter corner (and this is the prime reason that I will not be providing ground-motion prediction equations for PGD).

Table G.1 Geometric-mean peak ground motions for Bajestan and Tabas recordings of 1978 Tabas earthquake from records processed by PEER NGA and by D. Boore, showing influence of filter corner.

Station

Bajestan

data source	f_{LC} (Hz)	PGA(cm/s/s)	PGV(cm/s)	PGD(cm)
PEER NGA:	**0.02**	**77.89**	**6.60**	**10.39**
Filter only	**0.02**	**74.64**	**34.52**	**183.46**
Filter only	**0.1**	**76.02**	**6.84**	**5.02**
Filter only	**0.2**	**76.48**	**4.30**	**1.37**
Constant step correction	**0.02**	**74.77**	**37.76**	**194.87**
Constant step correction	**0.1**	**75.98**	**7.42**	**5.29**
Constant step correction	**0.2**	**76.48**	**4.30**	**1.28**
Polynomial step correction	**0.02**	**76.27**	**13.88**	**46.34**
Polynomial step correction	**0.1**	**76.15**	**6.02**	**3.58**
Polynomial step correction	**0.2**	**76.48**	**4.30**	**1.15**

Tabas

data source	f_{LC} (Hz)	PGA(cm/s/s)	PGV(cm/s)	PGD(cm)
PEER NGA:	**0.05**	**827.96**	**109.00**	**59.09**
Filter only	**0.05**	**949.84**	**105.47**	**80.91**
Filter only	**0.1**	**952.11**	**105.56**	**53.24**
Filter only	**0.2**	**980.82**	**78.16**	**31.35**

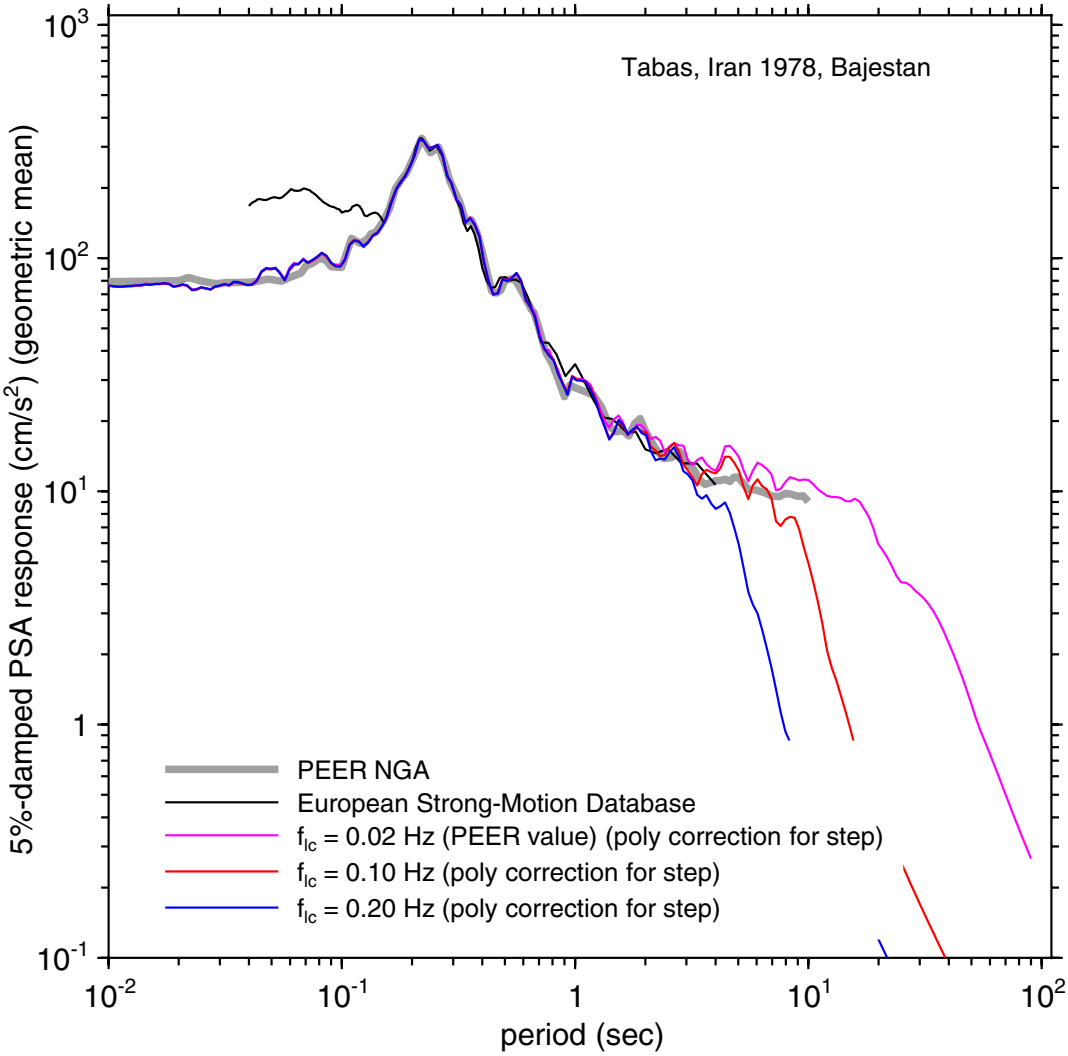

Fig. G.8 Geometric-mean SA for Bajestan record of Tabas earthquake, processed by different groups and using different filter corners. Note that D. Boore's processing included a polynomial step correction for one component and despiking of other component (not done for processing of records available from European Strong-Motion Database website, which explains divergence at short periods).

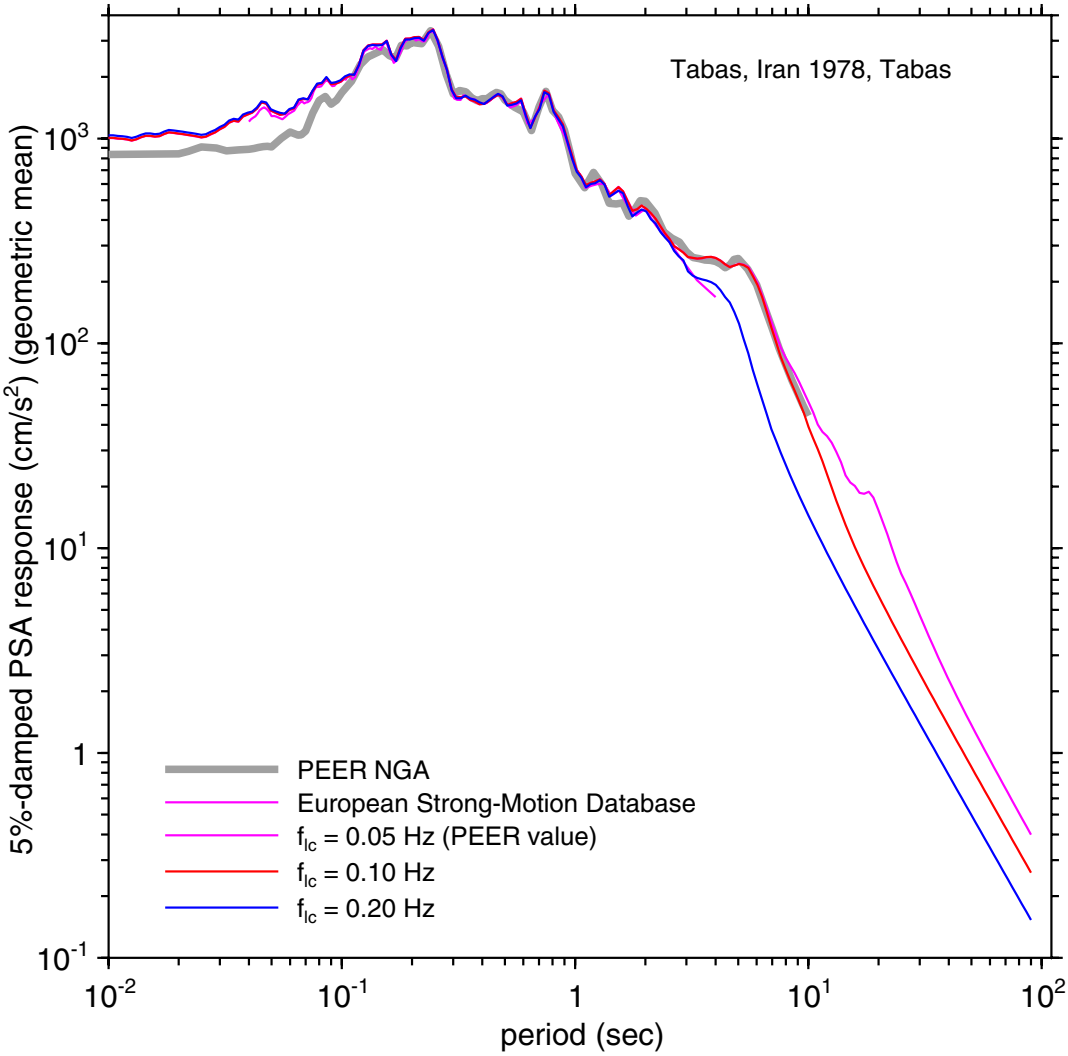

Fig. G.9 Geometric-mean SA for Tabas record of Tabas earthquake, processed by different groups and using different filter corners. Note difference between PEER–NGA and other values at short periods.

The pseudo-acceleration spectra for the Bajestan and Tabas recordings are shown in Figures G.8–G.9. The high value at short periods for the European Strong-Motion Database results are due to the presence of a large-amplitude spike on the Bajestan y-component (Fig. G.2) that was not removed during data processing. Otherwise the agreement is good over the period range 0.2–2 s. Note that the PEER NGA PGA value, and thus the short-period response spectrum, at Tabas is lower than the others (but recall that I used the European uncorrected data, so agreement should be expected between the non–PEER values at short periods, which are not as sensitive to filtering). (The processed data available from the European Strong-Motion

Database website, as opposed to the recently released CD, use a low-frequency filter of 0.25 Hz for all records.)

Another potential problem: Kashmar is an S-triggered record (Fig. G.10).

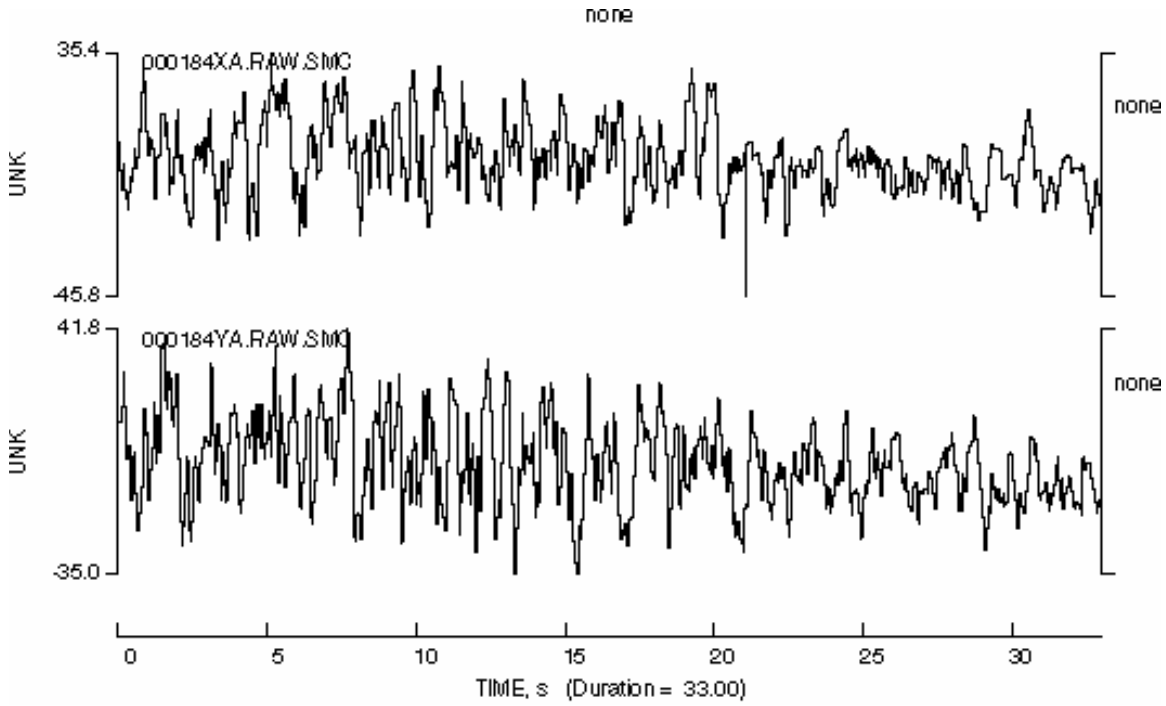

Fig. G.10 Unprocessed x- and y-component accelerations for Kashmar recording of 1978 Tabas earthquake, showing it is an S-triggered record.

Conclusions: (1) the low-cut filter corners of all but the Tabas recording of the 1978 Tabas earthquake are probably too small; (2) the PGD is sensitive to the filter corner; (3) the PEER NGA PGA for Tabas is about 15 percent lower than the value from the European Strong-Motion Database website; (4) Kashmar is an S-triggered record.

Appendix H: Notes on UCSC Recording of 1989 Loma Prieta Earthquake at Los Gatos Presentation Center

The response spectra computed by me and available in an early version of the NGA flatfile showed some disagreements for records obtained at the University of California Santa Cruz (UCSC) stations. In response to my email of July 6, 2004, Walt Silva et al. recently sent newly processed data from UC Santa Cruz for the 1989 Loma Prieta earthquake. The new spectra now seem to be in better agreement with those I computed. Figure H.1 shows a direct comparison at the UCSC station. Also shown in that figure are spectra at the Lick station on the UCSC campus.

The main topic of these notes is the Los Gatos Presentation Center (LGPC) data. I think that the data are so full of erroneous spikes (even after despiking and high-cut filtering by Silva et al.) and are so different from the relatively nearby Lexington Dam (LEXD, my code for this station) record that the motions from LGPC should not be used. As a side note, I also discovered that the coordinates of LEXD in the CGS data files and website are incorrect. Using the Topo! Program, I find that the proper coordinates for the strong-motion recorder are 37.20080 and -121.99032 (NAD27) (the other coordinates are for the center of the dam). This appendix is mainly a series of figures.

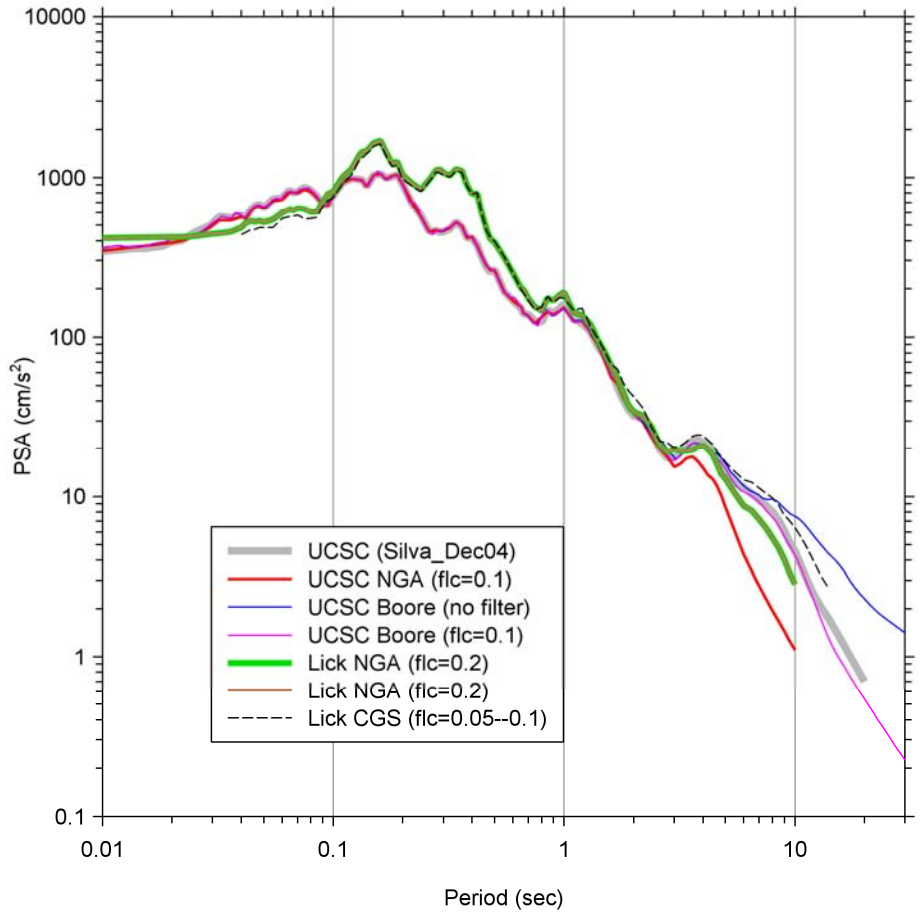

Fig. H.1 Spectra of data recorded on UCSC campus. New spectrum at UCSC (gray) is in good agreement with my spectrum of filtered motion (magenta). Note difference between Lick and UCSC spectra is probably real.

Figure H.2 is a map of the locations of LGPC and LEXD, as well as the surface projection of the Loma Prieta mainshock that Bill Joyner and I used for distance calculations in our 1993 regression work (note that with our surface projections that the JB distance is not zero for the stations, as it is for LGPC in the NGA flatfile; this is an example of differences that can occur due to the subjective choice of the dimensions and location of rupture surfaces in earthquakes. A more detailed map is given in Figure H.3.

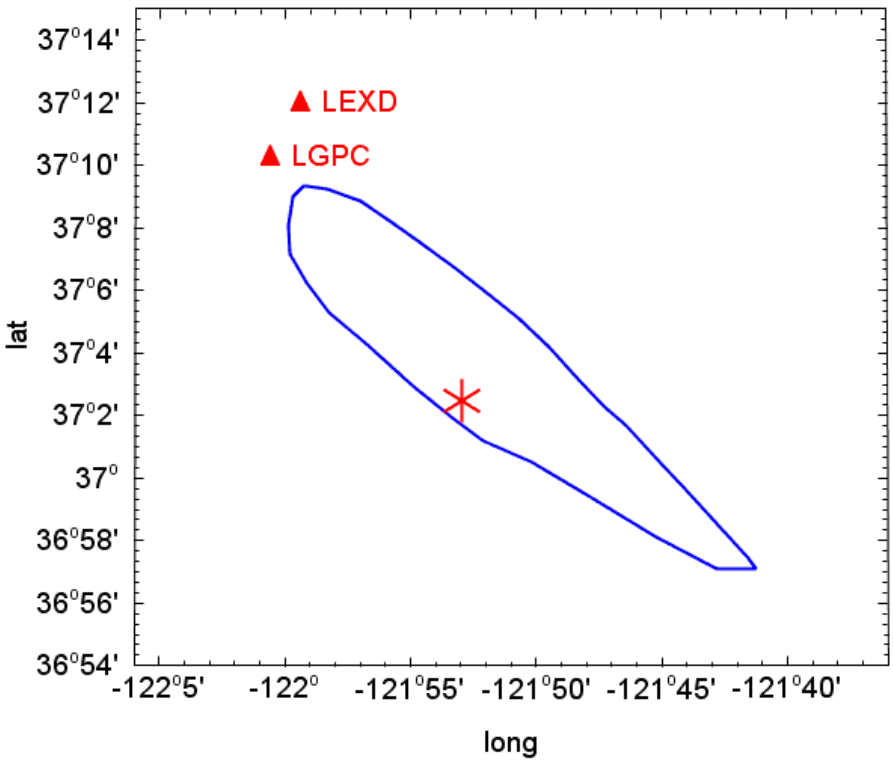

Fig. H.2 Map of surface projection of fault, epicenter (asterisk), and stations.

Fig. H.3 Map showing locations of LGPC and Lexington Dam stations (stations 3.6 km apart).

The accelerations at LGPC before despiking are shown in Figure H.4, and the first derivative of the original accelerations are given in Figure H.5 (these time series are useful for identifying spikes). Recalling that spikes in acceleration show up as double-sided pulses in jerk, the plot above suggests that there are many more spikes on the records than identified by Silva et al. To see the effect of the Silva et al. despiking (and 80 Hz high-cut filtering), I show the same two figures as before, but using the data recently sent by Silva et al. The results are shown in Figures H.6–H.7. It seems to me that much of the high-frequency chatter remains. Notice that some of the spikes in the jerk trace are single sided, implying steps in the acceleration. It is not clear to me that the despiked record (Figs. H.6–H.7) is that much better than the original record (Figs. H.4–H.5).

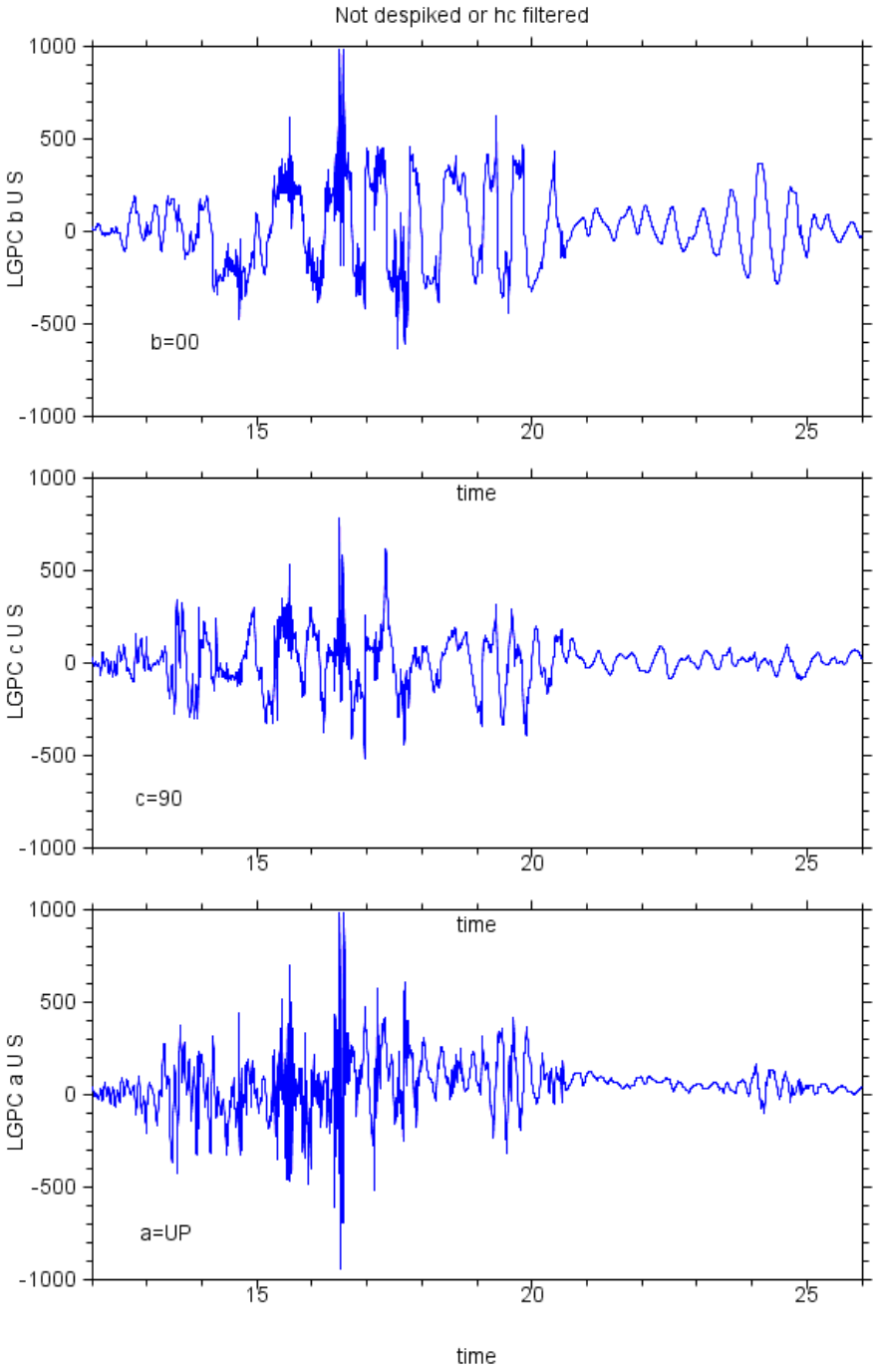

Fig. H.4 Accelerations at LGPC, before despiking.

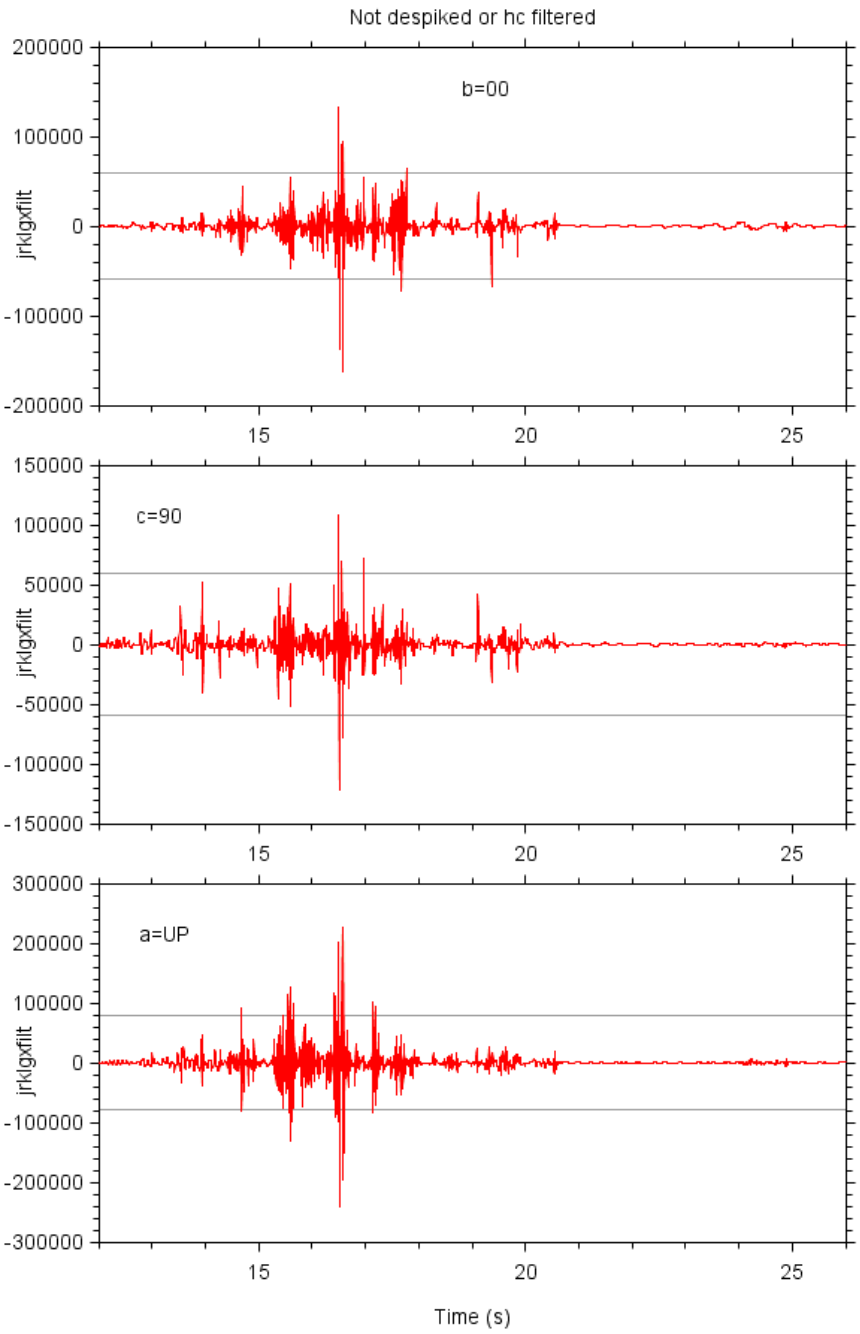

Fig. H.5 "Jerk" (first difference of acceleration) at LGPC, using original record (not despiked). Horizontal gray lines correspond to jerk level used by Silva et al. in despiking record (first difference would be 981*0.3/0.005 = 58,860 for horizontal components and 981*0.4/0.005 = 78,480 for vertical component).

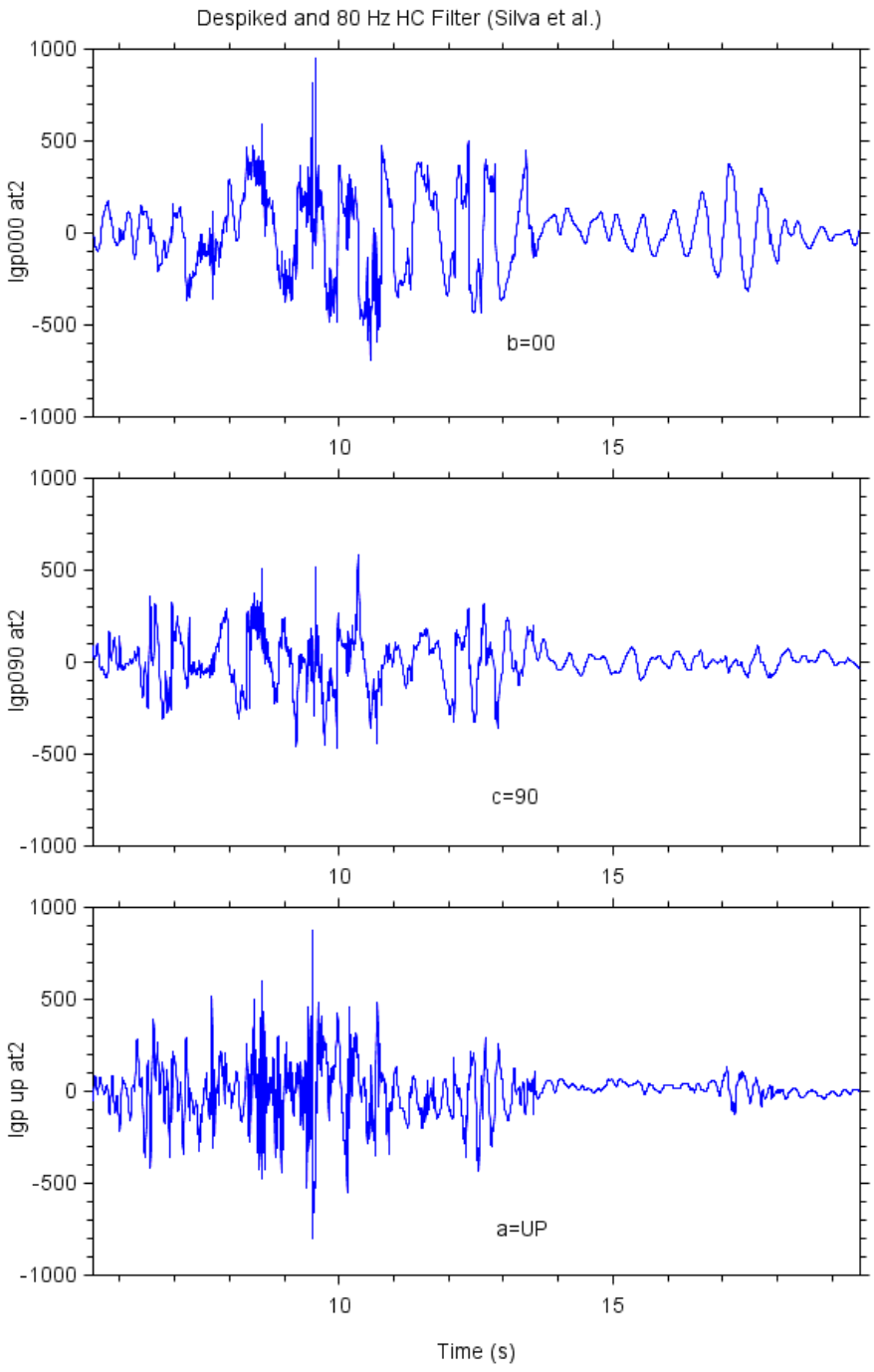

Fig. H.6 Despiked and high-cut filtered by Silva et al.

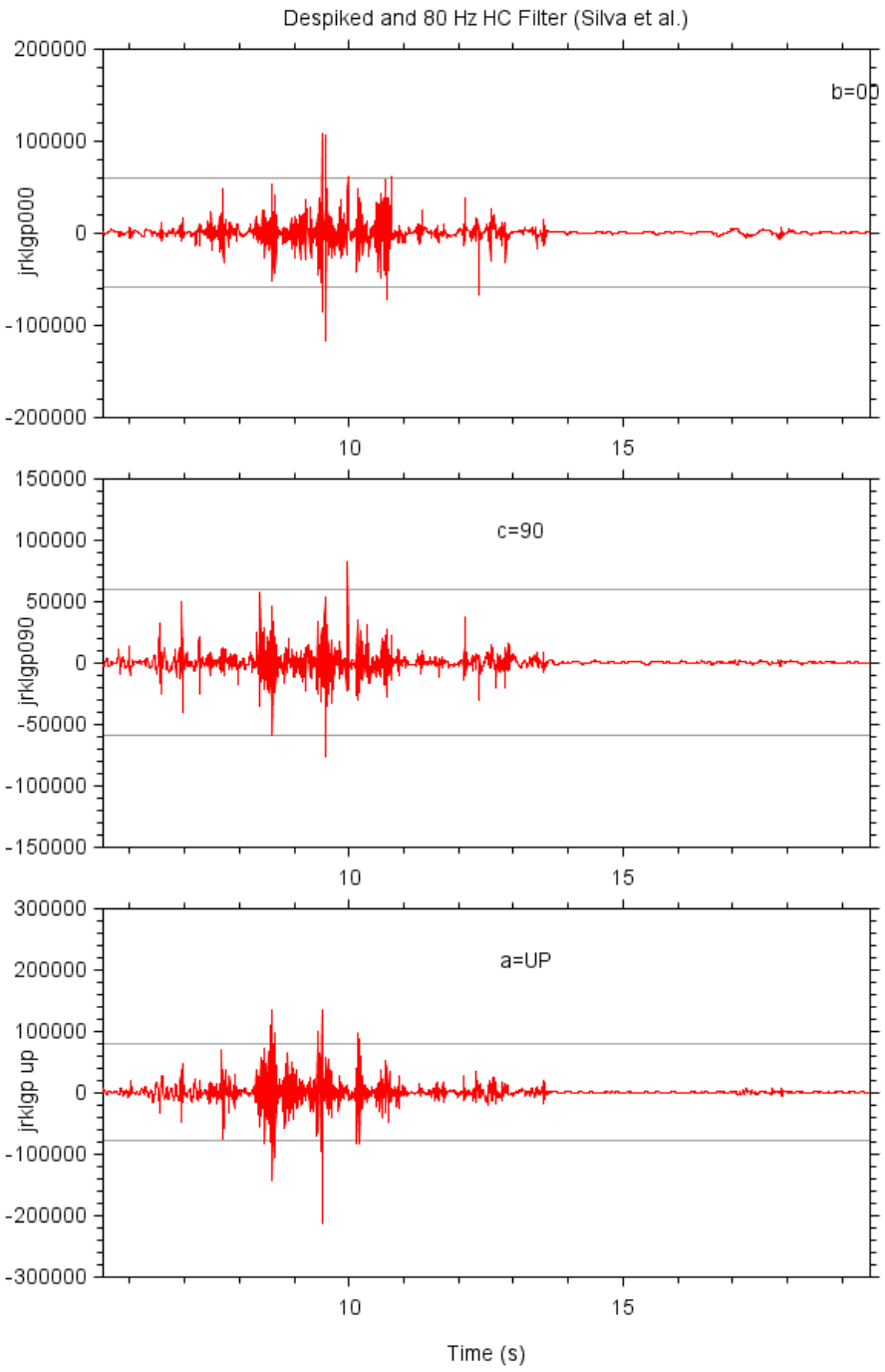

Fig. H.7 Jerk time series for despiked records.

The waveforms at LEXD and LGPC are quite different, even though the stations are only 3.6 km from one another. This is shown in the Figure H.8. The spectra of all but the EW component for $T > 1\,\mathrm{s}$ are also very different in general, as shown in the Figure H.9.

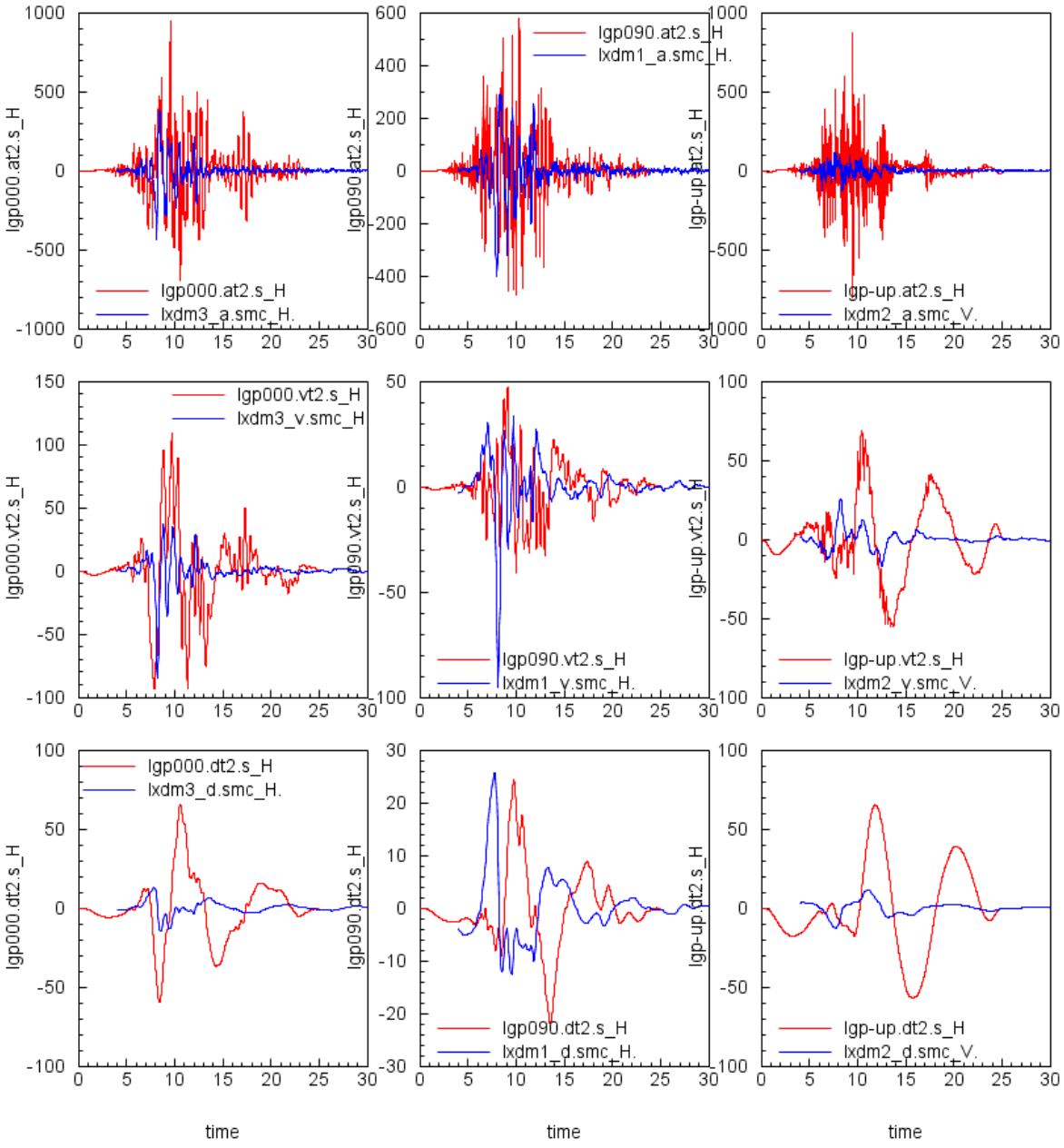

Fig. H.8 Comparison of acceleration, velocity, and displacement traces at Lexington Dam and LGPC. Lexington Dam record low-cut filtered between 0.05 and 0.10 Hz. LGPC record low-cut filtered with causal 0.1 Hz filter. Time alignment is arbitrary; all Lexington Dam components shifted by same amount to produce general coincidence of acceleration traces.

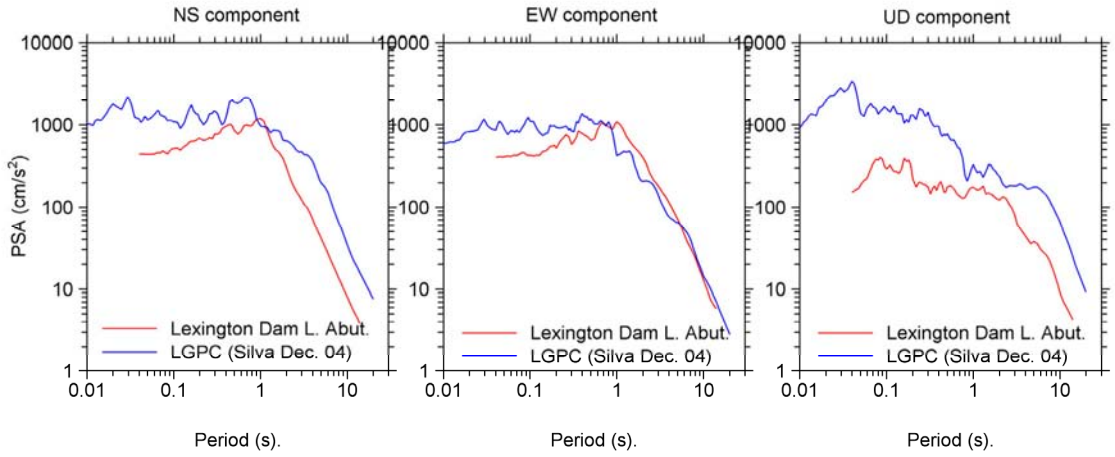

Fig. H.9 Spectra at LEXD and LGPC

Unless someone can convince me otherwise, I think that the recordings at LGPC should not be used for any analyses. The acceleration record at LGPC is very strange looking, with numerous spikes that have not been removed by despiking and high-cut filtering. In contrast, the LEXD record does not seem at all strange. If I knew what produced the spikes on the LGPC record and could be assured that the spikes only affect high frequencies, I could see using a high-cut filtered version of the record. But the comparisons of velocity and displacement waveforms at LEXD and LGPC does not give me much confidence that the problems on the LGPC record are restricted to high frequencies (with the possible exception of the EW component record).

Appendix I: USGS Data for 1992 Cape Mendocino Not Included in NGA Flatfile

I noticed in early January 2005 that there are no USGS data in the NGA database for the 1992 Cape Mendocino mainshock. This appendix, originally written on 8 January 2005, was an unsuccessful appeal that the USGS data be included.

Unprocessed data have been available for at least four years from *http://nsmp.wr.usgs.gov/data_sets/petrolia.html*. For use in the subduction ground-motion paper that Gail Atkinson and I published (Atkinson and Boore 2003), I did some quick processing of the data (using a low-cut filter of 0.2 Hz for all records), and summaries of the results of the accelerations and velocities for those records are included in Table I.1. For comparison, Table I.2 contains information for the CGS recordings. Note that the USGS data are at relevant distances and amplitudes, with a number of peak accelerations between about 0.2 and 0.4g, and PGV as large as 75 cm/s. It is quite likely that the data would permit filtering at lower frequencies (see below for one example)—the choice of 0.2 Hz was conservative, and no effort was made to explore lower-frequency filters.

One possible reason that the USGS data were not included is that the file headers indicate that there were stalls on a number of recordings. This is probably not a good reason to exclude the data: there are indications of definite stalls on 3 of the 8 recordings, possible stalls on 2 recordings, and no stalls on 3 recordings. In addition, the times of the stalls for several of the records identified as having stalls do not coincide with the portion of strong shaking. Finally, Chris Stephens looked at what seems to be the worst case (Ferndale), and thinks that the record has had a first-order correction applied to account for the stalls (he also points out that there are stretches as well as stall). It is possible to do a correction because time code traces are available on the recordings (unlike the Rinaldi Receiving Station record of the 1994 Northridge

mainshock, which also had stalls (Trifunac et al., 1998)). I also studied the displacements from two closely located stations in Fortuna (see Fig. I.1 for locations). The CGS recordings used a low-cut filter tapering from 0.07 to 0.05 Hz; in order to use a similar filter for the USGS data, I applied an acausal Butterworth filter with a 0.06 corner frequency. The comparisons are in Figure I.2. Although the file header indicates possible stalls at 50+0.5 and 50+6 s ("50" is the length of the zero pad applied before filtering), they do not seem to have had much effect on the motions (judging from the relatively good match with the CGS displacements).

In addition to the data, there are shear-wave velocity profiles at Ferndale (from Shannon and Wilson) and Loleta, College of the Redwoods, Fortuna Fire Station, Redwood Village Mall (Fortuna), and the Rio Dell overcrossing free field (the latter two are CDMG strong-motion stations for which data are in the NGA database). The velocities are in USGS OFR 02-203 and are available from the compilation I put together (see my website: *http://quake.usgs.gov/~boore*).

For the reasons above, I recommended that the USGS data be included in the NGA database. It is unfortunate that these date were not included in the flatfile.

Table I.1 USGS recordings (with 0.2 Hz low-cut filter).

Station Name	R_{EP}	ivrt	ihrz	fltr1	fltr2	PGA(cm/s/s)	PGV(cm/s)
Butler Valley Sta. 2	**60**	********	**60**	**0.2**	**-2**	**152.1**	**14.1**
Butler Valley Sta. 2	**60**	**0**	********	**0.2**	**-2**	**72.7**	**10.7**
Butler Valley Sta. 2	**60**	********	**330**	**0.2**	**-2**	**136.7**	**20.4**
Ferndale FS	**24**	********	**360**	**0.2**	**-2**	**266.5**	**39.3**
Ferndale FS	**24**	**0**	********	**0.2**	**-2**	**61.9**	**7.4**
Ferndale FS	**24**	********	**270**	**0.2**	**-2**	**452.3**	**74.8**
Loleta FS	**32**	********	**360**	**0.2**	**-2**	**251.5**	**24.5**
Loleta FS	**32**	**0**	********	**0.2**	**-2**	**132.4**	**5.7**
Loleta FS	**32**	********	**270**	**0.2**	**-2**	**246.8**	**29.4**
Centerville Beach	**22**	********	**360**	**0.2**	**-2**	**451.3**	**59.4**
Centerville Beach	**22**	**0**	********	**0.2**	**-2**	**137.2**	**11.5**
Centerville Beach	**22**	********	**270**	**0.2**	**-2**	**302.7**	**48.4**
College of the Redwoods	**38**	********	**360**	**0.2**	**-2**	**170.5**	**29.3**
College of the Redwoods	**38**	**0**	********	**0.2**	**-2**	**73.5**	**7.1**
College of the Redwoods	**38**	********	**270**	**0.2**	**-2**	**168.7**	**25.1**
South Bay Union School	**42**	********	**360**	**0.2**	**-2**	**189.6**	**23.2**
South Bay Union School	**42**	**0**	********	**0.2**	**-2**	**64.9**	**6.6**
South Bay Union School	**42**	********	**270**	**0.2**	**-2**	**149.3**	**23.5**
Fortuna FS	**29**	********	**360**	**0.2**	**-2**	**281**	**27.4**
Fortuna FS	**29**	**0**	********	**0.2**	**-2**	**80.5**	**6.3**
Fortuna FS	**29**	********	**270**	**0.2**	**-2**	**348.5**	**33.7**
Bunker Hill	**15**	********	**360**	**0.2**	**-2**	**225.5**	**29.1**
Bunker Hill	**15**	**0**	********	**0.2**	**-2**	**76.6**	**12.4**
Bunker Hill	**15**	********	**270**	**0.2**	**-2**	**185**	**46.6**

Table I.2 CGS data.

Station Name	R_{EP}	ivrt	ihrz	fltr1	fltr2	PGA(cm/s/s)	PGV(cm/s)
CAPE MENDOCINO	**10**	**90**	**90**	**0.05**	**0.07**	**1019.4**	**40.5**
CAPE MENDOCINO	**10**	**0**	**0**	**0.05**	**0.07**	**738.9**	**60.3**
CAPE MENDOCINO	**10**	**90**	**0**	**0.05**	**0.07**	**1468.3**	**126.1**
EUREKA - 5TH & H FEDERAL BLDG.	**52**	**90**	**80**	**0.12**	**0.24**	**152.7**	**28.6**
EUREKA - 5TH & H FEDERAL BLDG.	**52**	**0**	**0**	**0.12**	**0.24**	**35.4**	**6.2**
EUREKA - 5TH & H FEDERAL BLDG.	**52**	**90**	**350**	**0.12**	**0.24**	**86.4**	**17**
EUREKA - MYRTLE & WEST AVENUE	**52**	**90**	**90**	**0.08**	**0.16**	**174.7**	**28.6**
EUREKA - MYRTLE & WEST AVENUE	**52**	**0**	**0**	**0.08**	**0.16**	**41.6**	**7.3**
EUREKA - MYRTLE & WEST AVENUE	**52**	**90**	**0**	**0.08**	**0.16**	**151**	**20**
FORTUNA - 701 S. FORTUNA BLVD.	**28**	**90**	**90**	**0.05**	**0.07**	**111.9**	**20.9**
FORTUNA - 701 S. FORTUNA BLVD.	**28**	**0**	**0**	**0.05**	**0.07**	**47.9**	**5.8**
FORTUNA - 701 S. FORTUNA BLVD.	**28**	**90**	**0**	**0.05**	**0.07**	**113.6**	**28.8**
PETROLIA	**5**	**90**	**90**	**0.05**	**0.07**	**649.4**	**89.5**
PETROLIA	**5**	**0**	**0**	**0.05**	**0.07**	**159.7**	**20.9**
PETROLIA	**5**	**90**	**0**	**0.05**	**0.07**	**578.1**	**48.3**
RIO DELL - 101/PAINTER ST. OVE	**21**	**90**	**272**	**0.05**	**0.07**	**378.3**	**44.7**
RIO DELL - 101/PAINTER ST. OVE	**21**	**0**	**0**	**0.05**	**0.07**	**191.5**	**10.2**
RIO DELL - 101/PAINTER ST. OVE	**21**	**90**	**2**	**0.05**	**0.07**	**538.5**	**42.6**
SHELTER COVE - AIRPORT	**36**	**90**	**90**	**0.25**	**0.5**	**173**	**6.9**
SHELTER COVE - AIRPORT	**36**	**0**	**0**	**0.25**	**0.5**	**49.5**	**1.8**
SHELTER COVE - AIRPORT	**36**	**90**	**0**	**0.25**	**0.5**	**222**	**7**

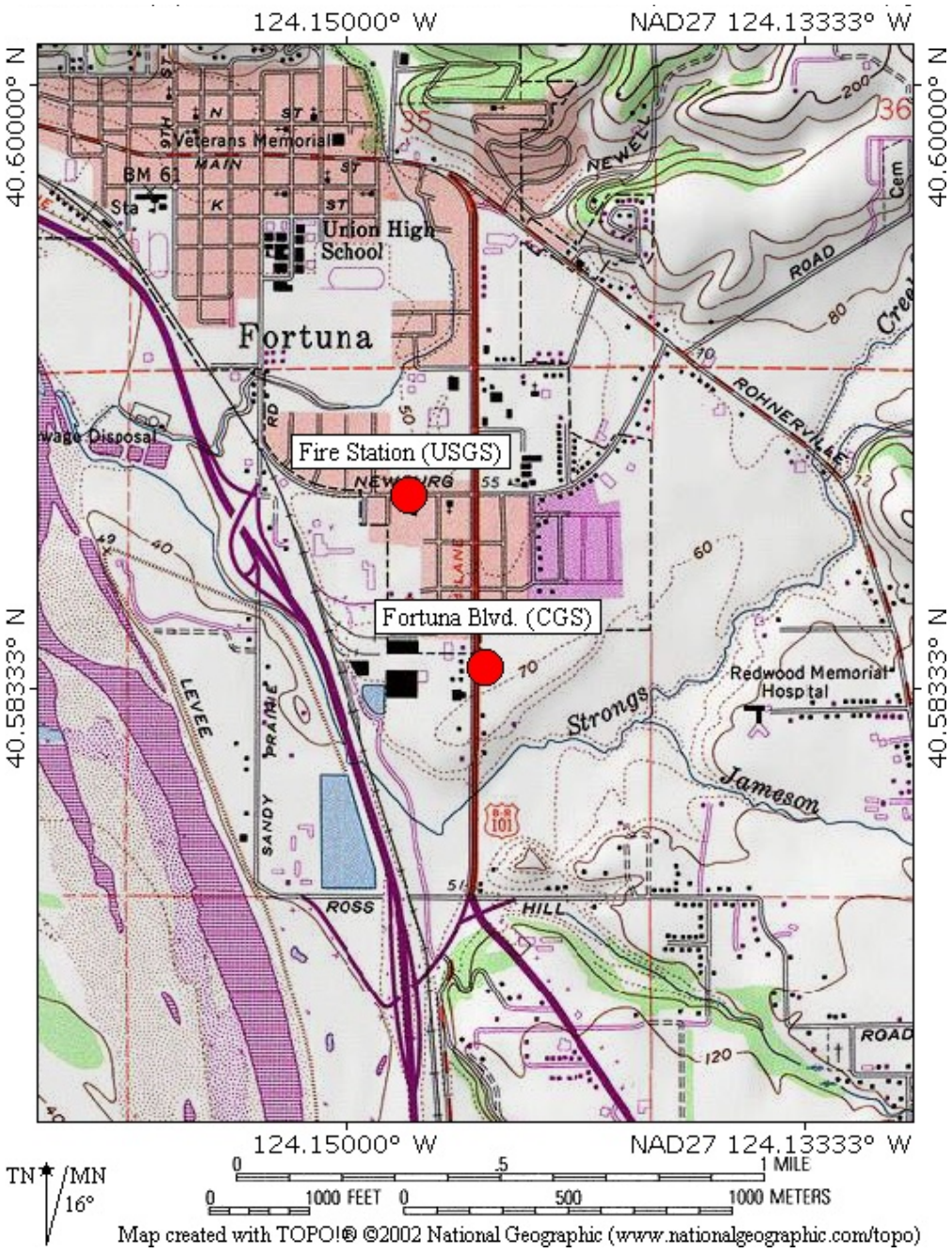

Fig. I.1 Map of two nearby stations that recorded 1992 Cape Mendocino earthquake.

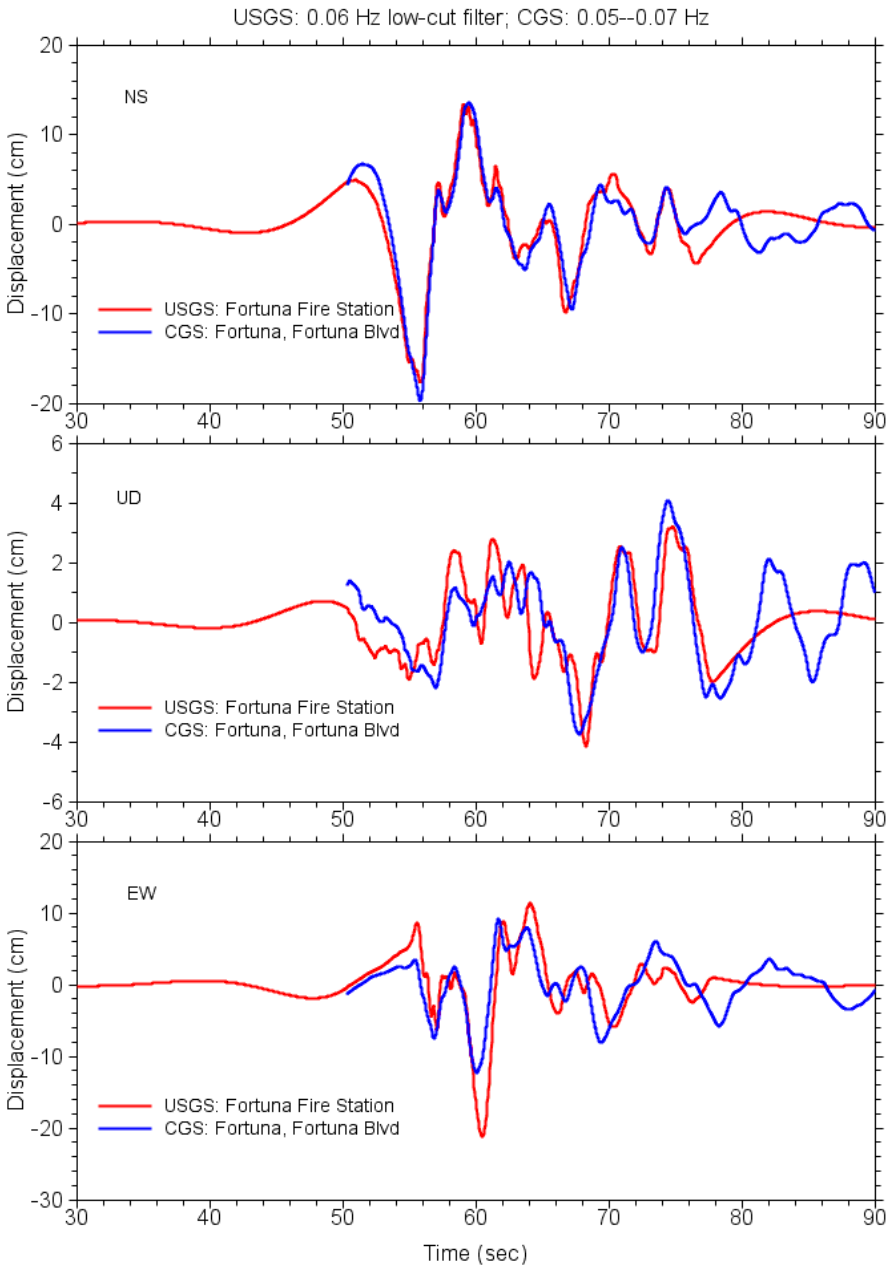

Fig. I.2 USGS records include padded portions before (less than 50 s) and after (greater than 78 s) recorded motions.

Appendix J: Notes on Rinaldi Receiving Station Recording of 1994 Northridge Earthquake Used in NGA Flatfile

For the Rinaldi Receiving Station recording of the 1994 Northridge mainshock, I happened to notice in early 2005 that the low-cut filter corner in the PEER NGA flatfile is 0.3 Hz, which struck me as being too high. I confirmed this with Walt Silva via telephone conversations in the first week of 2005. He is not sure where he obtained the data or what processing was done on the record. On looking into the issue, I discovered that the data in the flatfile correspond to the "old" data (with a duration of about 16 s). Trifunac et al. (1998) redigitized the data. Their version of the data differs in several ways from the old version: they included more of the record, they captured peaks not properly digitized in the old version, and they corrected for more stalls on the record. As a matter of interest, it should be noted that no internal time code marks are available for this record, and thus the peak velocities and peak displacements, as well as the spectral amplitudes, are dependent on the assumption that 1 cm = 1 s.

To see how the "new" data might differ from that used in the NGA flatfile, I include here a series of plots comparing waveforms and response spectra (Figs. J.1–J.8). I processed the new data using both causal and acausal filters, each with different rolloffs. The processed data available from USC has filtered the 228-degree trace with a transition from 0.09 to 0.11 Hz and the 318-degree component with a transition between 0.15–0.20 Hz. In Trifunac et al. (1998) the transition from 0.07 to 0.09 Hz is used for both components. In this note I used Butterworth filters with corners of 0.01, 0.02, 0.10, and 0.20 Hz. I did no baseline corrections before filtering. I show plots of the waveforms only for the recorded section of time. Because I have not included the padded portions in the plots, the displacements sometimes do not return to around zero at the end of the recorded time, although plots of the complete time series that was filtered do show

that the displacements return to zero (in other words, the filtering was done correctly and no "wrap-around" pollution exists—see Boore 2005, for a discussion).

Please note that waveforms plots were made using a quick plotting program and as a result, the traces appear to have dropouts. But they should be adequate for purposes of comparisons, and the peak motions along the ordinate axes are accurate.

Here are some observations:

1. At short periods, there are systematic differences between NGA and new for the 318-degree component, although the short-period response is essentially identical for all acausal filters. The NGA spectra are given at 0.01 and 0.02 s, but the similar values at both periods are not consistent with the new results, and, furthermore, the abrupt leveling off of the NGA spectrum for periods shorter than about 0.02 s looks strange (the spectrum for the 228-degree component also levels off at about 0.02 s, but more gradually). The spectra for the 228-degree component are similar for NGA and new (as long as acausal filtering is used).
2. At long periods, there are differences between NGA and new for periods longer than about 2 to 3 s (depending on component), but here the new results vary with the filter corner (as expected). For the 228-degree component, the NGA results are greater than the new results for periods between about 2 to 5 s and tend to lower values for greater periods. For the 318-degree component, the NGA values are lower than the new values for periods greater than about 6 s (except for the new results using a filter corner of 0.2 Hz).

Bottom line: I recommend replacing the NGA values for the Rinaldi Receiving Station recording of the 1994 Northridge mainshock with the USC digitized data, corrected for stalls. The processing of the corrected data should use acausal, not causal filters (note the sensitivity of the short-period response on the 228-degree component to long-period cutoffs for the causal filter, as well as the greater sensitivity of the peak velocity to filter corner for causal filters).

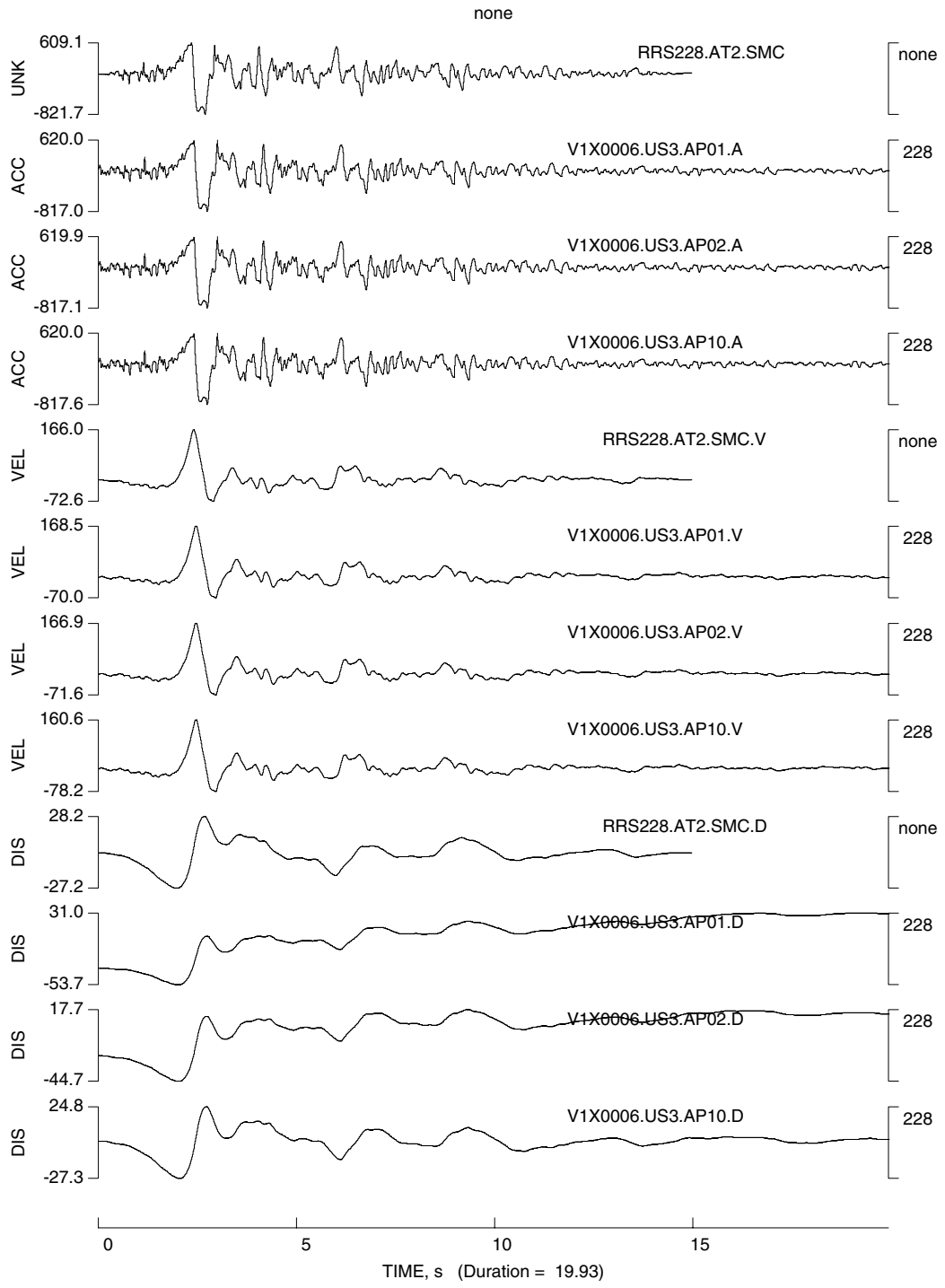

Fig. J.1 NGA time series ("RRS" file name), and acausally filtered, 228-degree component using filter corners of 0.01, 0.02, 0.1, and 0.2 Hz.

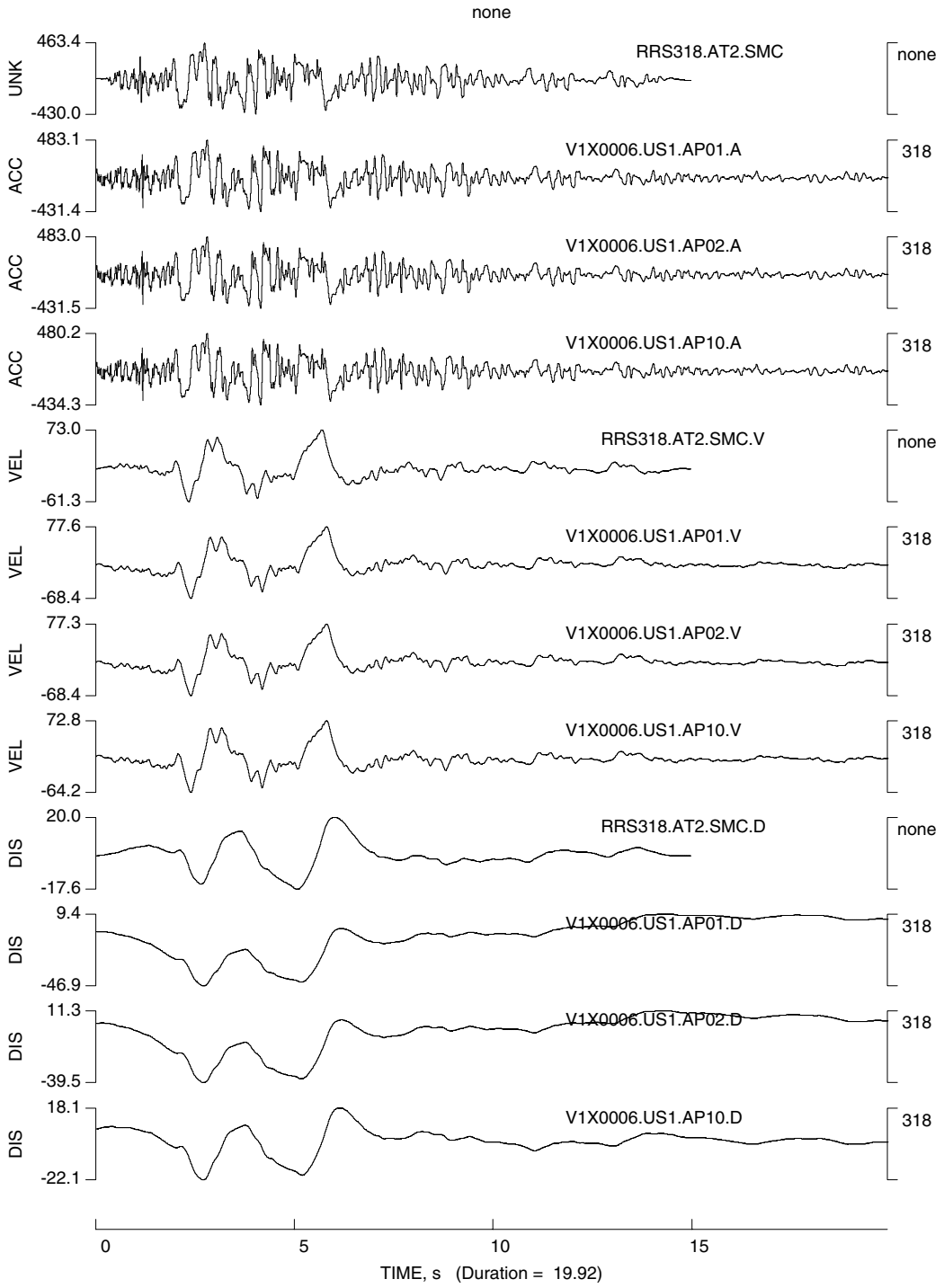

Fig. J.2 NGA time series ("RRS" file name), and acausally filtered, 318-degree component using filter corners of 0.01, 0.02, 0.1, and 0.2 Hz.

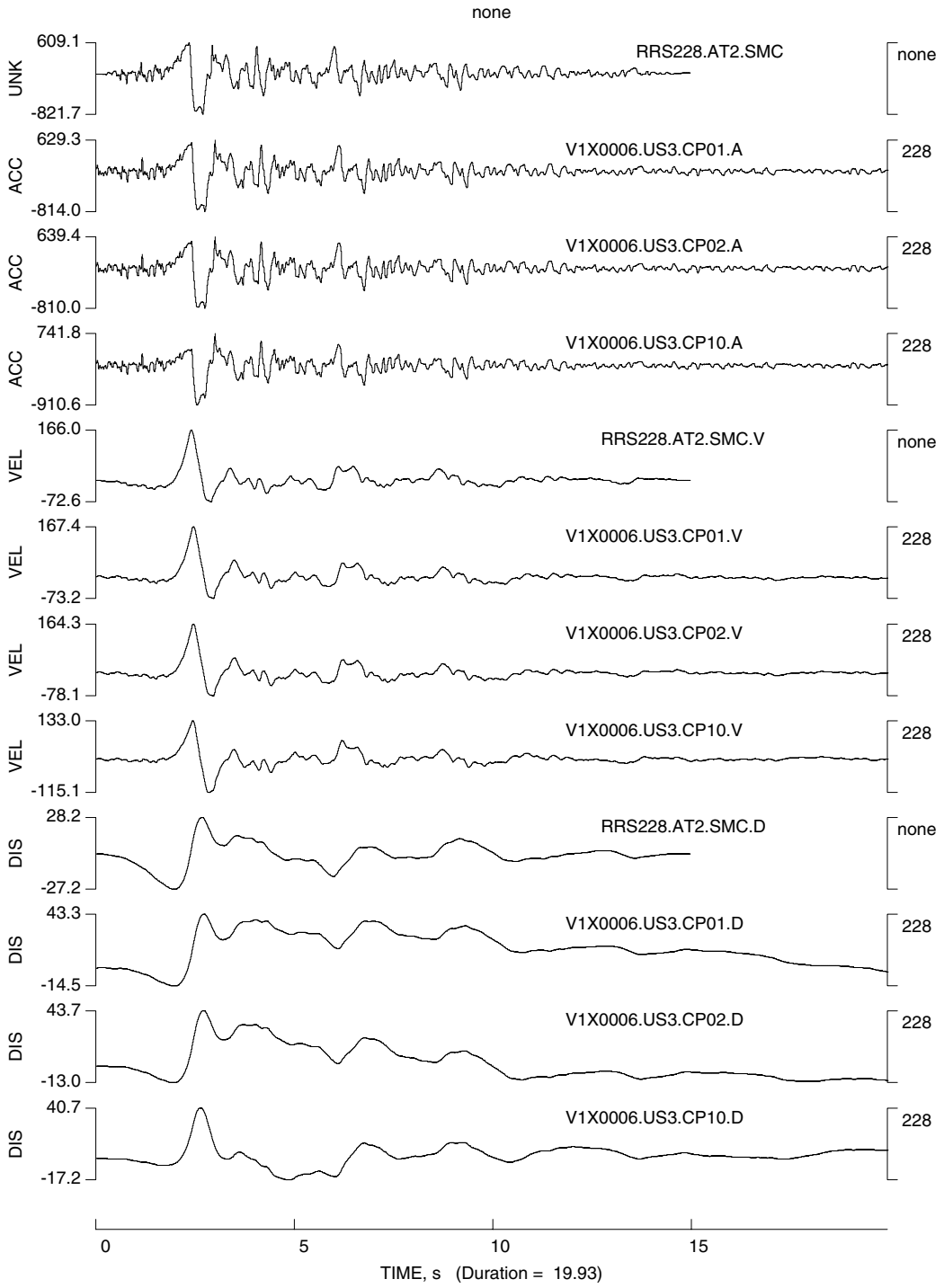

Fig. J.3 NGA time series ("RRS" file name), and causally filtered, 228-degree component using filter corners of 0.01, 0.02, 0.1, and 0.2 Hz.

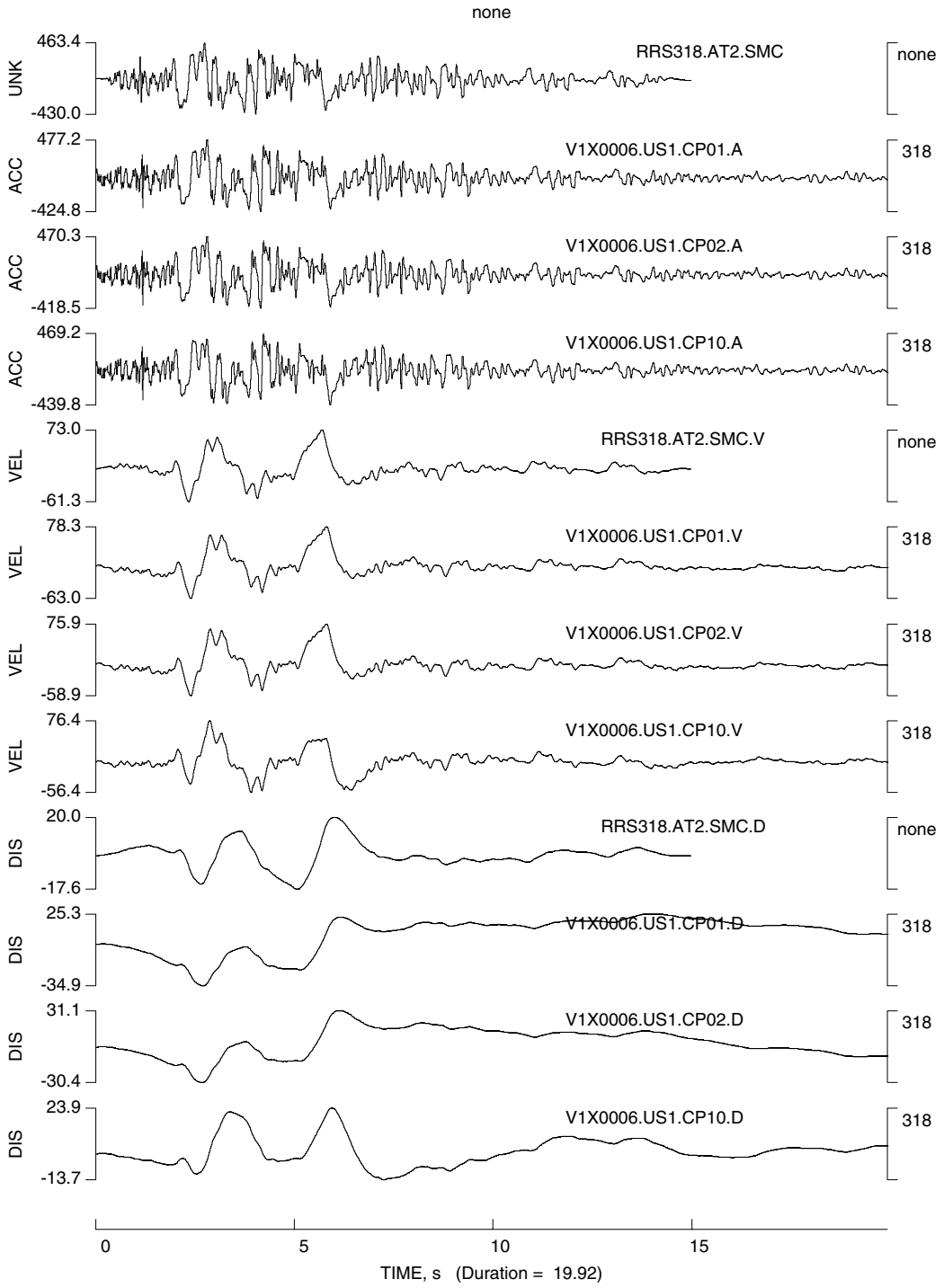

Fig. J.4 NGA time series ("RRS" file name), and causally filtered, 318-degree component using filter corners of 0.01, 0.02, 0.1, and 0.2 Hz.

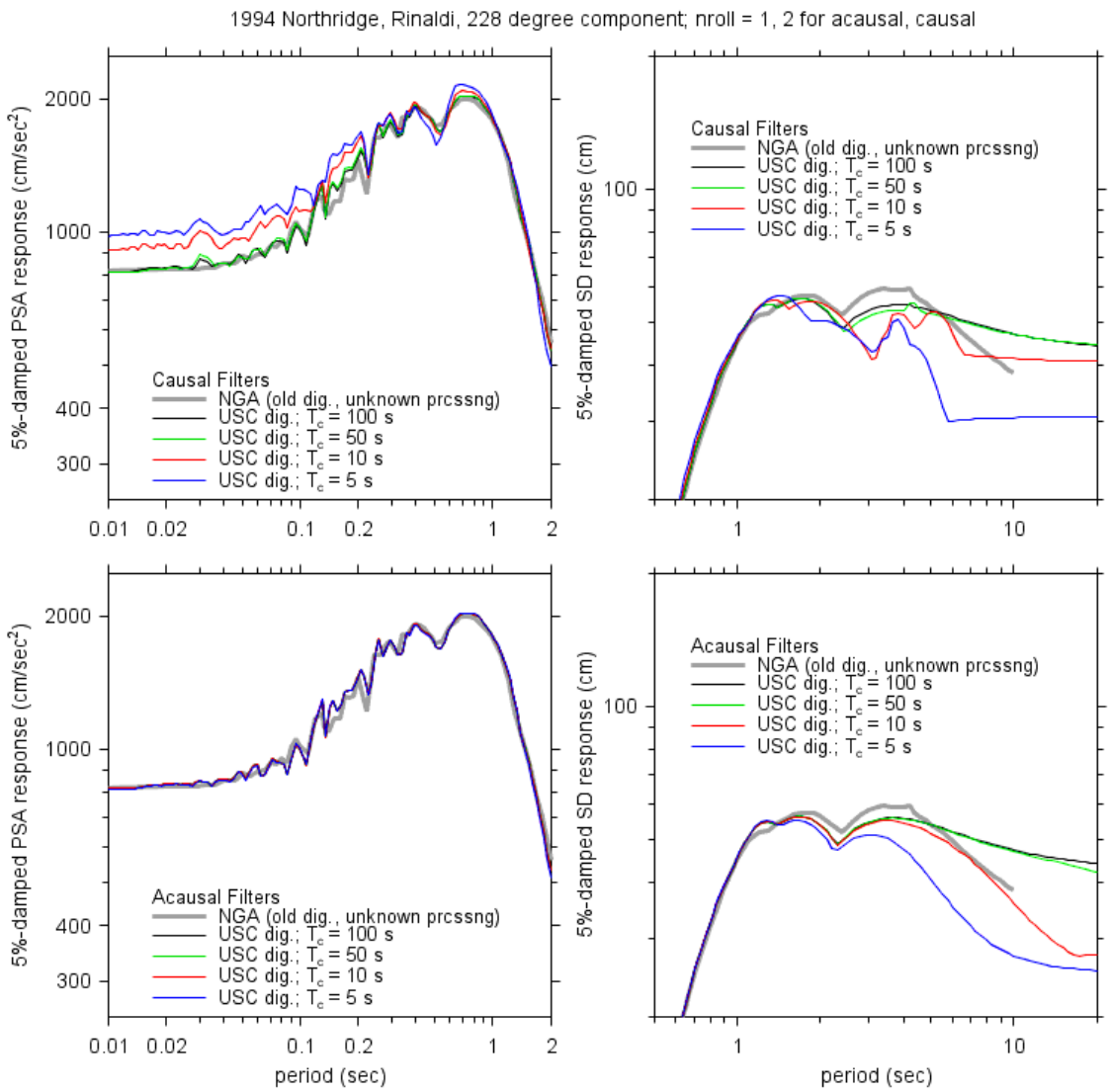

Fig. J.5 PSA and SD response, acausal and causal filters, as well as NGA spectra, for 228-degree component. Lowest order time-domain filters used.

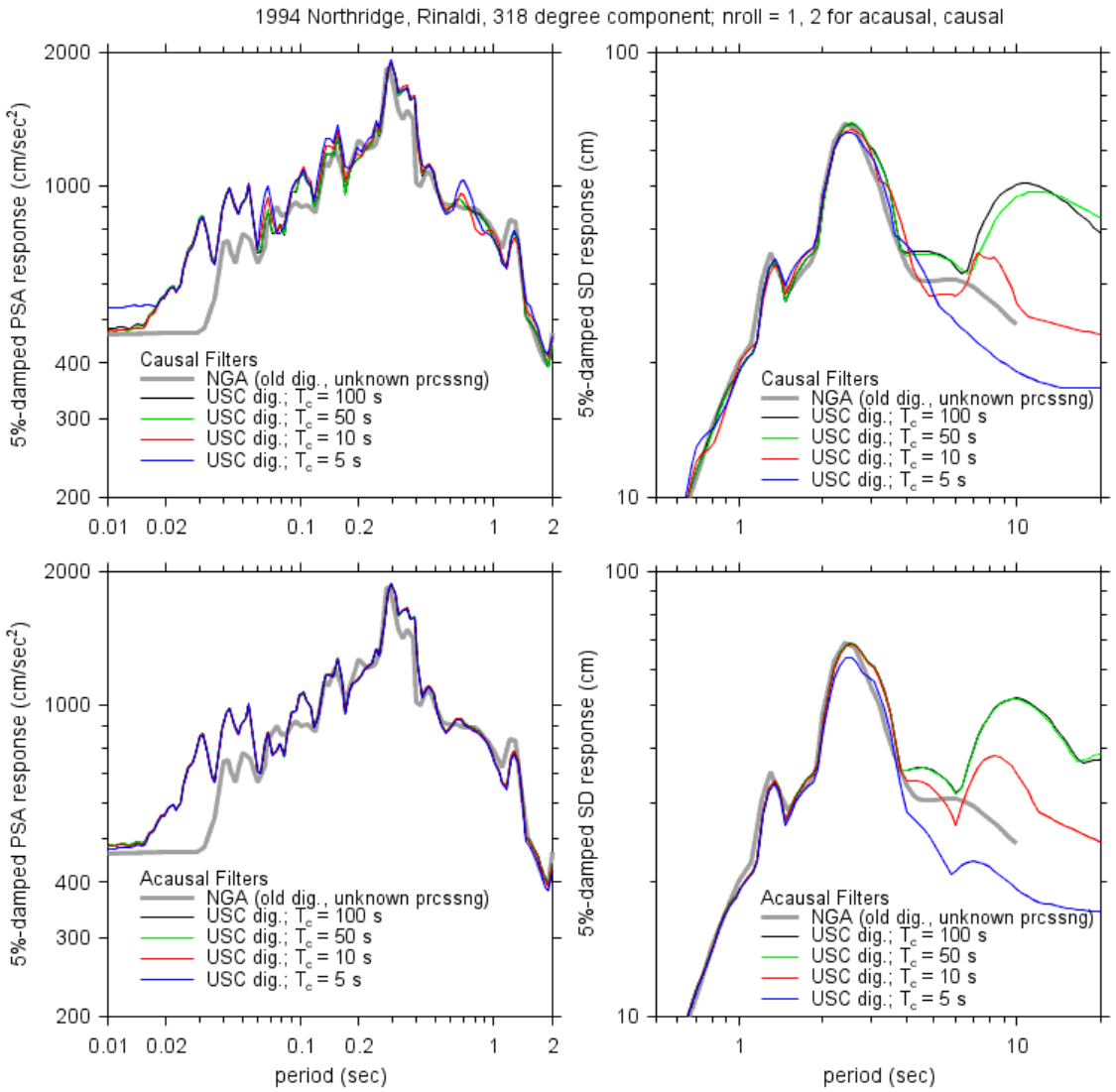

Fig. J.6 PSA and SD response, acausal and causal filters, as well as NGA spectra, for 318-degree component. Lowest order time-domain filters used.

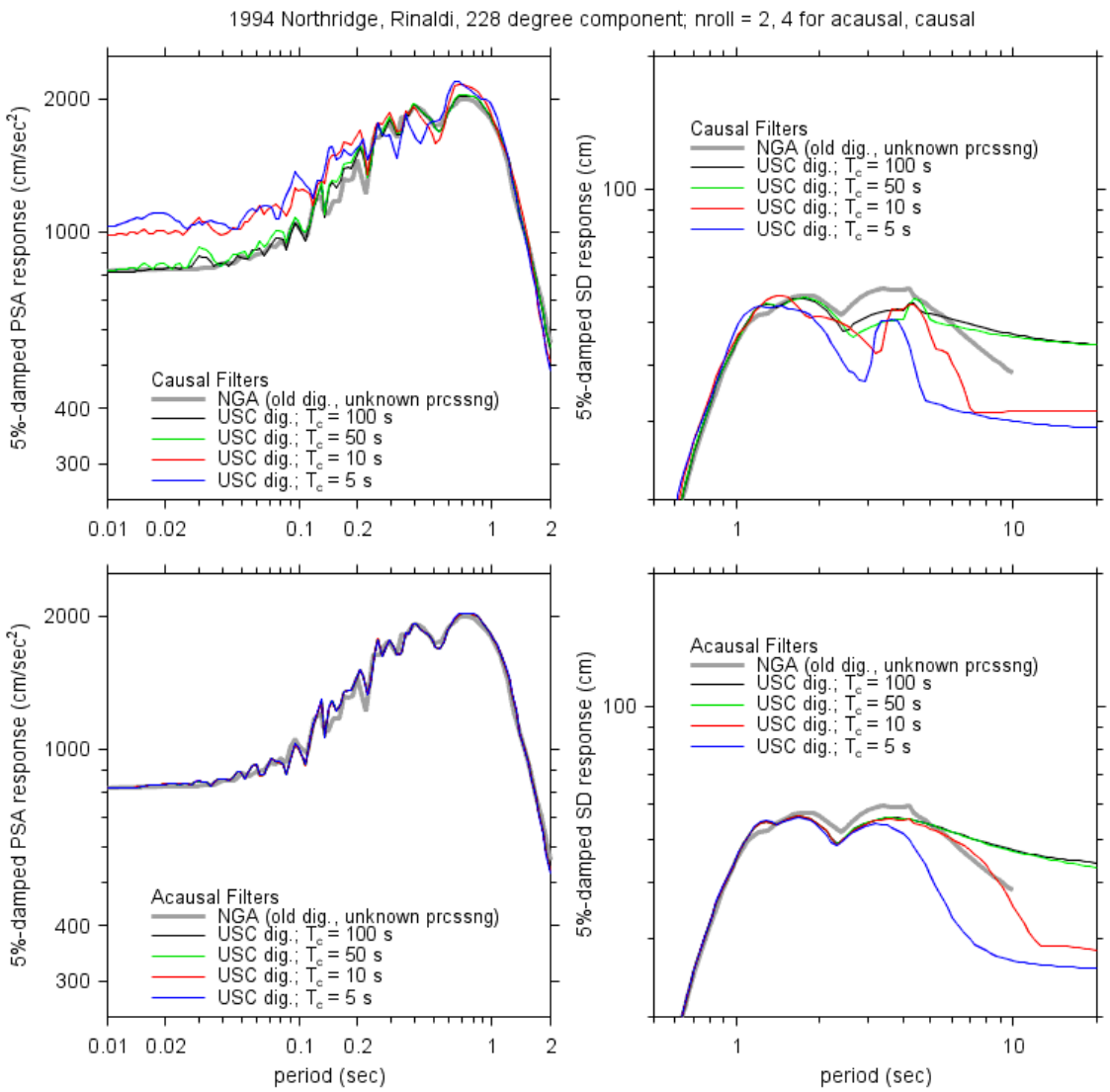

Fig. J.7 PSA and SD response, acausal and causal filters, as well as NGA spectra, for 228-degree component. Order of filters twice that used in previous two figures.

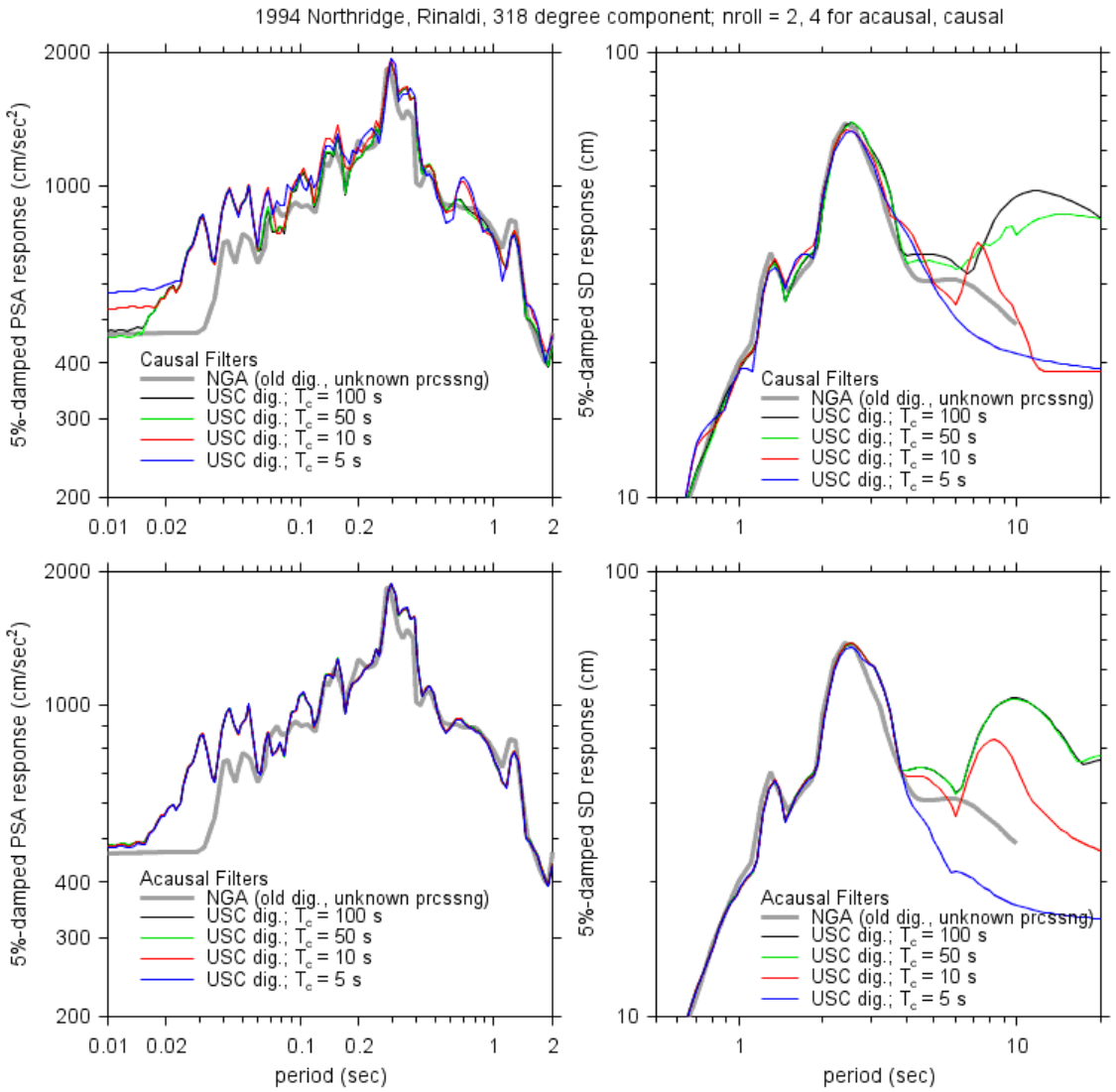

Fig. J.8 PSA and SD response, acausal and causal filters, as well as NGA spectra, for 318-degree component. Order of filters twice that used in Figs. 2.4–2.5.

Appendix K: Notes on 1999 Düzce Recordings

I noticed in the plots of events terms (Figs. K.1–K.3, updated from the figures that accompanied the original version of this note, 30 July 2005) that the Düzce event is low relative to the other strike-slip earthquakes for periods less than 5 s. This was also found by Ambraseys et al. (2005).

Figures K.4–K.9 show plots for three earthquakes with similar magnitude (corrected for site response to $V_{S30} = 760$ m/s, using the BJF97 site amplification factors—these plots were made before we settled on the site amplifications to be used in the BA07 NGA equations). It turns out that most of the Düzce $V_{S30} > 360$ m/s records are from the Lamont stations, and it was recognized earlier in the NGA project that the records from these stations seemed to be peculiar—but I cannot remember details. I've indicated the Lamont stations in the plots. Although there is little distance overlap in the Lamont versus other stations, the motions from the more distant stations for the Düzce earthquake seem low with respect to those from the other events, so perhaps there is nothing peculiar about the Lamont stations. For more information on shear-wave velocities at some stations that recorded the 1999 Düzce earthquake, see Rathje et al. (2003, 2004).

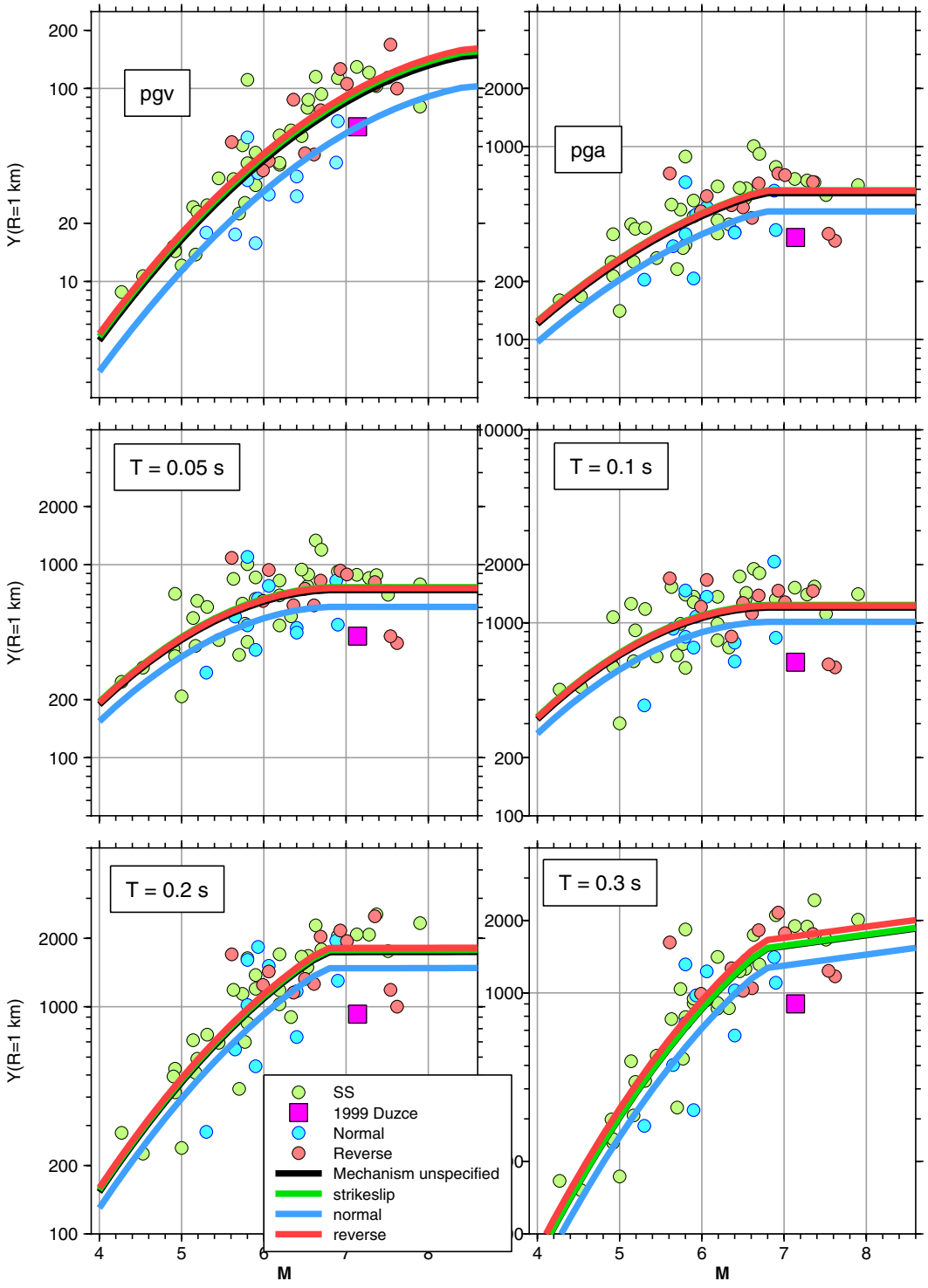

Fig. K.1 Event terms plotted against M. Same as Fig. 4.15(a), but with event term for 1999 Düzce earthquake identified.

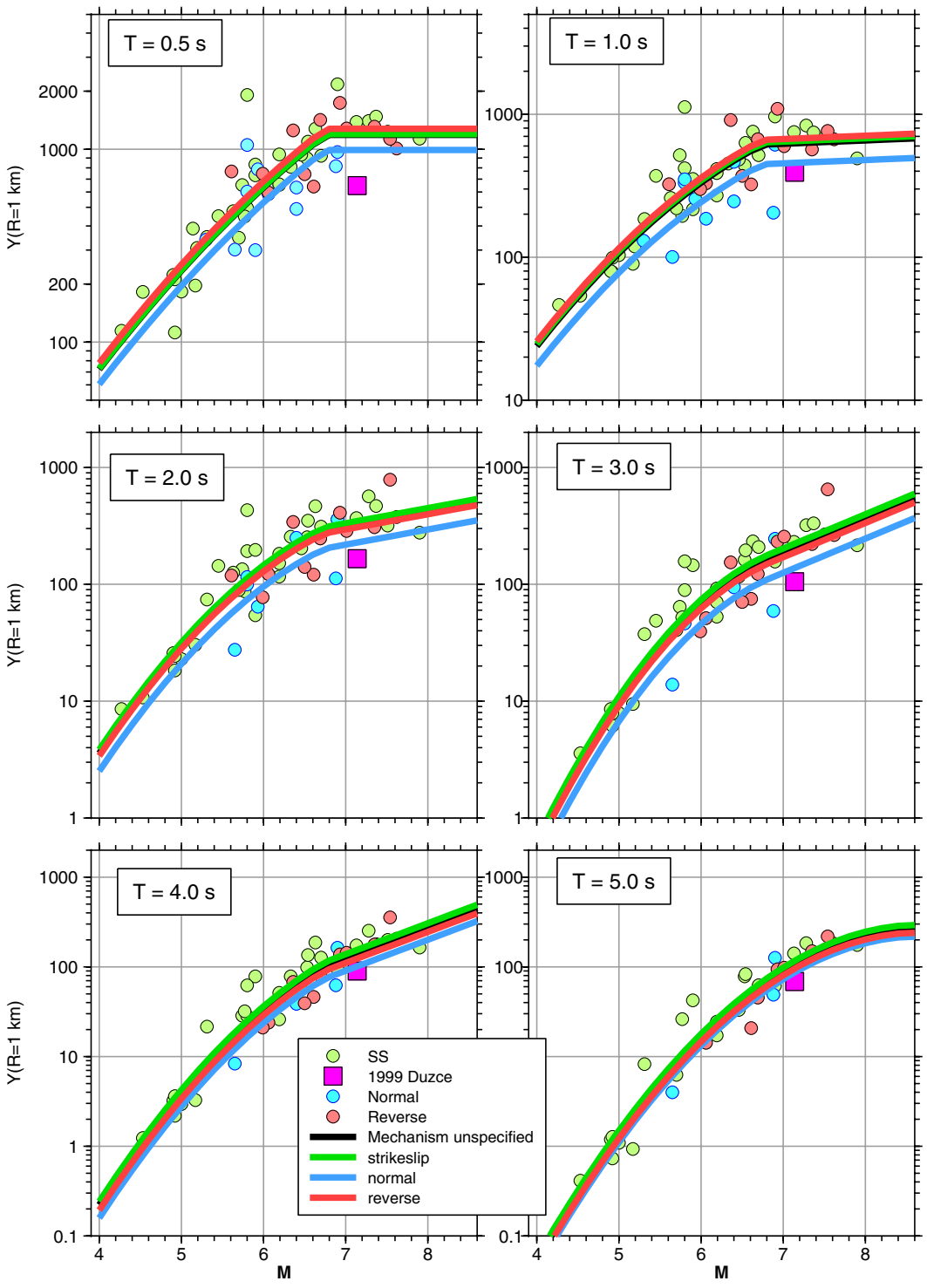

Fig. K.2 Event terms plotted against M. Same as Fig. 4.15(b) but with event term for 1999 Düzce earthquake identified.

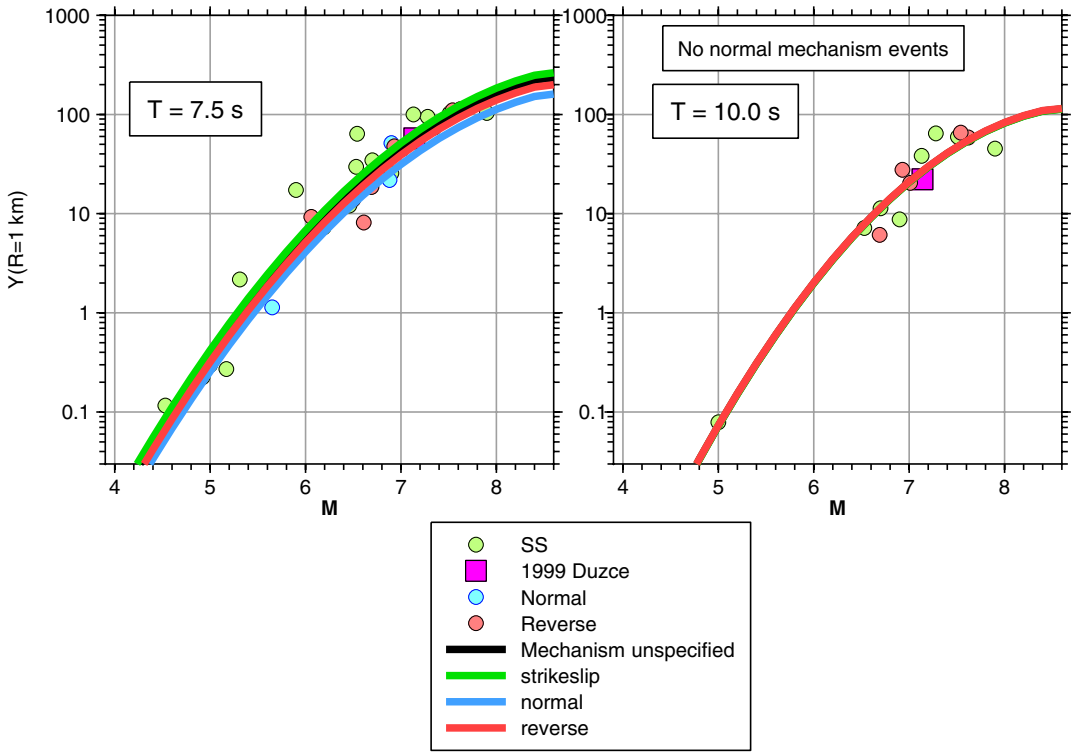

Fig. K.3 Event terms plotted against M. Same as Fig. 4.15(c), but with event term for 1999 Düzce earthquake identified.

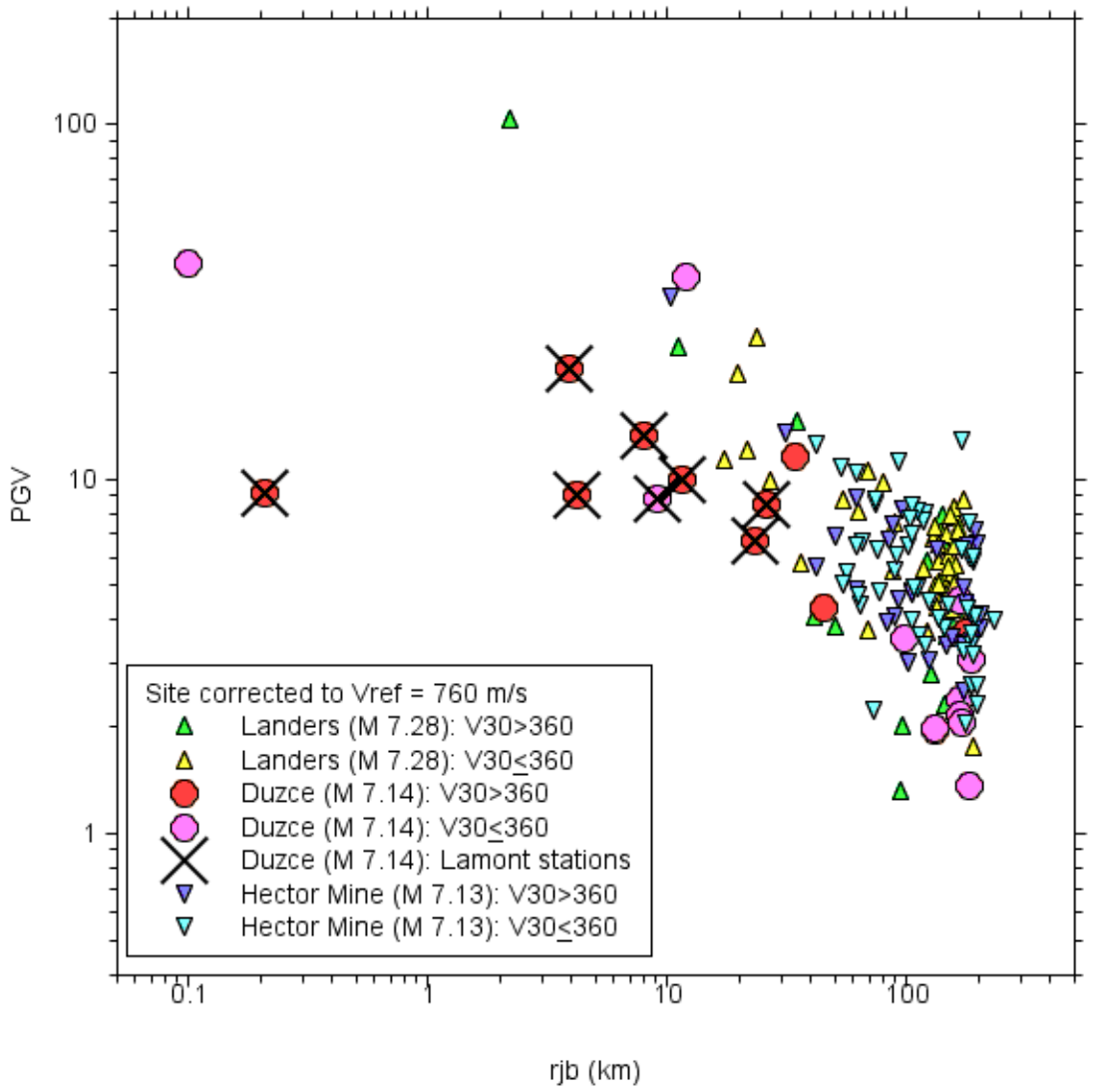

Fig. K.4 PGV (cm/s) vs. R_{JB} for several earthquakes of comparable magnitude. For Düzce earthquake, values from temporary Lamont stations shown by large crosses. Values from Düzce earthquake from all stations, not just Lamont stations, seem low compared to motions from other earthquakes.

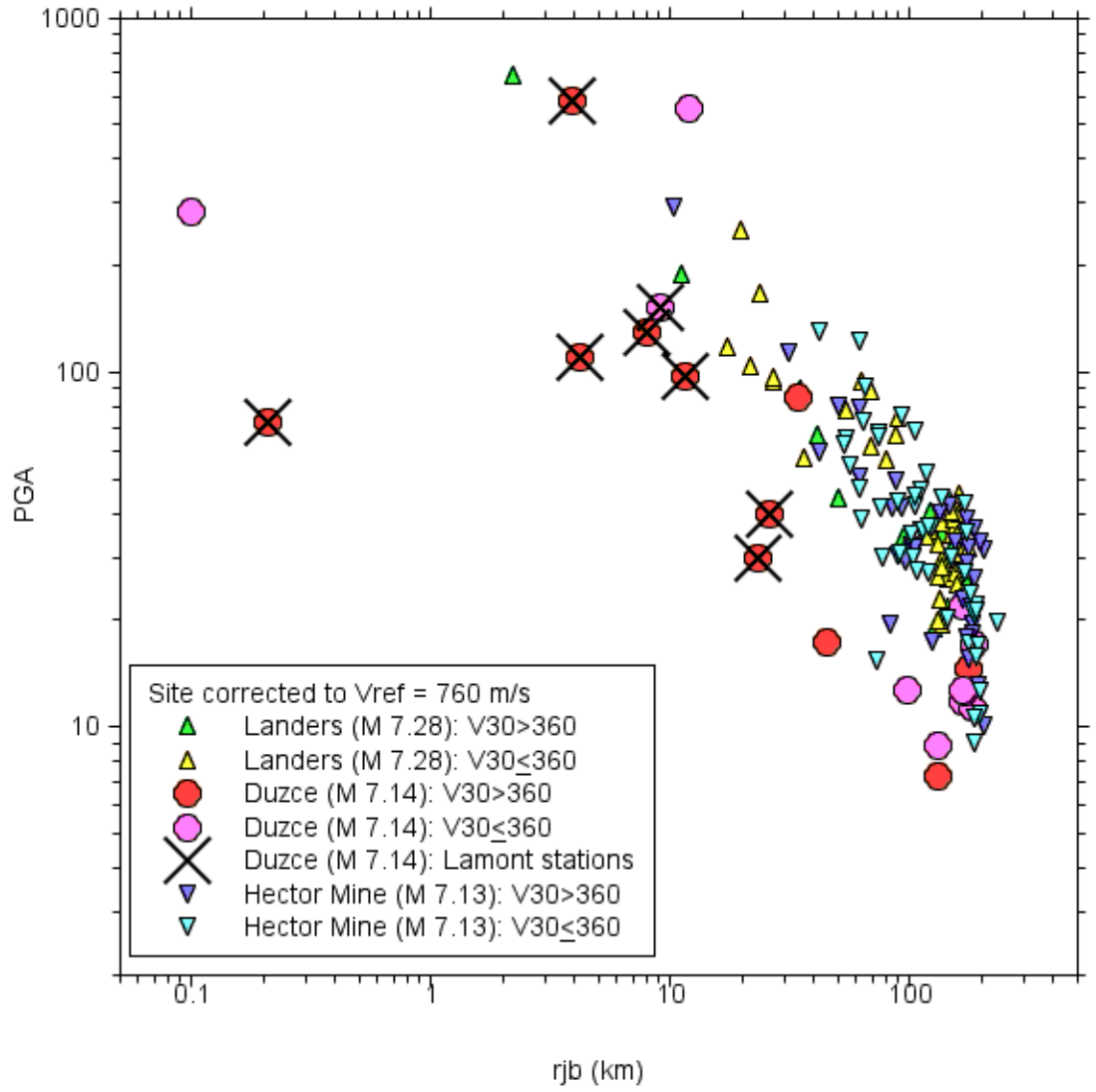

Fig. K.5 **PGA (cm/s/s) vs. R_{JB} for several earthquakes of comparable magnitude. For Düzce earthquake, values from temporary Lamont stations shown by large crosses. Values from Düzce earthquake from all stations, not just Lamont stations, seem low compared to motions from other earthquakes.**

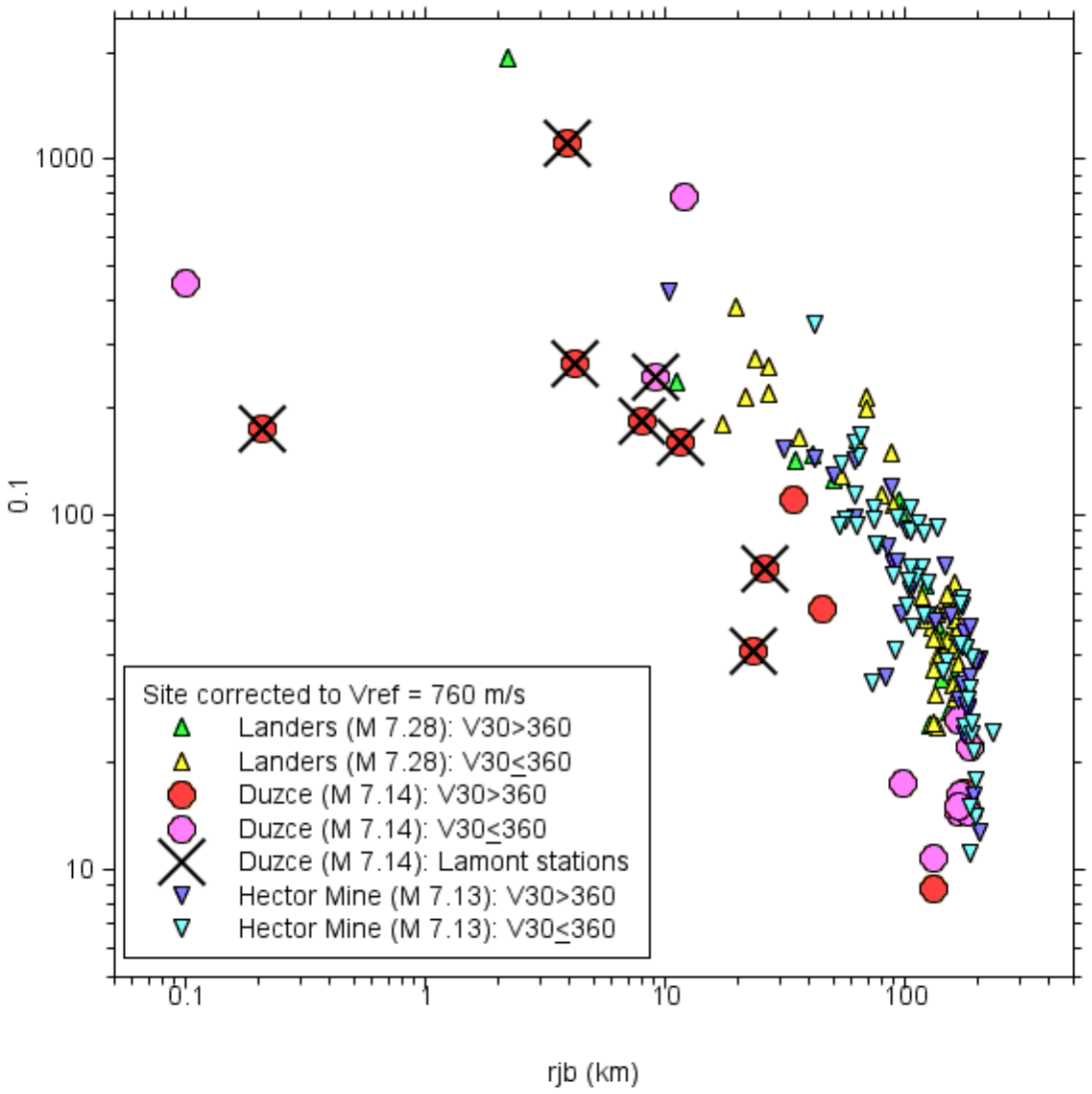

Fig. K.6 0.1 s PSA (cm/s/s) vs. R_{JB} for several earthquakes of comparable magnitude. For Düzce earthquake, values from temporary Lamont stations shown by large crosses. Values from Düzce earthquake from all stations, not just Lamont stations, seem low compared to motions from other earthquakes.

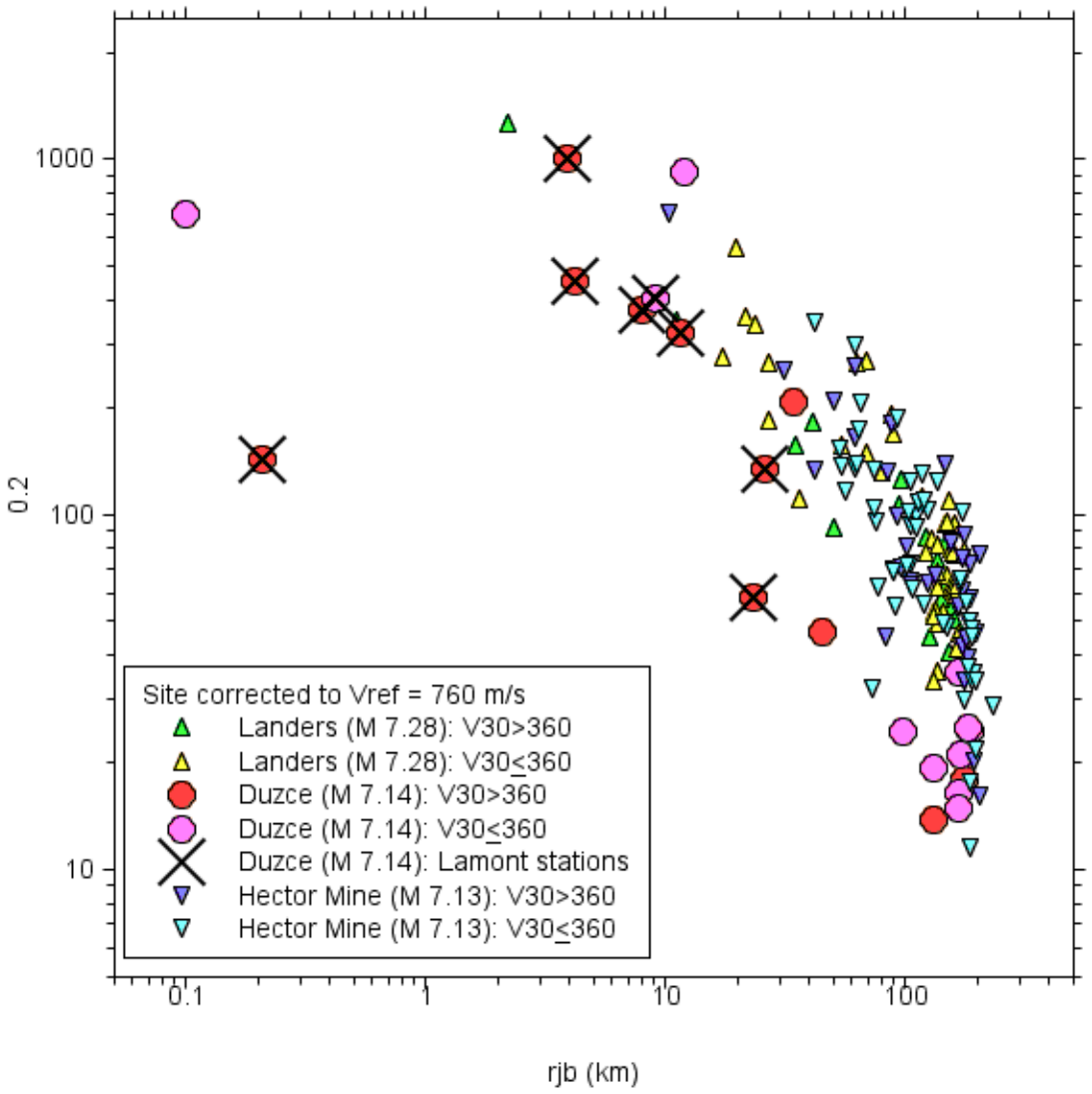

Fig. K.7 0.2 s PSA (cm/s/s) vs. R_{JB} for several earthquakes of comparable magnitude. For Düzce earthquake, values from temporary Lamont stations shown by large crosses. Values from Düzce earthquake from all stations, not just Lamont stations, seem low compared to motions from other earthquakes.

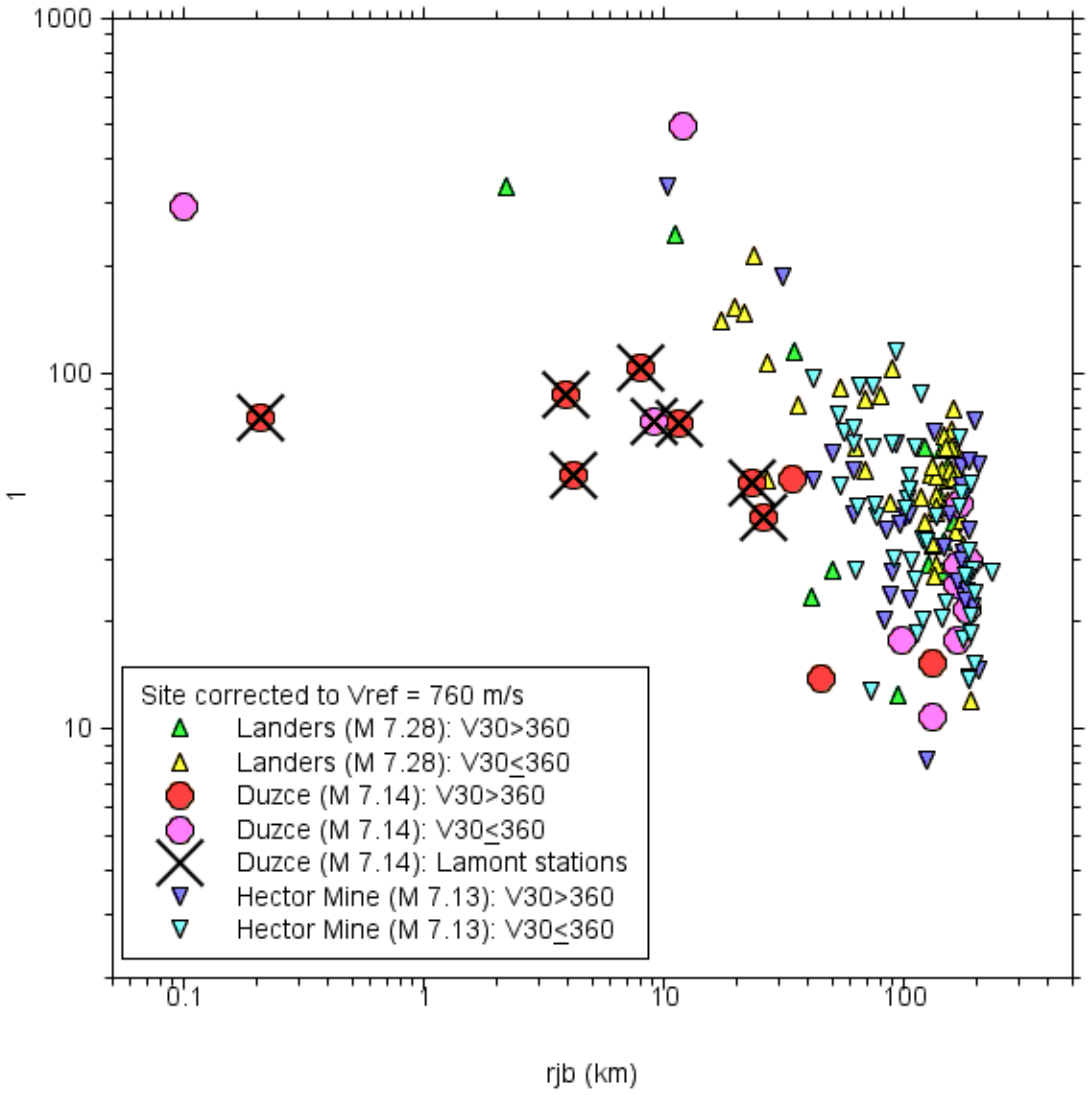

Fig. K.8 1.0 s PSA (cm/s/s) vs. R_{JB} for several earthquakes of comparable magnitude. For Düzce earthquake, values from temporary Lamont stations shown by large crosses. Values from Düzce earthquake from all stations, not just Lamont stations, seem low compared to motions from other earthquakes.

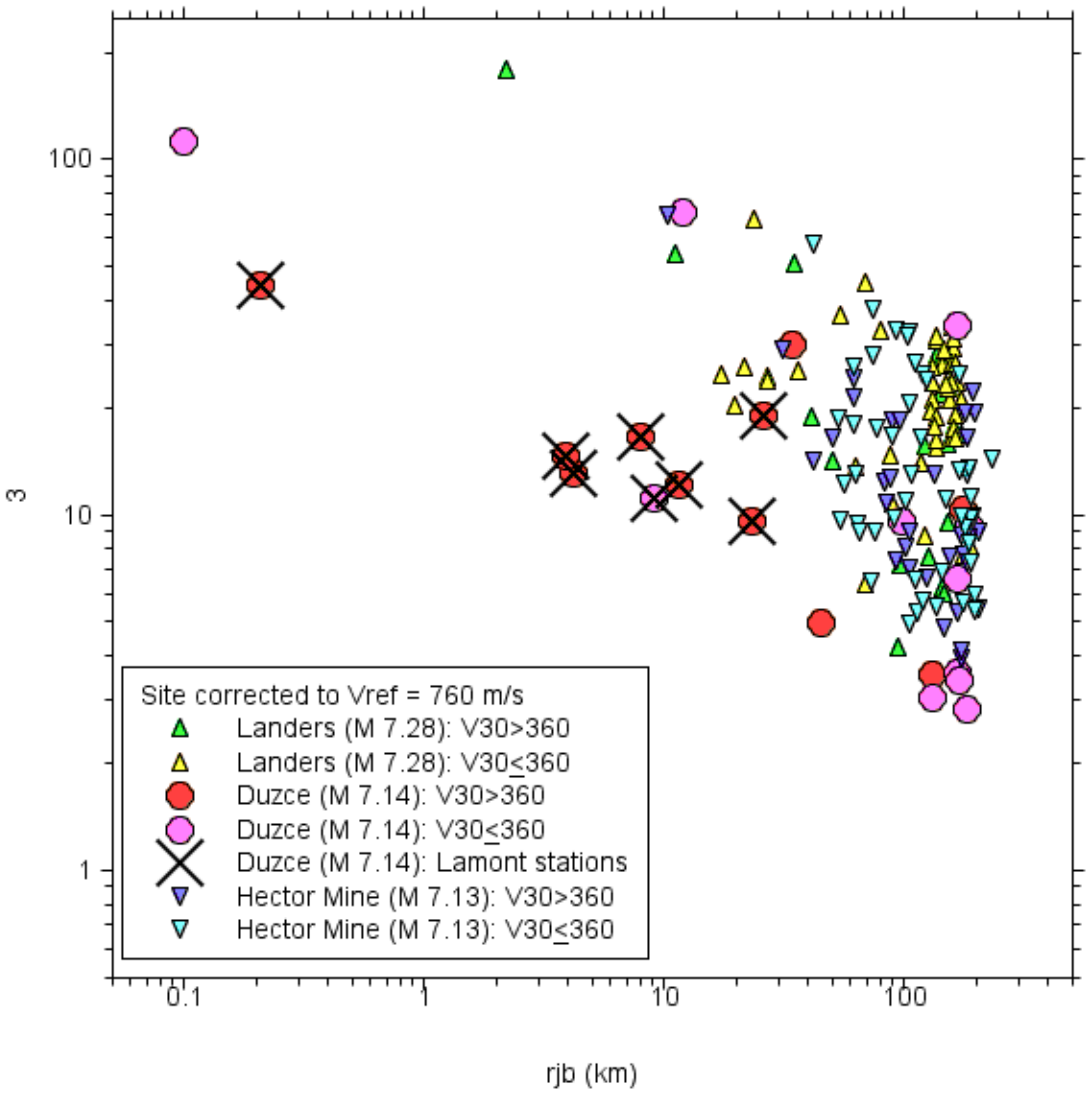

Fig. K.9 3.0 s PSA (cm/s/s) vs. R_{JB} for several earthquakes of comparable magnitude. For Düzce earthquake, values from temporary Lamont stations shown by large crosses. Values from Düzce earthquake from all stations, not just Lamont stations, seem low compared to motions from other earthquakes.

Appendix L: Notes Regarding Record Obtained at Pump Station 10 from 2002 Denali Fault Earthquake

At Workshop 7 Walt Silva asked me about the Pump Station 10 record of the 2002 Denali fault earthquake. There was some confusion about what version of the record was used in the NGA database. Here is a short history of the record, as I know it. When first put on the USGS NSMP website (http://nsmp.wr.usgs.gov/), there was a statement that the hardware low-cut filter was at a very low frequency, on the order of 0.01 Hz. But then it was discovered that the hardware filter was actually about 0.1 Hz. The statement on the website, as shown below, has been changed. The changes are indicated by italics.

> Revised information about the nominal filter characteristics, as determined from an analysis of a circuit diagram for the filter. *Note in particular that the highpass corner is at 0.1 Hz, not 0.01 Hz* as was indicated in the files originally provided by Alyeska, *and that the highpass and lowpass filters each have 2 poles rather than 1.* Details of the nominal filter characteristics are provided in the headers.
> Due to uncertainties in the instrument response, *only uncorrected acceleration time series data are currently being served.* Results from bench tests using components similar to those deployed in the field show deviations from nominal characteristics that could produce variations of up to 20% in displacements determined by double integration of the acceleration time series. The USGS is working with Alyeska to determine more accurate calibrations, and any new information will be released as soon as it is available.

Bill Ellsworth applied a correction for the instrument filter and used this in his recent *Earthquake Spectra* paper (Ellsworth et al., 2004). His corrected data can be obtained from ftp://clover.wr.usgs.gov/pub/ehz/PS10/. I reformatted his corrected version of the data into the standard USGS NSMP SMC format. When integrating to velocity and displacement. I discovered some drifts that were easy to remove by applying a simple "v0" baseline correction (details are in the headers of the smc files, available from me). Figure L.1 is a plot of the acceleration, velocity, and displacement for the three components of motion. Figure L.2 is a plot of the geometric mean PSA and SD compared to the spectrum from the NGA flatfile. As can be seen most readily from the SD plot, there are significant differences between the NGA spectrum

(as contained in the flatfile available on 07 December 2004) and that from the instrument-filter, baseline-corrected data, the latter being higher at short and long periods. Note that the difference at long periods starts at about 6 s, so it is probably important to replace the spectrum in the flatfile with the new spectrum. The difference is in the direction expected if the NGA values are based on the uncorrected data (email from W. Silva subsequent to this confirmed my suspicions). The difference at short periods might be due to the use of a causal high-pass filter by NGA—Boore and Akkar (2003) show the surprising result that causal filters can affect short-period motions, at periods much shorter than the filter corner period. This has been confirmed in studies of a number of other records. The geometric means of the PGA are as follows: NGA: 0.316g; Dave: 0.346g. And for PGV: NGA: 85 cm/s; Dave: 128 cm/s. The difference in PGV might be explained by the use of a 0.1 high-pass filter in the data (or are the filter characteristics in the flatfile simply reporting the hardwired instrument filter? Was an additional filter applied by Walt?)

An issue not discussed by the group is that the geometric means of the two horizontal components is not invariant under rotation. This may become important when the developers are studying fault-parallel and fault-normal motions. At the time that the material in this appendix was originally prepared, I had not seen a systematic study of the dependence of geometric mean on rotation, For that reason, I was the lead author in developing a measure of strong ground motion that is independent of instrument orientation (Boore at al., 2006). For the interest of the reader, I show in Figure L.3 the acceleration, velocity, and displacement traces for the motions after rotating into fault-normal and fault-parallel directions. Figure L.4 shows the PSA and SD response spectra for the fault-normal and fault-parallel direction; note that the fault-normal spectrum exceeds the fault-parallel spectrum for the period range from about 2 s to 20 s, after which the large residual displacement in the fault-parallel direction produces a much larger response spectrum. Both the time series and the response spectra show that the character of the waveforms can depend strongly on instrument orientation, particularly at longer periods. For that reason, there can be significant differences in the geometric-mean spectra for different orientations, as shown in Figure L.5.

In summary, the NGA flatfile entries for Pump Station 10 are based on data uncorrected for the hardware instrument filter. Using corrected data leads to differences in the PGA, PGV, and PGD values, as well as short- and long-period response spectra. In addition, as a side issue I show that there can be substantial differences in the geometric mean computed from unrotated

and rotated horizontal components. This might be important in studies of fault-normal and fault-parallel motions.

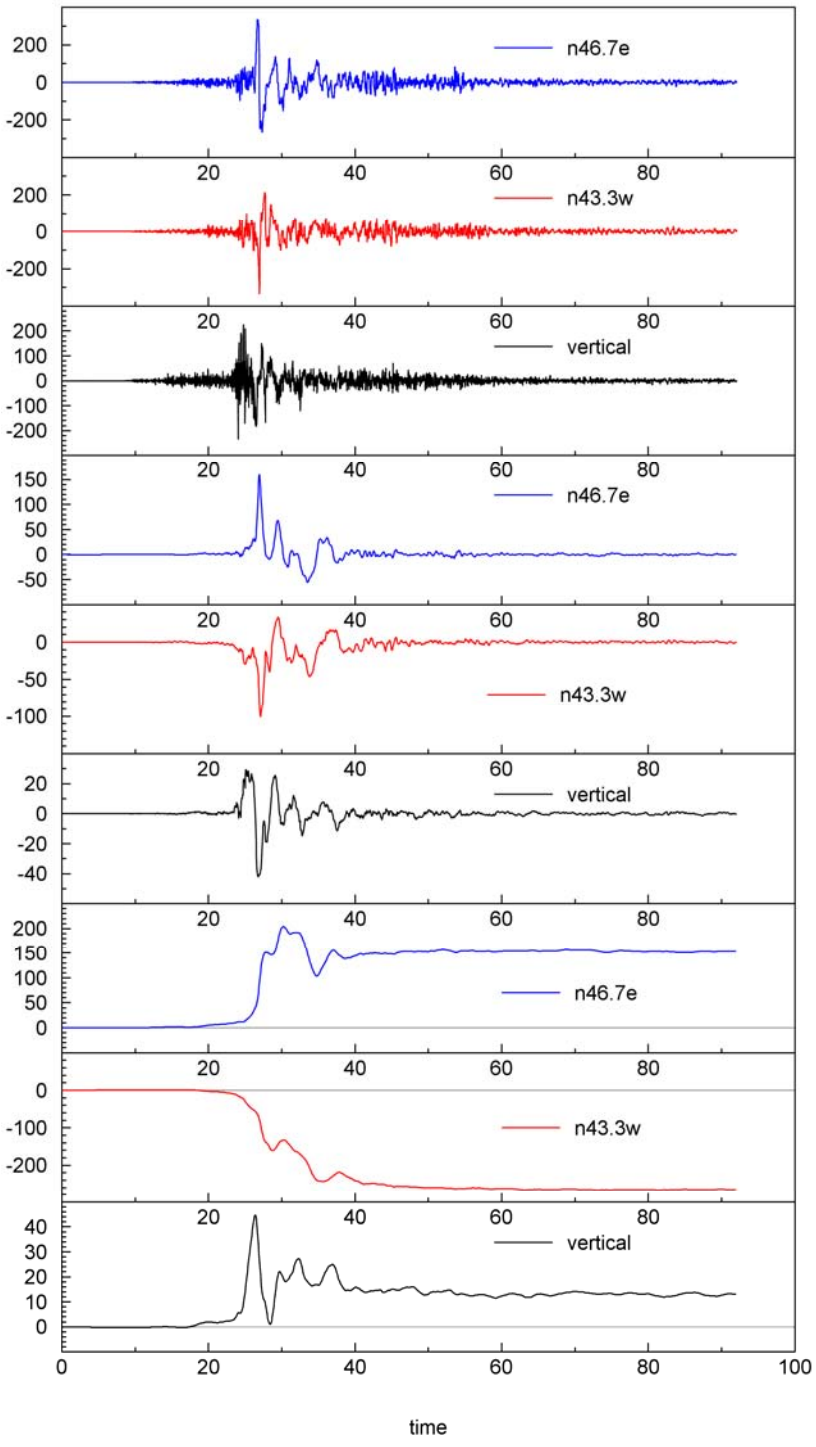

Fig. L.1 Pump Station 10 data from 2002 Denali fault earthquake (from Ellsworth), reprocessed using "V0" baseline correction.

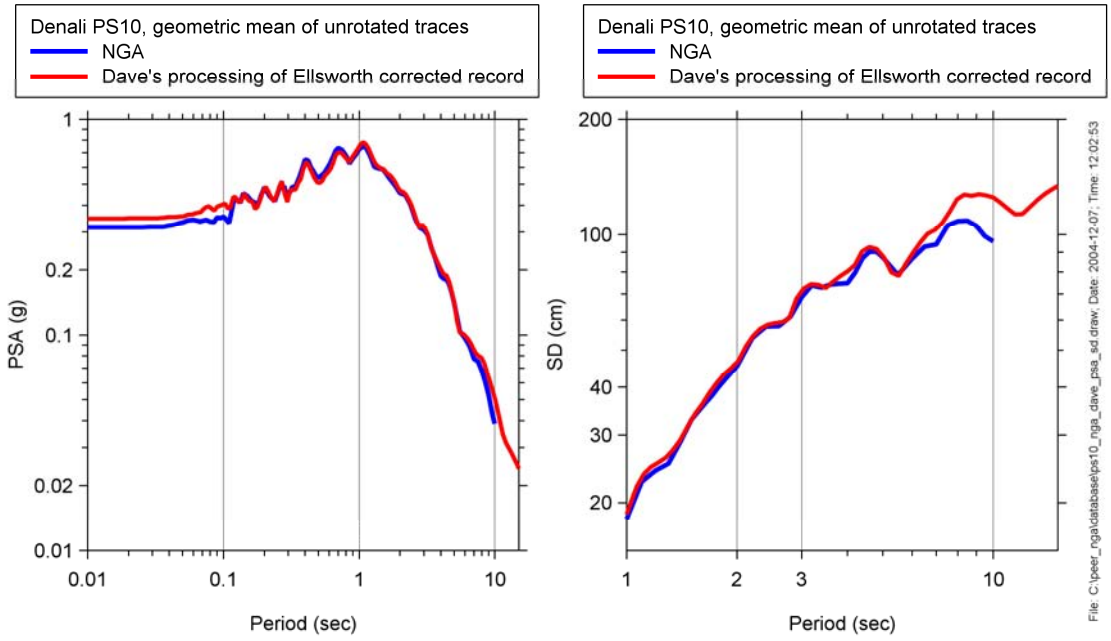

Fig. L.2 Comparison of NGA and D. Boore's PSA for Pump Station 10 data from 2002 Denali fault earthquake (from Ellsworth), reprocessed using "V0" baseline correction.

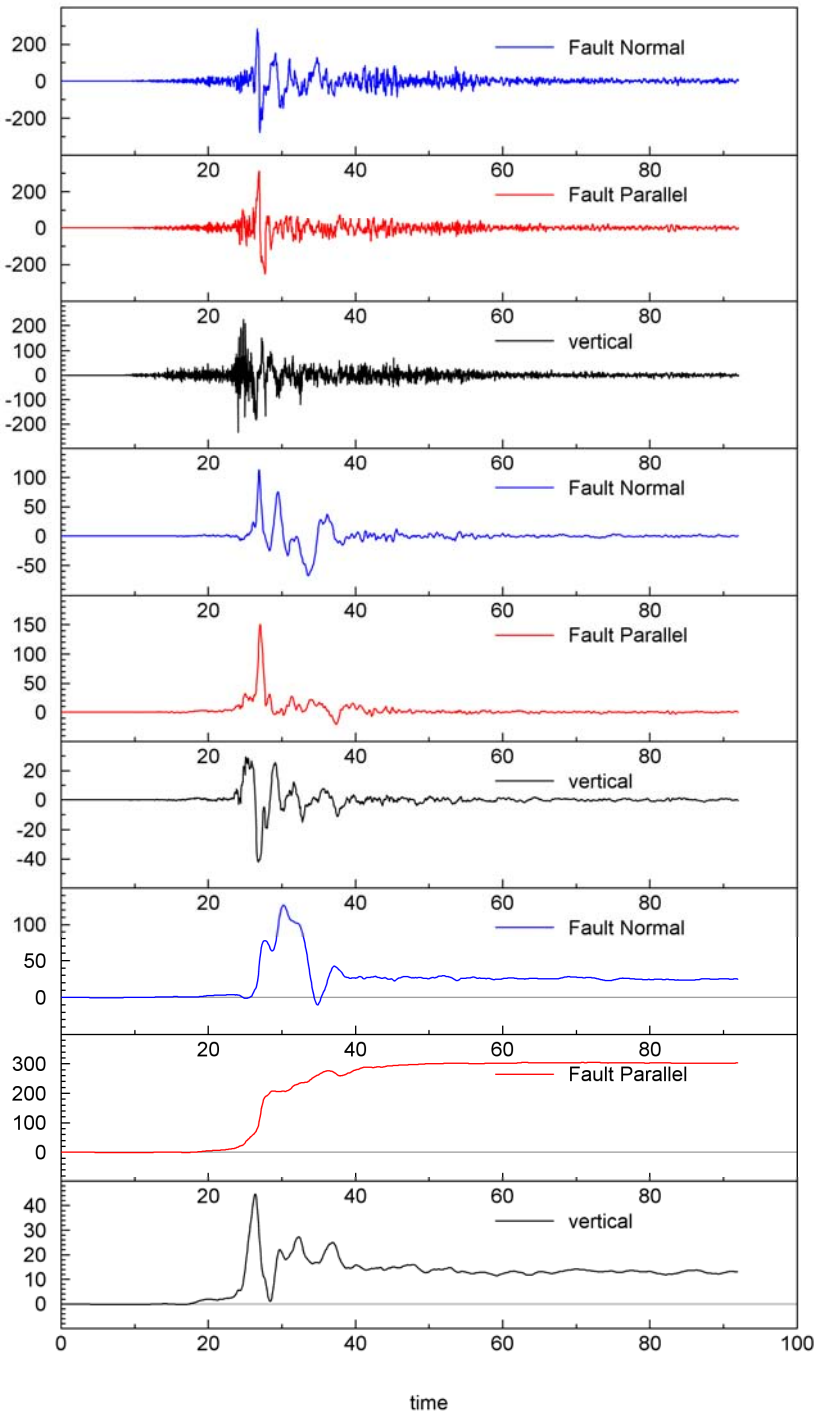

Fig. L.3 Pump Station 10 data from 2002 Denali fault earthquake (from Ellsworth), reprocessed using "V0" baseline correction and rotated into fault-normal and fault-parallel directions.

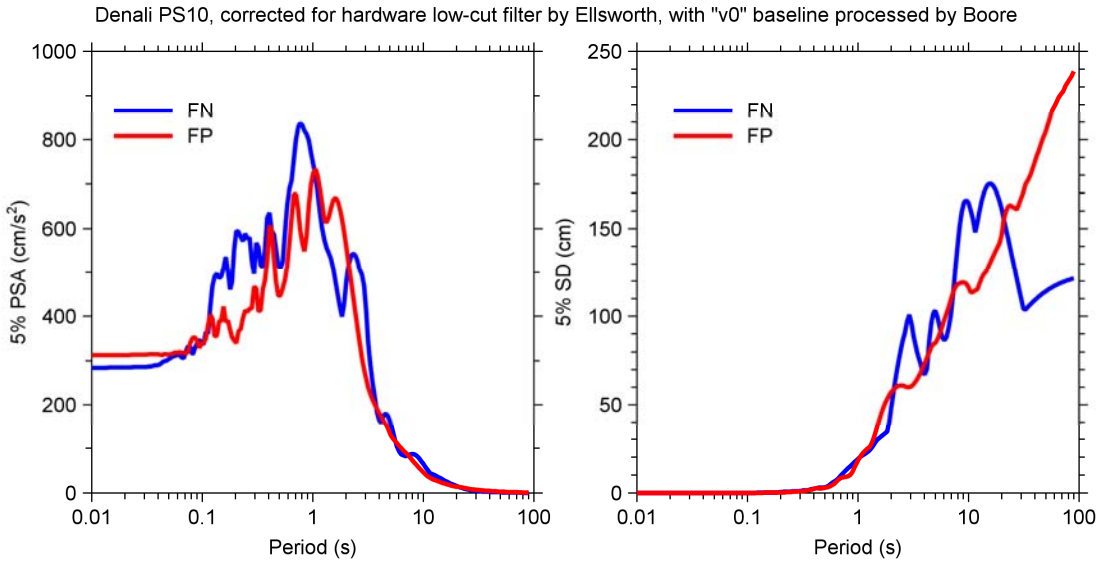

Fig. L.4 PSA and SD for Pump Station 10 data from 2002 Denali fault earthquake (from Ellsworth), reprocessed using "V0" baseline correction and rotated into fault-normal and fault-parallel directions.

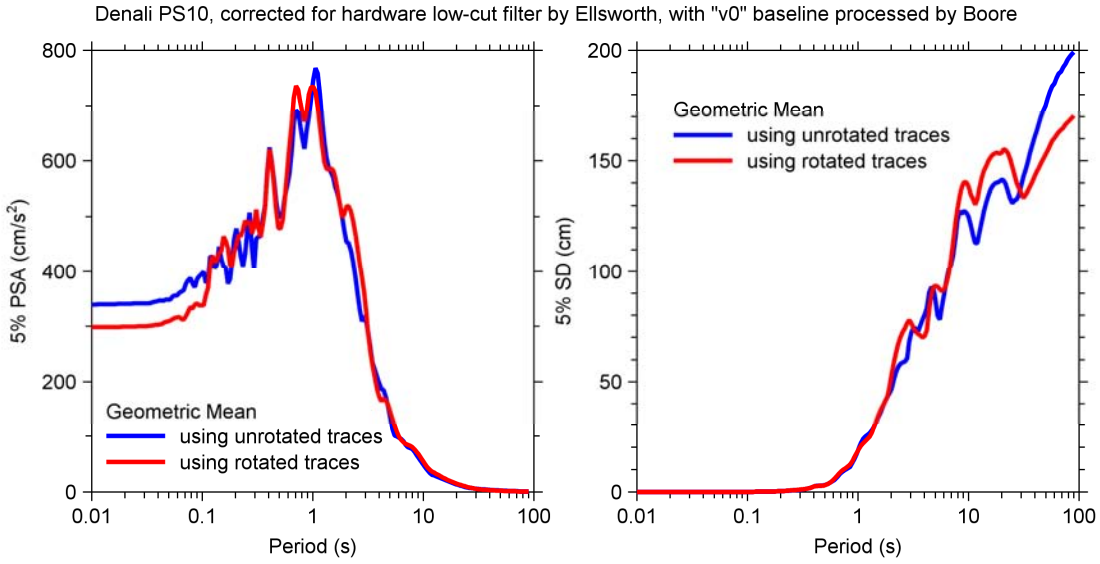

Fig. L.5 PSA and SD from geometric means of unrotated and rotated traces for Pump Station 10 data from 2002 Denali fault earthquake (from Ellsworth), reprocessed using "V0" baseline correction.

Appendix M: Magnitudes for Big Bear City and Yorba Linda Earthquakes

In a presentation given at an NGA developers workshop on 12 April 2005, I showed that the data from the 2002 Yorba Linda earthquake were systematically smaller than for other earthquakes with magnitudes near the M 4.8 given for the event in the then-current NGA flatfile. Ken Campbell's event terms from his regression confirmed this. Soon after the workshop, I came across the paper by Komatitisch et al. (2004), in which they model long-period (greater than 6 s) displacements for the event, using **M** = 4.2 rather than 4.8. They do not state how they obtained **M** for the event, but I imagine it is based on their modeling (and the method of Liu et al. 2004). As shown previously (Fig. 4.34), the ground motions from the Yorba Linda earthquake are lower than for the Anza and Big Bear City earthquakes (whose magnitudes in the flatfile are 4.92 and 5.0, respectively). Clearly, the Yorba Linda event is smaller than the other two. In addition, the attenuation with distance seems to be different for Yorba Linda than for the other two at shorter periods. In the original notes on this subject, I showed a comparison with an earlier version of the BA equations determined assuming that the magnitude of the Yorba Linda earthquakes was 4.8. I pointed out that the magnitude scaling from these earlier GMPEs gave an offset between the Yorba Linda and the other two events similar to the offset of the observations in Figure 4.34 if Komatitisch et al.'s (2004) magnitude was correct. On this basis I suggested that the magnitude for the Yorba Linda earthquake be lowered. I also pointed out that the Liu et al. (2004) paper gives **M** = 4.92 and depth = 6.3 km for the 22 February 2003 Big Bear City earthquake. The NGA flatfile gives **M** = 5.0 and 1.2 km for that event. I suggested that the flatfile values should be changed, and this was done. Some indication that the magnitudes are correct is given in Figures M.1–M.3, in which I compare the observations from the three earthquakes with simulations using the Joyner (1984) source model and the Raoof et al. (1999)

path function. The comparison is quite good considering that no effort was made to adjust the parameters of the simulation to fit the observations.

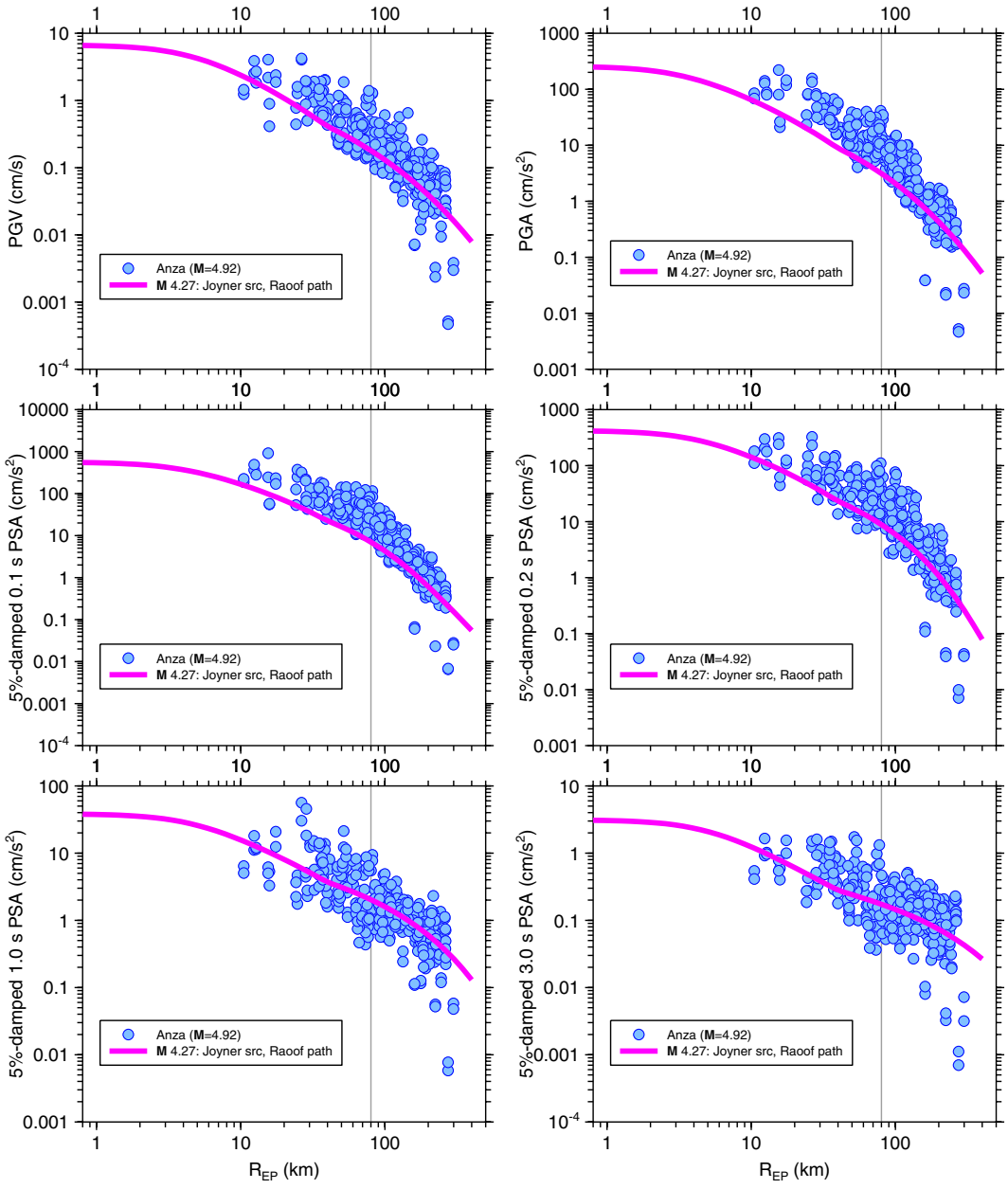

Fig. M.1 Ground motions from Anza earthquake, with simulated motions (using Joyner (1984) source model and path model from Raoof et al. (1999)).

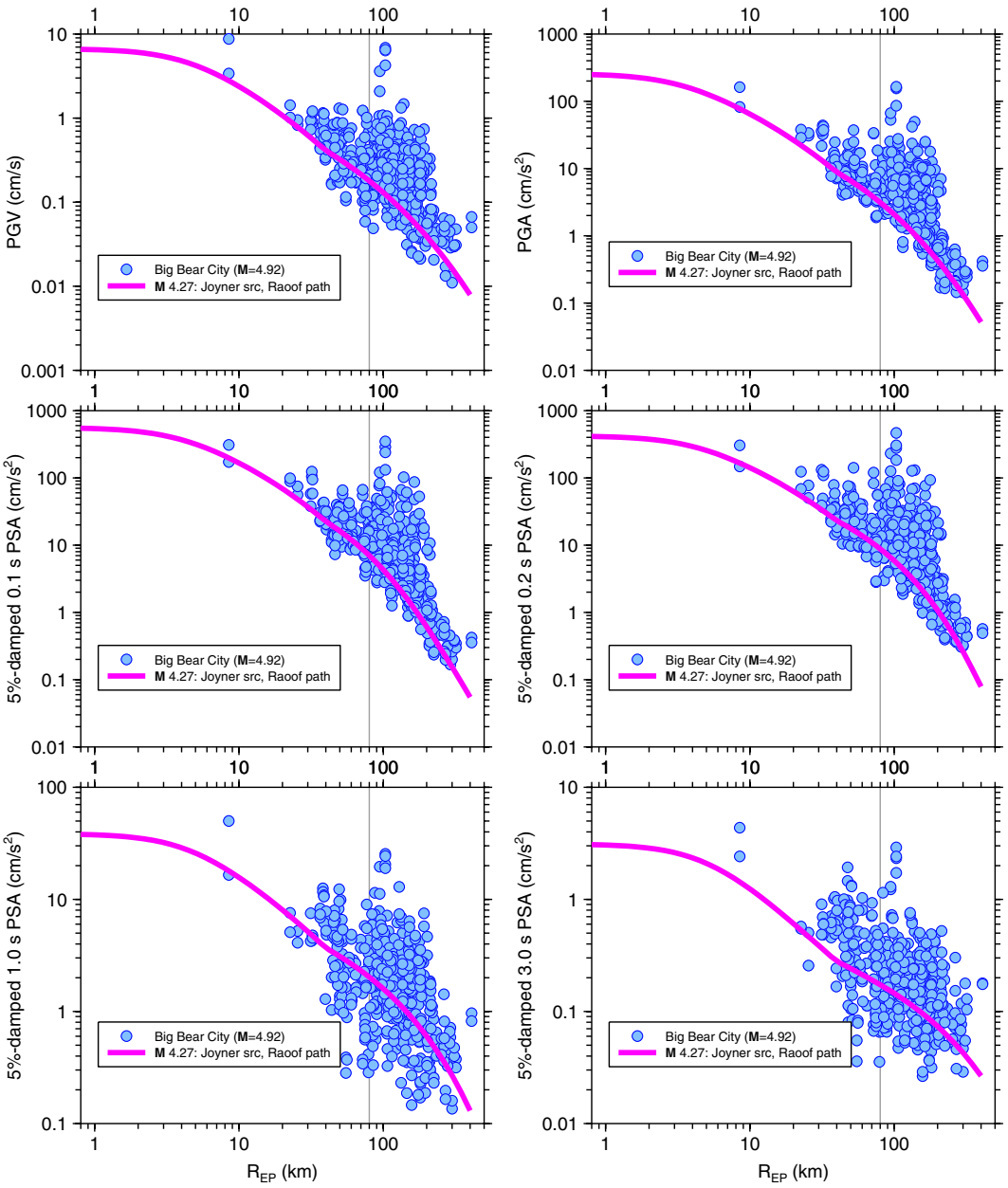

Fig. M.2 Ground motions from Big Bear City earthquake, with simulated motions (using Joyner (1984) source model and path model from Raoof et al. (1999)).

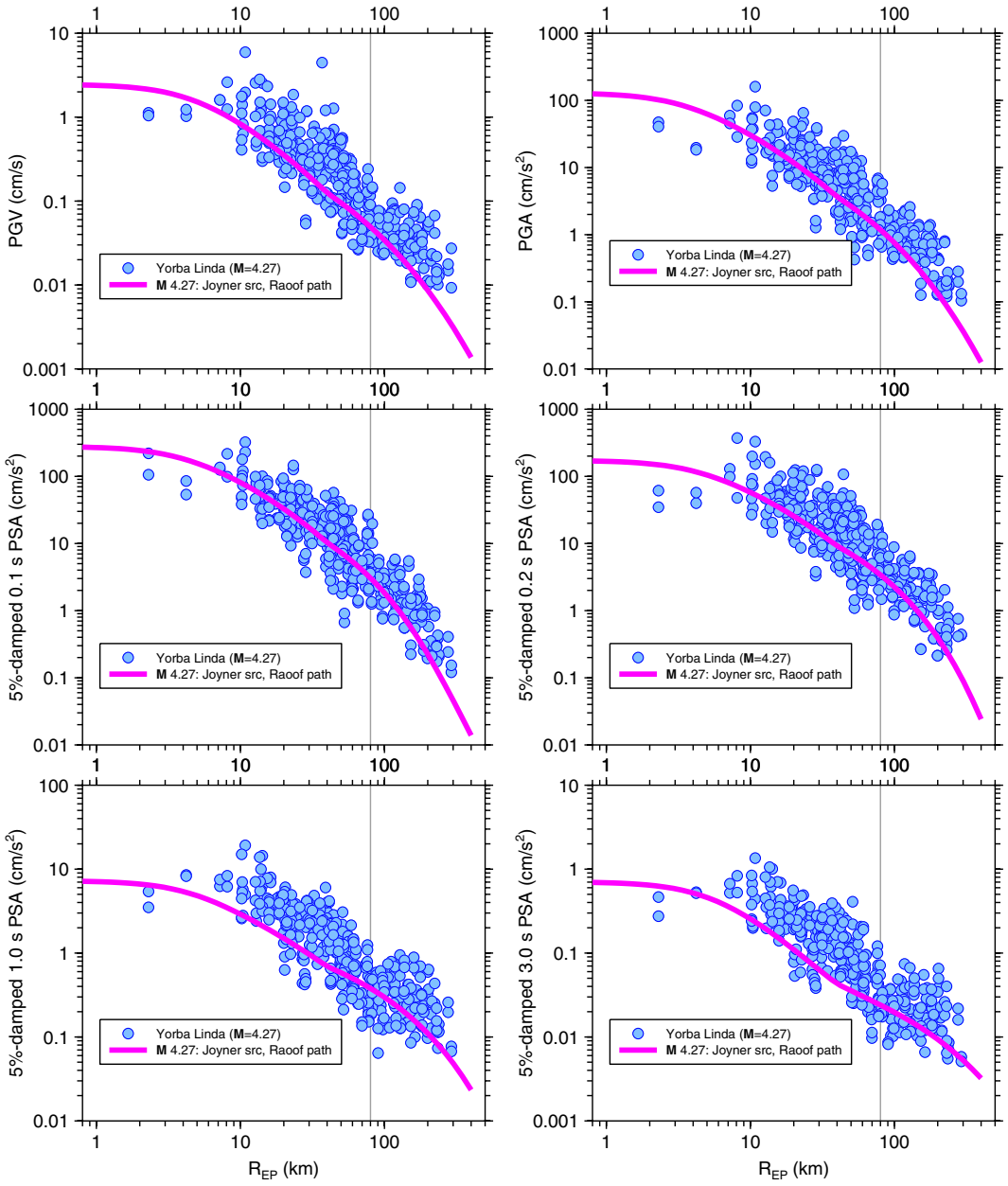

Fig. M.3 Ground motions from Yorba Linda earthquake, with simulated motions (using Joyner (1984) source model and path model from Raoof et al. (1999)).

Appendix N: Comparison of Ground Motions from 2001 Anza, 2002 Yorba Linda, and 2003 Big Bear City Earthquakes with 2004 Parkfield Earthquake

In the course of the NGA project, there was some discussion regarding the validity of the non-strong-motion source data for the three small earthquakes. The data for the three small events were gathered by Linda Seekins for Jack Boatwright. According to an email from her to me on 15 September 2005, "*All of the data from the Anza earthquake that I generated for Jack from the SCEC database was from the HLE and HLN recorders. They are low gain. accelerographs."* I understand from conversations with Linda that this is also true for the other two small events; thus no velocity sensor data from these three earthquakes were used in the analyses in this report. It is unfortunate that the extended data sets for the three small earthquakes were not included in the NGA flatfile; just because the data don't come from the USGS or CGS strong-motion groups does not make the data any different. According to the SCSN website (http://www.trinet.org/instr.html#analogvsdig), the accelerograph data come from K2 accelerographs.

One way of judging whether there is anything peculiar about the motions is to compare plots of the motions against distance with motions from the 2004 Parkfield earthquake from traditional (with one exception) strong-motion stations (many more data from non-traditional sources are available for the Parkfield earthquake, but I have not obtained those data). These comparisons are shown in Figures N.1–N.3 for PGV, PGA, and 5%-damped PSA for 0.1, 0.2, 1.0, and 3.0 s. The distance for the Parkfield earthquake is R_{JB} and for the others is R_{EP}. No site correction has been applied to the Parkfield data, but the data for the other quakes have been corrected to $V_{S30} = 760$ m/s using BJF97 amp factors (no nonlinear correction). The ground-

motion intensity measures from the two horizontal components have *not* been merged—the plots show both the intensity measures for both components for each station.

I see nothing strange in the distance decay of the three smaller events compared to the Parkfield data, although it is interesting to note that the level of motions at high frequency for the Anza and Big Bear City earthquakes is comparable to that from the larger Parkfield earthquake, although the magnitudes are quite different.

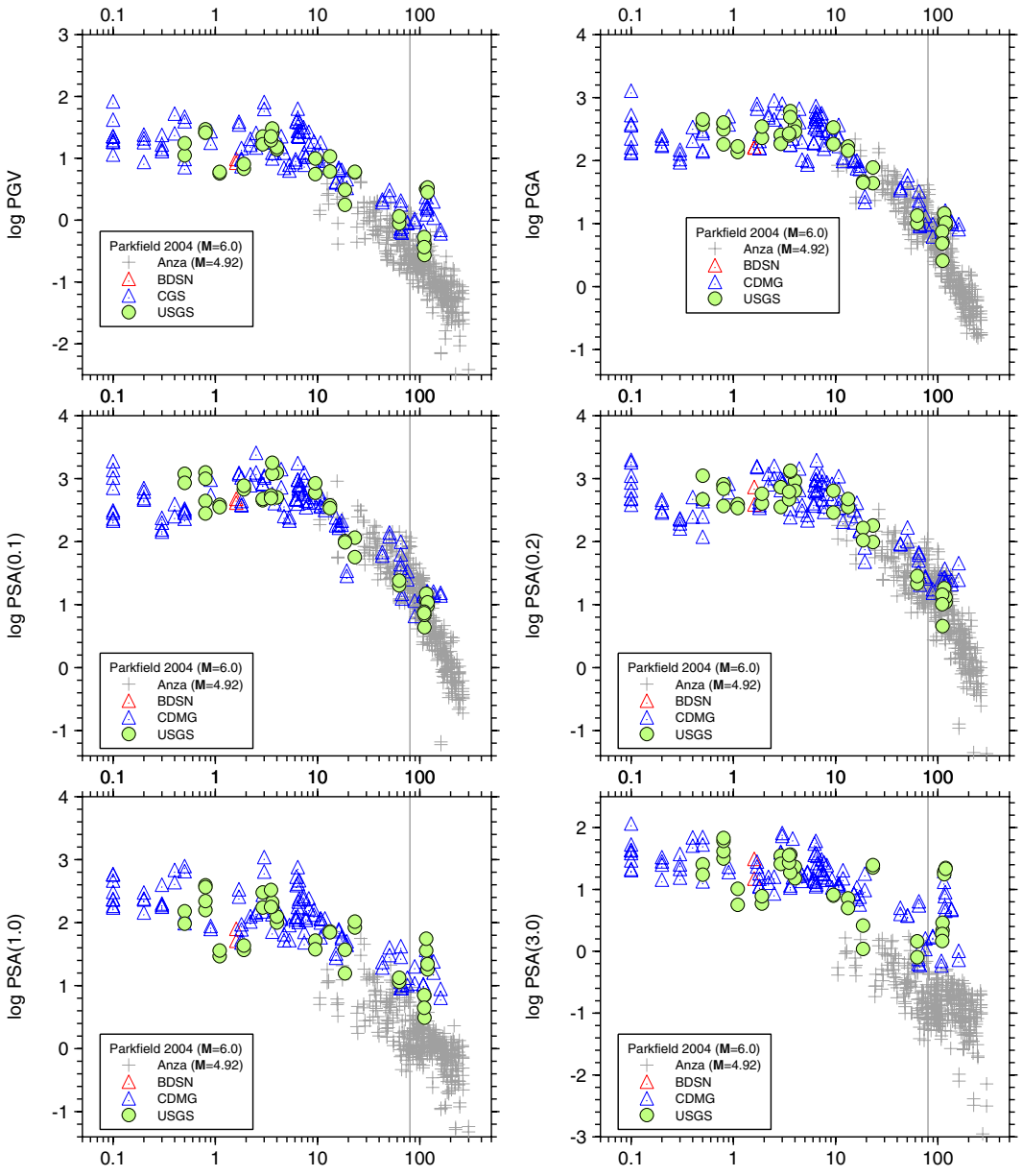

Fig. N.1 Ground motions from 2004 Parkfield earthquake compared to ground motions from smaller Anza earthquake.

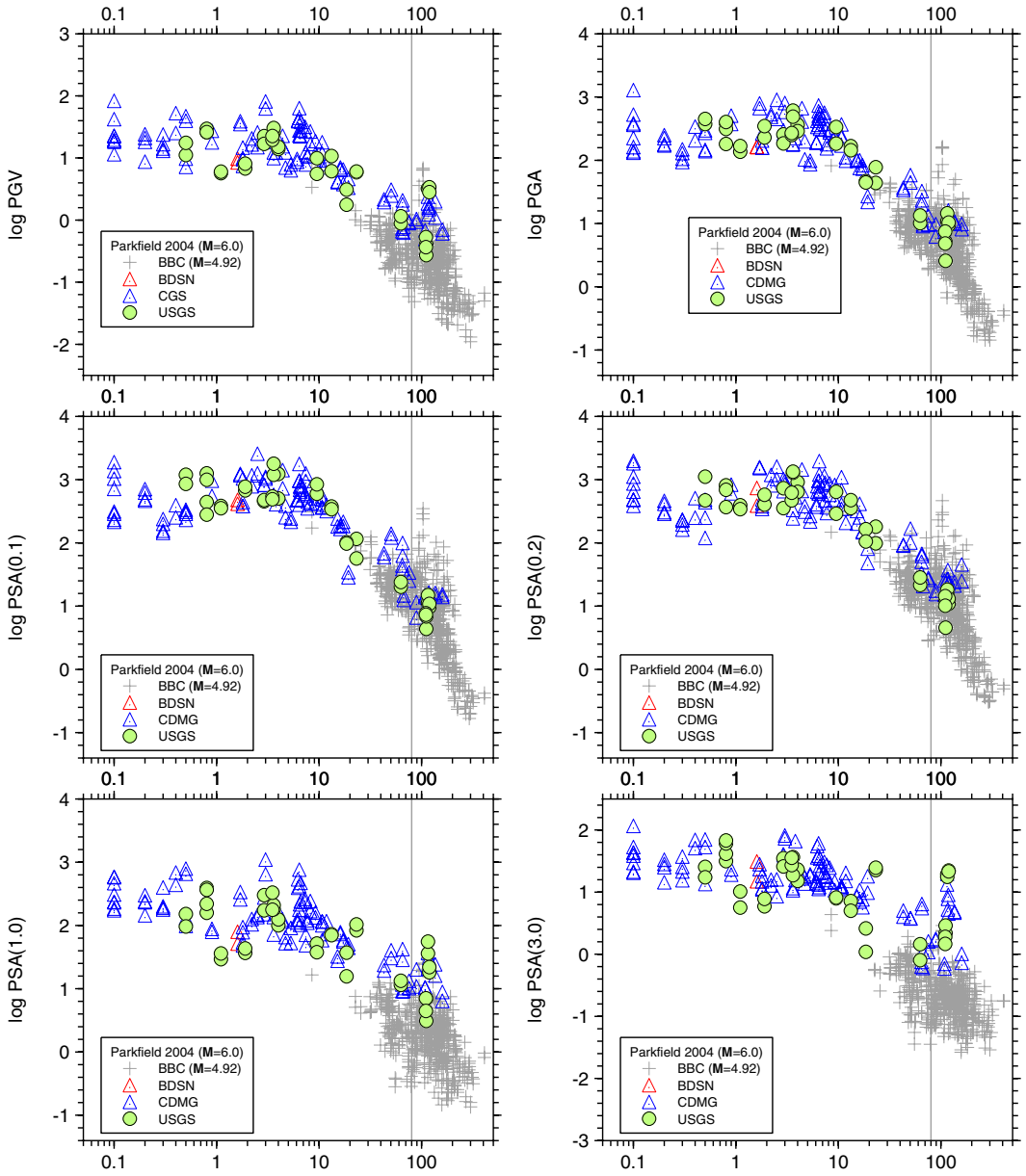

Fig. N.2 Ground motions from 2004 Parkfield earthquake compared to ground motions from smaller Big Bear City earthquake.

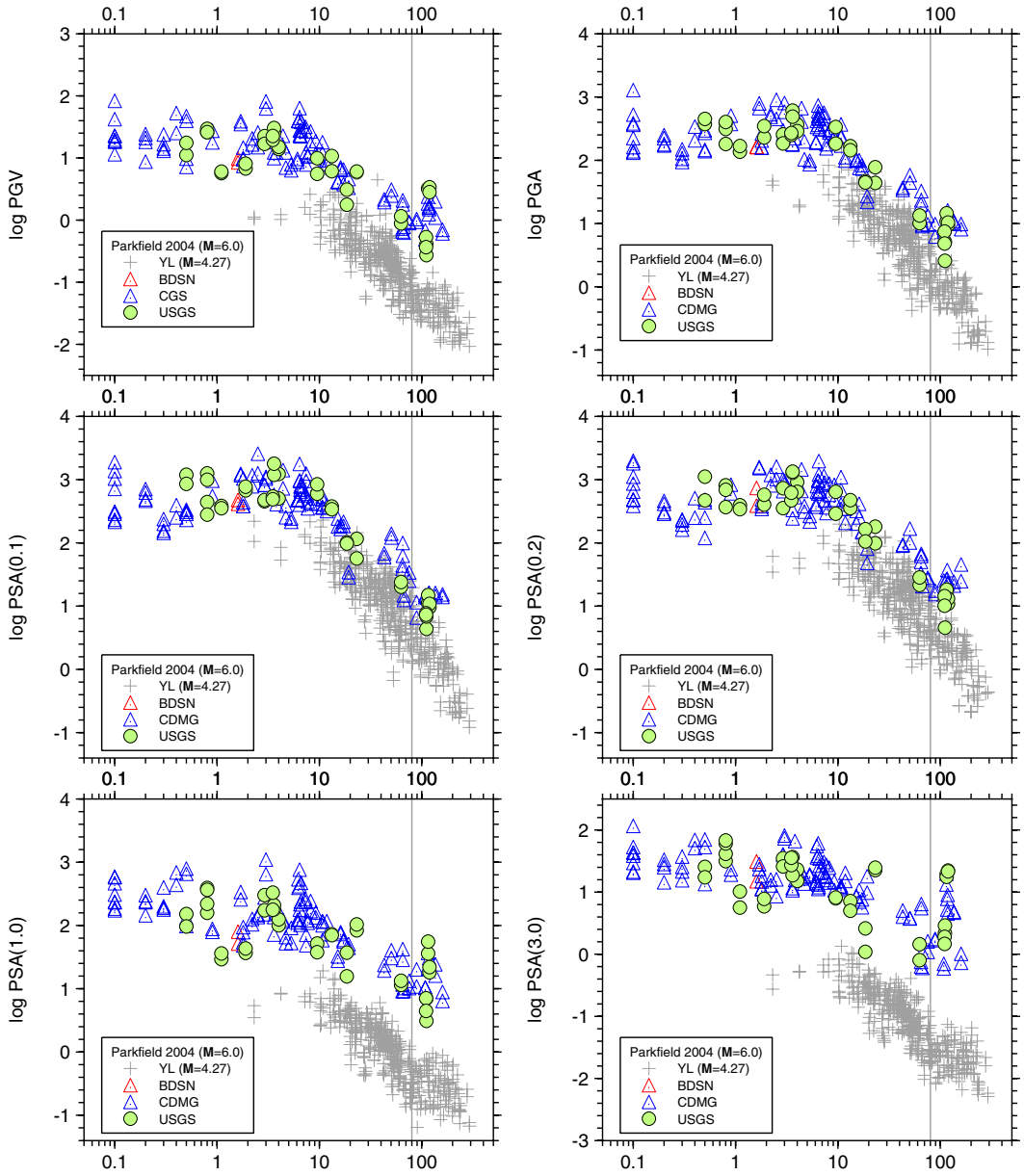

Fig. N.3 Ground motions from 2004 Parkfield earthquake compared to ground motions from smaller Yorba Linda earthquake.